Zeitschrift: IABSE reports = Rapports AIPC = IVBH Berichte
Band: 54 (1987)

Rubrik: Session 2: Computational models (advances)

SESSION 2

August 26, 1987 (afternoon)

Computational Models (Advances)

Modèles de calcul par ordinateur (progrès)

Rechenmodelle (Fortschritte)

Chairman: H. Mang, Austria

Invited Lecturers: E. Ramm, Fed. Rep. of Germany
Ultimate Load and Stability Analysis of Reinforced Concrete Shells

R. de Borst, The Netherlands
Stability and Uniqueness in Numerical Modelling of Concrete Structures

Leere Seite
Blank page
Page vide

Ultimate Load and Stability Analysis of Reinforced Concrete Shells

Charge de rupture et stabilité de coques en béton armé

Traglast- und Stabilitätsberechnung von Stahlbetonschalen

Ekkehard RAMM
Prof. of Civil Eng.
Univ. of Stuttgart
Stuttgart, FRG

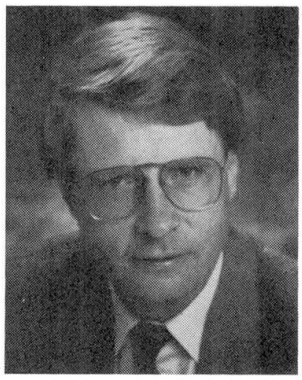

Ekkehard Ramm, born in 1940, earned his Dipl.-Ing. degree in civil engineering at the Technical Universities of Darmstadt and Stuttgart. He finished his Ph.D. in 1972 and his habilitation in 1976. Being a professor since 1976 he is now head of the Institute of Structural Analysis at the University of Stuttgart.

SUMMARY

The paper firstly discusses the fundamental behaviour of RC-shells in the ultimate load range which is characterized by a strong interaction of buckling and strength. It reviews current design procedures, few reported structural failures as well as RC model tests and finite element formulations for geometrically and materially nonlinear finite element analyses of RC-shells. Finally a brief description of one specific numerical model is given. It is applied to the ultimate load and stability analyses of conically shaped cooling towers.

RÉSUMÉ

Le rapport traite du comportement fondamental des coques en béton armé dans le domaine de la charge de rupture qui est caractérisé par l'interaction de la résistance moindre du matériau et du voilement. Il présente la pratique de projet actuelle, quelques cas de dommage et des expériences à l'aide de modèles en microbéton. Des calculs de coques en béton armé sur la base de la méthode des éléments finis sont présentés, en tenant compte de la non-linéarité géométrique et matérielle. Finalement un modèle numérique est décrit brièvement et appliqué aux calculs de charge de rupture et de stabilité des tours de réfrigération de forme conique.

ZUSAMMENFASSUNG

Der Beitrag diskutiert zunächst das prinzipielle Verhalten von Stahlbetonschalen im Grenzlastbereich, der durch kombiniertes Beul- und Materialversagen charakterisiert ist. Es wird ein Überblick gegeben über die gegenwärtige Entwurfspraxis, einige Schadenfälle, Modellversuche aus Mikrobeton und finite Elementformulierungen für geometrisch und materiell nichtlineare Berechnungen von Stahlbetonschalen. Schließlich wird ein numerisches Modell kurz beschrieben und auf Traglast- und Stabilitätsberechnungen von kegelförmigen Kühlturmschalen angewandt.

1. INTRODUCTION: BUCKLING OR STRENGTH?

RC - shells are extremely thin structures with radius to thickness ratios from 300 to 800, in particular if they are compared to classical domes or even natural egg shells with ratios up to 50 and 100, respectively. Therefore, it is obvious that each designer immediately is concerned that buckling may be a dominant phenomenon. However, most engineers have in mind the classical elastic stability problems when they think of buckling where the failure is usually caused by extreme symmetry in geometry, load, boundary conditions, stress state (uniform membrane) etc. Typical examples are the diamond shaped buckling of axially loaded cylinders or the snap - through behaviour of spherical shells under external pressure. It is natural that problems associated with buckling like imperfection sensitivity then have to be considered. This is the reason that for many RC - shell structures elastic model tests have been carried out in order to investigate the safety against buckling.

The question has to be raised whether this kind of buckling phenomenon can be met with RC - shells. It is well-known that the material behaviour may have a severe influence on stability, f.e. in the range of plastic buckling. The strong interaction can already be seen in the simple formula for classical linear buckling of shells with double curvature under external pressure:

$$p_{cr,ideal} = c \cdot E \cdot t^2/R_1 \cdot R_2$$

The buckling load depends on the material stiffness (Young's modulus E), the thickness t and the Gaussian curvature $1/R_1 \cdot R_2$. The factor c varies from one shell to the other, it is 1.15 for spheres. Quality and nonlinear behaviour of the concrete, creep and shrinkage, yielding of the reinforcement enter the formula via the material property E. The effective thickness is influenced by cracking, the percentage of the reinforcement and the number of layers (single or double). Moreover, creep may drastically change the original shape (flattening). All together these material effects may contribute more to the failure of the structure than the purely geometrical phenomenon of buckling.

Even if most people call a collapse of a shell structure in analysis, test or reality a buckling problem it is better to distinguish between the influence of material and geometrical nonlinearities. Therefore, let us call the collapse of a shell a buckling phenomenon when it is a finite deformation problem with little influence of the material failure and a strength problem when it is just the other way around (Fig. 1).

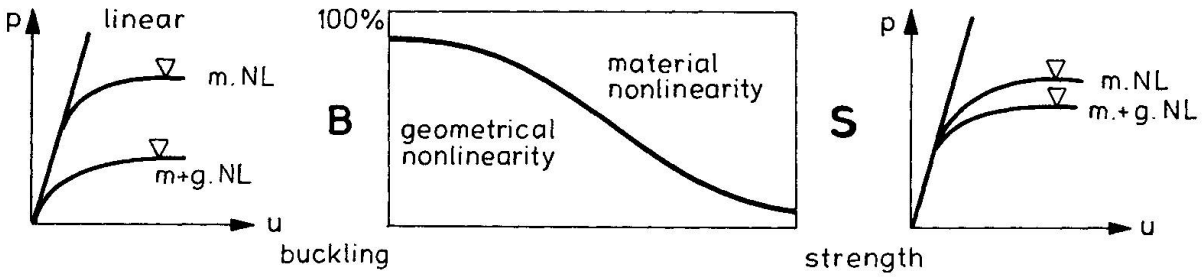

Figure 1: Contribution to Collapse

Unfortunately it is often not known in advance in what range the real structure has to be classified. However, certain parameters exist which qualitatively

indicate the tendency to the one or the other kind of failure (Fig. 2). Many practical cases are located in the intermediate range where both effects influence each other.

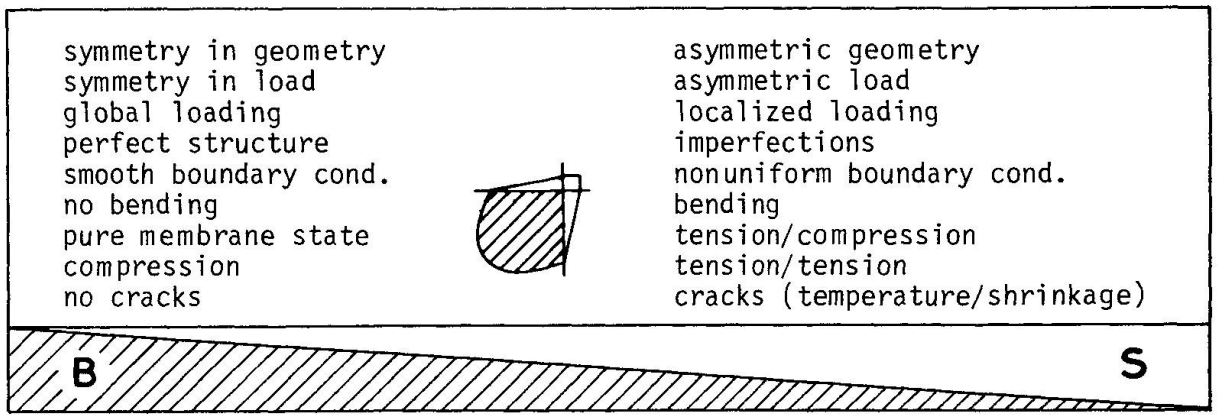

Figure 2: Buckling versus strength

The purpose of this paper is to review the literature with respect to this topic, to give some remarks to existing finite element models and first of all to call attention to this problem.

2. BASIC NONLINEAR STRUCTURAL BEHAVIOUR OF RC - SHELLS

An excellent compilation of the current state of understanding of concrete shell buckling is the ACI publication [1]. But the report also makes clear that beyond the classical type of buckling a considerable lack of information exists.

2.1 Current Design Procedures

Most codes on concrete structures only briefly stress the importance of shell buckling, enumerate several buckling load reducing effects and specify high safety factor, e.g. 5, in order to indicate the uncertainty of parameters and analysis (DIN 1045, ACI Standard 318). No details are given how the check against buckling has to be made. An exception are the IASS Recommendations [2] which are mostly based on the work of Dulácska [3]. The procedure contains five steps reducing the linear elastic buckling load of the homogeneous uncracked shell to the design load p (Fig. 3).

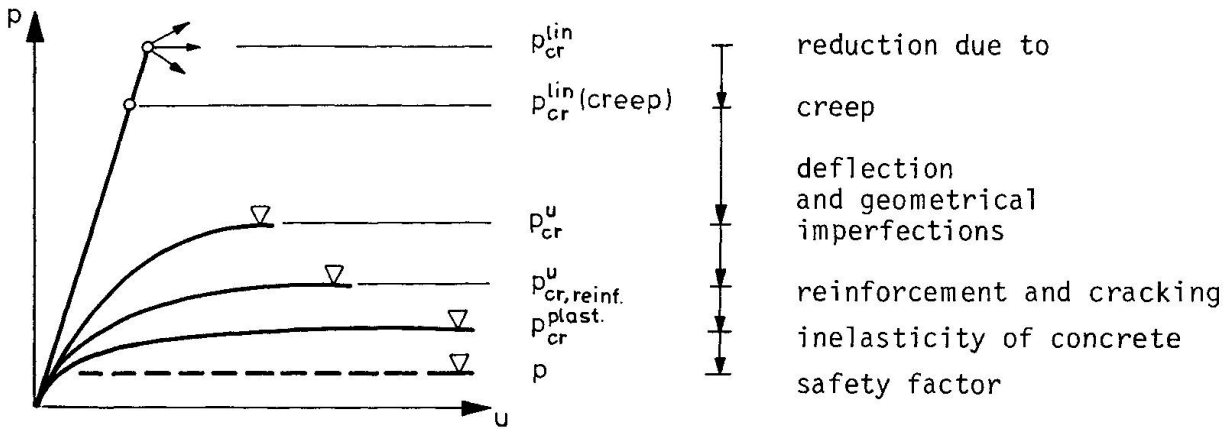

Figure 3: Buckling load according to IASS Recommendation [2]

The calculation which is essentially based on a local failure criterion does not cover the realistic situation because it accumulates all effects neglecting their different interactions. Despite the fact that it leads to a conservative design the scatter of results may be very large depending on the size of imperfections assumed. Reduction factors of less than 0.01 are possible. The Recommendations also address the possibility of one middle layer of reinforcement, a case which should not be used in practise due to unexpected local bending effects like concentrated loading (wind gusts), temperature change etc.

The situation with concrete cooling towers - even though more extensively investigated - is nearly the same [1], [4], [5]: independent design procedures against buckling on one side and yielding on the other side determining the wall thickness and the amount of reinforcement, respectively. The buckling analysis is mostly based on linear stability analyses or elastic model tests using reduction factors to account for imperfections, nonlinear behaviour, creep, cracking etc. In addition, high safety factors, e.g. 5, compared to the regular values of 1.75 for the yielding or the reinforcement, are introduced. In [6] it has been demonstrated through nonlinear finite element analyses that this discrepancy in safety factors is unrealistic since both effects strongly interact. A factor of safety 2.8 against buckling is proposed.

Although the more empirical approach is not satisfactory from the scientific point of view it has nearly always led to safe designs. A perfect example is the Swiss engineer Isler who has built more than 1400 concrete shells without any failure [7], [8].

2.2 Structural Failures

Very few failures of RC - shells have been reported (Table 1). Non of them can be attributed to buckling in the real sense. In most cases poor design and/or

Hungary [9], [10]	1954	EP 19 x 18 m	near collapse after 2 years, shell weakened by small glass skylights
Ferrybridge, GB	1965	cooling towers	poor design (membrane theory, working load design, one layer, no ring reinforcement)
Virginia [11]	1970	HP-gable shell 31 x 31 m	collapse after 7 years due to creep
Ardeer, GB	1973	cooling towers	low circumference reinforcement, vertical cracking due to thermal gradients
Latin America [12]	1975	EP 27 x 27 m	collapse after 4 days, poor concrete quality, significant geometrical imperfections, earthquake excitation
Port Gibson, USA	1978	cooling towers	damaged by toppling tower crane due to tornado
Berlin [13]	1980	HP	not a shell design, partly collapsed due to corrosion of tendons

Table 1: Failures of RC - shells

manufacturing can be made responsible, so that finally material failure caused the damage. On the other side there are several examples where well designed RC - shell structures withstood unexpected loadings, f.e. tornado (Port Gibson, 1978) or earthquake (Mexico, 1985).

2.3 Model Tests

The literature on small scale buckling tests of shells made of elastic material or metal is immense. In contrast to this very little information exists on model tests of RC - shells using microconcrete or mortar with and without reinforcement. In Table 2 some documented experiments are classified with respect to their kind of failure. This underlines the statements given in Fig. 2. If the structure is thick the crushing strength is decisive. If certain cracking is possible, for example due to boundary conditions, a combined buckling/material failure takes place. The more cracking is excluded and the thin structure is in a uniform compression state buckling becomes dominant. In this case the tangent modulus approach for buckling can be applied [18]. In [20] the important influence of creep on instability is stressed.

Schubiger [14]	ellipsoid (R), lateral load	628 *	combined buckling/strength
Bouma et al. [15]	cylindrical roof (R), lateral load	100	material failure (bending), small influence of geometrical nonlinearity
Distefano et al. [16]	HP (R), lateral load	a) shallow b) deep	a) buckling with material cracking b) pure buckling
Haas et al. [17]	cylinders (U), axial compression	50 - 120	material failure (crushing)
Griggs [18]	cylindrical roof (R), lateral load	238	combined buckling/strength
	spheres (R), ext. pressure	340	buckling with some material influence
	cylindrical panel (R), biaxial compression	200	
Müller et al. [19]	spheres (R), lateral load	a) 218 - 370 b) 303 perfect	a) material failure (bending) b) material failure (comp. strength)
Vandepitte et al. [20]	spheres (U), external pressure	~ 350	a) combined buckling/strength b) creep buckling

Table 2: RC - model tests (U = unreinforced, R = reinforced, * = r/t)

2.4 Nonlinear Analyses

Very few existing RC - shells have been investigated by a fully nonlinear analysis taking into account geometrical as well as material nonlinearties. The reason is that numerical models which are to some extend reliable came up only recently (see Chapter 3.1). Here few selected examples are mentioned. In the work of Scordelis and Chan [11], [21] an HP - gable shell is investigated which is patterned from a real structure. The collapse analysis indicates a strong interaction between both nonlinearities; it also points out the severe influence of creep on the ultimate load.

Significant work on the analysis of cooling towers under dead and wind load has been reported [4] but, as already mentioned in Chapter 2.1, most is based on elastic bifurcation and geometrical nonlinear analyses. For example a buckling criterion, the so-called buckling stress state (BSS), in conjunction with an equivalent axisymmetric stress approach is proposed in [22]. It has already been pointed out by Mang [23] that this assumption leads to the wrong conclusion that the structure would fail by buckling due to biaxial compression. Through elaborate materially and geometrically nonlinear analyses of two built cooling towers the authors in [24], [25] demonstrated that the loss of structural integrity is caused by cracking of the concrete on the windward side with some subsequent redistributions of stresses in the postcracking range. It is rather a material failure with little influence of large deformation effects than a buckling problem. This has been confirmed for the same cooling tower in [26] where in addition the noticeable influence of tension stiffening has been investigated.

For conical type of cooling towers see Chapter 3.2.

3. FINITE ELEMENT MODELS FOR RC - SHELLS

3.1 Review

The brief review is restricted to large deformation finite element models of general RC - shells. It is not considered to be complete. Either flat, curved shell or degenerated solid elements are applied. Due to the size and complexity of the problem neither a microscopic nor a macroscopic modelling is used. It is rather an intermediate type of idealization. That means that neither discrete cracks, strain localization or individual rebars on one side nor material laws defined in stress resultants like moment curvature relationships on the other side are introduced. To the author's knowledge all models use a smeared crack, layered approach. In each individual concrete layer a 2D stress state is assumed, in most cases referring to Kupfer's 2D failure envelope. The majority (Table 3) applies a nonlinear elastic, orthotropic material model introducing the equivalent uniaxial strain concept by Darwin and Pecknold. The fact that this semi-empirical formulation violates invariance requirements seems to be of little consequence since the principal stress direction does not rotate very much. Nearly all models assume a tension stiffening effect, either referred to the concrete or to the steel and use a fixed or variable shear retention factor after cracking. The steel layers always have uniaxial properties based on a bi- or multilinear stress - strain curve with hardening and elastic unloading. Large deformation effects are covered in the conventional way as in elastic analysis.

The assumption of a 2D stress state is certainly justified for most shell problems in which the load is mainly carried by membrane action. But it has to be noted that certain limitations exist: All stress states which deviate from the 2D situation like concentrated loading or localized support conditions cannot be properly analysed. For such local problems the design anyway requires special care, f.e. stirup reinforcement. In this case it is necessary to increase locally

the strength reflecting the existence of confined concrete. Otherwise premature failure occurs. Another possiblity is to resort to a 3D concrete model.

	ref.	material model	tension stiffening	extras
Ghoneim/Ghali	[33]	NE	C	prestress, creep, shrinkage
Arnesen/Bergan	[28]	EC	-	combined tensile strain/stress, criterion f. cracking
Floegl/Mang	[24], [29]	NE	S (bond slip)	influence of stress gradient
Chan/Scordelis	[21], [11]	NE	S	creep, shrinkage
Kompfner/Ramm	[30], [31]	NE	C	-
Figueiras/Owen	[32]	P (Kupfer)	C	w. & w/o hardening
Milford/ Schnobrich	[26], [27]	NE	S	rotated crack model
Cervera/Abdel Rahman/Hinton	[34]	P (v.Mises)	C	rotated crack model

Table 3: Large deformation RC - shell models
(NE: nonlinear elastic model, EC: endochronic model,
P: plasticity model, C/S: concrete/steel referred)

3.2 Present Model

The present model is described in detail in [30], see also [31]. The main characteristics of the formulation and the concrete model which is essentially an extended Darwin/Pecknold model are summarized in Tables 4 and 5.

formulation	arbitrarily large deformation, material mode (T.L.), incremental/iterative
iteration scheme	standard, modified, quasi Newton, load-, displacement-, arc-length-control, line search
shell element	isoparametric displacement model, degenerated solid, linear, quadratic or cubic interpolation (serendipity, Lagrange), full or reduced integration (Gauss), layered model (Simpson's integration)
material model	concrete: short time, nonlinear elastic, orthotropic, equivalent uniaxial strain concept (Darwin/ Pecknold), tension stiffening steel: smeared layers with uniaxial properties, multilinear, elasto-plastic, isotropic hardening

Table 4: RC - shell element formulation [30], [31]

The failure envelope renders the limit stresses σ_{ic} for each stress ratio α. Together with the limit strain ε_{ic} taken from test results it defines the corresponding stress - equivalent uniaxial strain curve, from which the material stiffness E_i is taken. In the finite element formulation nonproportional loading in each individual point cannot be avoided. In this case the stress - strain curve for that point varies. E_i is found according to the actual stress instead of the actual uniaxial strain; in the descending portion E_i is set to zero.

stress-equivalent uniaxial strain curve in compression	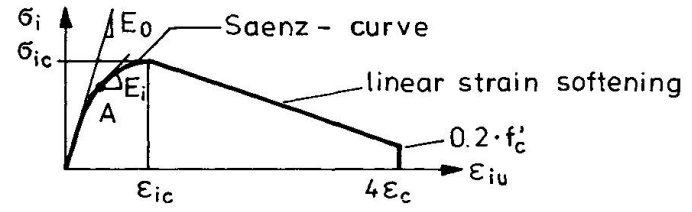
biaxial failure envelope (Kupfer/Gerstle) 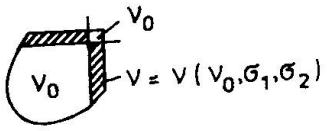	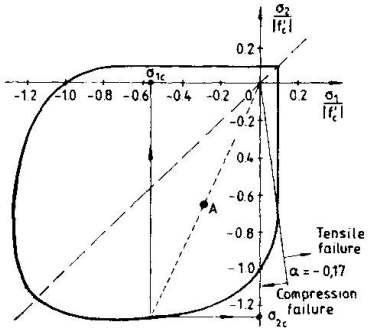
cracking fixed crack approach	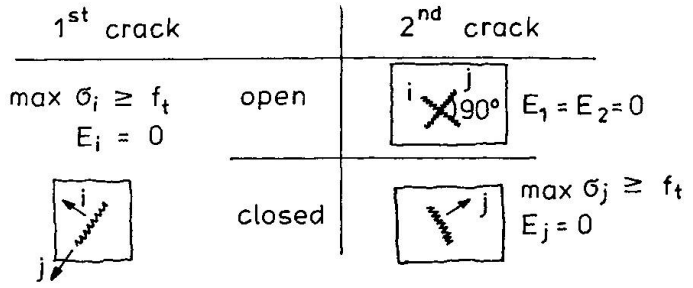
tension stiffening 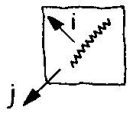	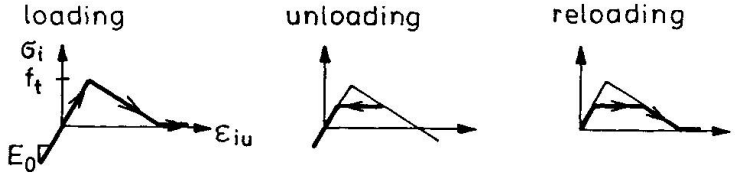
constitutive matrix for shell element	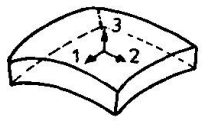 $\sigma_{33} = 0 \quad ; \quad \varepsilon_{33} = 0$ $G_{transverse} = \frac{5}{6} \cdot G_{inplane}$

Table 5: Concrete material model

Cracking follows the usual maximum principal stress criterion. Tension stiffening is included in a straightforward way. In the locally defined constitutive matrix the zero stress/strain condition is enforced. The inplane and transverse shear moduli are automatically adjusted according to the incremental orthotropic material tensor.

4. NUMERICAL EXAMPLES

In [30] ultimate load analyses of cylindrical roof shell and an HP-gable shell are described applying this model.

Recently in two power plants near Stuttgart two so-called hybrid (dry/wet) cooling towers have been built (Figures 5 and 7). Both towers with different size consist of a conventional (frame/ring wall) base structure with many openings and a shell shaped as a conical frustum, the latter being investigated in the following study, for details see [35]. The shell thickness is 16 cm (30 cm) for tower I (II); only in the lower part 3.06 m (4.50 m) it is increased to 30 cm (50 cm). In each production cycle one quarter section with a height of 1.45 m is poured. The extreme loading is dead load, wind - taken constant along the meridian - and concentrated loads at the free edge due to scaffolding on 90° with added life load and fresh concrete. Preliminary studies have shown:

* The structural response is completely different from that of conventional hyperbolic cooling towers.
* The critical period is the phase before the upper ring is built, leading to a free edge boundary condition at the critical height h_{cr}.
* The concentrated loading at the top could be localized at the free edge in order to simplify the input data.
* Linear elastic buckling analyses restricted to axisymmetric modes lead to unrealistic high buckling loads.
* The results are almost not influenced by the boundary conditions of the lower edge (clamped or hinged).

The material properties of both towers are given in Figure 4.

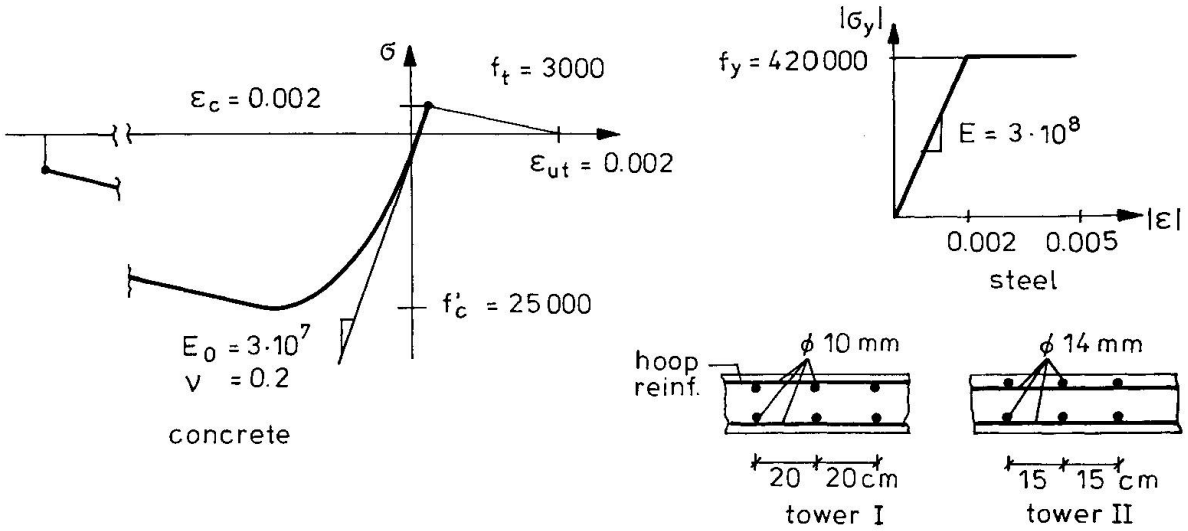

Figure 4: Material properties [kN/m²]

4.1 Cooling Tower I (Altbach)

The base structure of the small tower (Fig. 5) could be considered as very stiff. Therefore, clamped boundary conditions at the lower edge are introduced. As a conservative approach uniform thickness and axisymmetric loading is assumed. Linear elastic buckling analyses lead to a critical load factor λ = 15.7 with

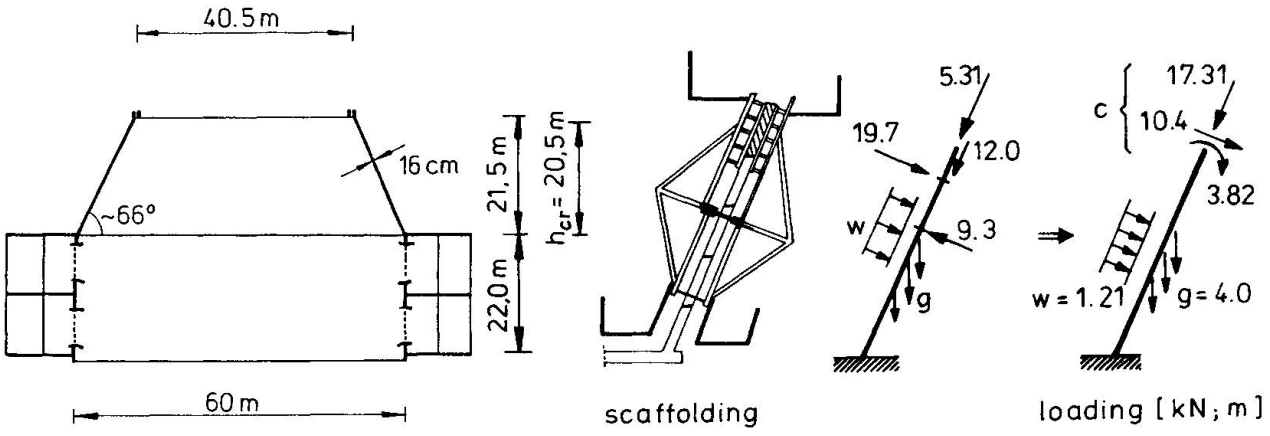

Figure 5: Cooling tower I (Altbach)

a buckling mode of 8 waves in hoop direction concentrated near the free edge. The corresponding stresses are far beyond the compressive strength of the concrete. A geometrically and materially nonlinear axisymmetric analysis of the perfect shell resulted in a failure load g + 5.4 (w + c). The load factor is reduced to 5.0 if tensile strength and ultimate strain are reduced (f_t = 10 kN/m²; $\varepsilon_{ut} = f_t / E_o$). Next nonsymmetric geometrical imperfections corresponding to the buckling wave pattern (n = 8) with a maximum amplitude of ± 5 cm are introduced. One half wave sector is modelled, assuming a reduced Young's modulus $E_o = 2.8 \cdot 10^7$ kN/m² for the upper 1.4 m and tension cut-off (f_c = 10 kN/m²; ε_{ut} = 0). These extreme conditions lower the load factor to 4.3 (Fig. 6). Cracking is concentrated to the upper ring portion.

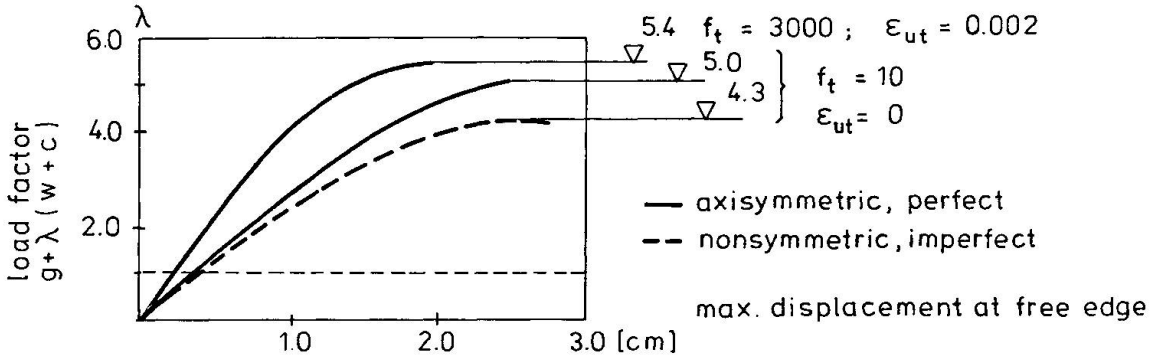

Figure 6: Load displacement diagram

4.2 Cooling Tower II (Neckarwestheim)

In contrast to tower I the base structure of cooling tower II (Fig. 7) is very flexible. Despite its size and dimensions it is a relatively slender contruction in which many precast elements are incorporated. Therefore, the shell itself has

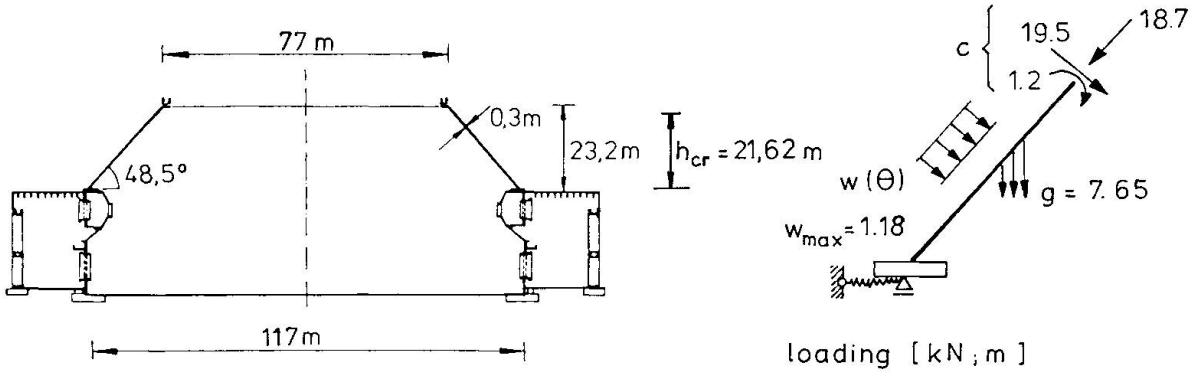

Figure 7: Cooling tower II (Neckarwestheim)

a lower ring beam (4.00 x 0.75 m; A_s = 482 cm²), but already under dead load the beam is partly cracked (state II) so that a reduced membrane and bending stiffness is introduced for the linear buckling analyses (EI^{I}/EI^{II} = 4.4; EA^{I}/EA^{II} = 8.5). Assuming that the ring/shell structure is hinged and radially as well as tangentially unrestrained - i.e. neglecting the stiffness of the base structure - a linear buckling analysis with axisymmetric loading leads to bifurcation loads 6.17 (g + w + c) or g + 13.50 (w + c) with five buckling waves in hoop direction. In this case a nonlinear study of a half wave sector of the imperfect shell - as for tower I - did not reflect the real situation since unsymmetric loading of wind and scaffolding causes considerable inextensional deformations (ovalization) due to the flexible base. Therefore, one half of the shell was modelled by a non-uniform mesh 15 x 32 eight-node shell elements and 32 quadratic beam elements for the edge beam which are compatible to the shell elements. Again the bending stiffness of the edge beam is reduced to that of state II; the membrane stiffness is restricted to the steel reinforcement alone. Regarding the different age of concrete the Young's modulus of the upper portion (2.9 m) of the shell is lowered by 20 percent. Now the base structure is simulated by radial and tangential springs at each node. The spring stiffnesses of k_r = 25675 kN/m and k_t = 8190 kN/m taken from a preliminary linear study of the entire structure under unfavourable conditions have been found essential for the safety of the structure. The concentrated load c of the scaffolding over a 90°-sector was located at the free edge on the windward side. Wind load and suction in hoop direction are defined in the following way:

$$w = (c_p \cdot 1.01 + 0.53)\ kN/m^2$$

with

$$c_p = \begin{cases} 1 - 2.1 \cdot [\sin(\Theta \cdot 90/71)]^n & 0 \leq |\Theta| \leq 71° \\ -1.1 + 0.6 \cdot [\sin(90 - 71) \cdot 90/22]^n & 71° \leq |\Theta| \leq 90{,}4° \\ -0.5 & 90{,}4° \leq |\Theta| \leq 180° \end{cases}$$

$$n = 2.395$$

The wind load is assumed constant along the meridian. Geometrical imperfections correspoding to the first buckling mode with a maximum horizontal amplitude of ± 10 cm were superimposed. For this a linear buckling analysis of the structure under nonsymmetric loading assuming a fixed lower boundary has been performed. Few circumferential waves are concentrated at the windward compression zone. In Figure 8 two materially nonlinear analyses with and without large deformation effects are compared indicating the considerable influence of the geometrical

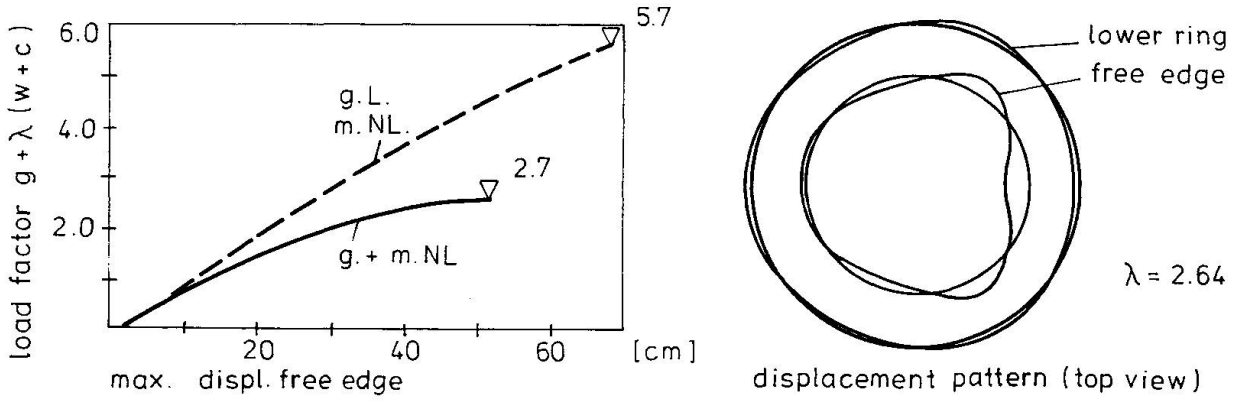

Figure 8: Load displacement diagram/failure mode

nonlinearity. The ultimate load is g + 2.70 (w + c). The ovalization of the entire shell can be seen in the failure mode (Fig. 8). A supplementary study with imperfections of ± 15 cm and a different loading sequence rendered an ultimate load of 1.45 g + 1.45 w + 2.51 c.

According to Figures 1 and 2 tower I could be classified as a primary strength problem whereas due to the flexible base structure tower II is located in the combined buckling/strength range.

5. CONCLUSION

The present study has shown:

* The knowledge of the fundamental response of RC-shells in the ultimate load range is still limited. Therefore, the question of reliable safety factors against failure is not yet answered.

* The current design procedures with a more or less empirical coupling of buckling with material failure is unsatisfactory.

* Elastic buckling analyses or tests are of limited value for RC-shells. They are necessary but not sufficient.

* The current development of numerical oriented RC material models including large deformation effects are a promising alternative to the current procedure.

* High quality of analysis based on conservative assumptions in loading, imperfections, boundary conditions, material properties allows to reduce safety factors against failure, e.g. to 2.5. However, these analyses are still expensive and need a lot of experience.

Further research is needed

* to gain further information on the basic nonlinear structural behaviour of RC - shells and

* to further improve existing or to develop new nonlinear material formulations.

ACKNOWLEDGEMENTS

The conceptual design of both cooling towers has been done by Balcke / Dürr, Ratingen. The contractor was Züblin AG, Stuttgart. The stability and ultimate load analyses have been carried out by Dr. A. Burmeister and Dr. H. Stegmüller, Institut für Baustatik, University of Stuttgart.

REFERENCES

[1] POPOV, E.P., MEDWADOWSKI, S.J. (eds.): Concrete Shell Buckling. ACI Publ. SP-67, 1981.

[2] Recommendations for Reinforced Concrete Shells and Folded Plates. Int. Association for Shell and Spatial Structures, IASS, Madrid, 1979.

[3] KOLLAR, L., DULACSKA, E.: Buckling of Shells for Engineers. Chapter 9.8: 'Problems of Reinforced Concrete Shells'. J. Wiley, 1984.

[4] GOULD, P.L., KRÄTZIG, W.B., MUNGAN, I., WITTEK, U. (eds.): Natural Draught Cooling Towers. Proc., 2 Int. Symp., Bochum, 1984, Springer-Verlag, 1984.

[5] BTR - Bautechnik bei Kühltürmen, Teil II. Bautechnische Richtlinie, Essen, VGB-Verlag, 1980.

[6] ZERNA, W., MUNGAN, I., WINTER, M.: Das nichtlineare Tragverhalten der Kühlturmschalen unter Wind. Bauingenieur 61 (1986) 149-153.

[7] ISLER, H.: The Stability of Thin Concrete Shells. Proc., State-of-the-Art Colloquium 'Buckling of Shells' (ed. E. Ramm), Springer-Verlag, 1982.

[8] RAMM, E., SCHUNCK, E.: Heinz Isler - Schalen. Kraemer-Verlag, Stuttgart, 1986.

[9] CSONKA, P.: The Buckling of a Spheroidal Shell Curved in Two Directions. Acta Technica Hung. 14 (1956) 425-437.

[10] CSONKA, P.: Die Verformung und nachträgliche Verstärkung einer kuppelartigen Schale in Ungarn. Bautechnik 35 (1958) 69 - 72.

[11] SCORDELIS, A.C.: Analysis of Thin Shell Roofs. Proc., IASS Symposium on Spatial Roof Structures, Dortmund, 1984, IASS-Bulletin 87 (1985) 5 - 19.

[12] BALLESTEROS, P.: Nonlinear Dynamic and Creep Buckling of Elliptical Paraboloidal Shells. IASS-Bulletin 68 (1978) 39 - 60.

[13] SCHLAICH, J., KORDINA, K., ENGELL, H.J.: Teileinsturz der Kongreßhalle Berlin - Schadensursachen - zusammenfassendes Gutachten. Beton- und Stahlbeton 75 (1980) 281 - 294.

[14] SCHUBIGER, E.: Die Schalenkuppel in vorgespanntem Beton der Kirche Felix und Regula in Zürich. Schweizer Bauzeitung 68 (1950) 223 - 228.

[15] BOUMA, A.L., VAN RIEL, A.C., VAN KOTEN, H., BERANEK, W.J.: Investigations on Models of Eleven Cylindrical Shells Made of Reinforced and Prestressed Concrete. Proc., IASS Symp. 'Shell Research', Delft, 1961.

[16] DISTEFANO, J.N., TORREGIANI, C.: A Simplified Method to Evaluate Critical Loads of Hyperbolic Paraboloidal Shells. Proc., IASS Symp. 'Shell Structures in Engineering Practice', Budapest, 1965.

[17] HAAS, A.M., VAN KOTEN, H., VAN LEEUVEN, J.: Stability of Thin Concrete Cylindrical Shells under Uniform Axial Compression. Proc., IASS Symp. 'Progress of Shell Structures in the Last Ten Years and its Future Development', Madrid, 1969.

[18] GRIGGS, P.H.: Buckling of Reinforced Concrete Shells. J. Eng. Mech. Div., ASCE 97 (1971) 687 - 700.

[19] MÜLLER, F.P., WEIDLICH, CH.: An Experimental Investigation of the Stability of Shallow Spherical Shells of Reinforced Concrete Subjected to Uniformly Distributed Load. Proc., IASS Symp., Darmstadt, 1978, 319-328.

[20] VANDEPITTE, D., RATHE, J., WEYMEIS, G.: Experimental Investigation into the Buckling and Creep Buckling of Shallow Spherical Caps Subjected to Uniform Radial Pressure. Proc., IASS World Congress on Shell and Spatial Structures, Madrid, 1979, 427 - 442.

[21] CHAN, E.C.: Nonlinear Geometric, Material and Time Dependent Analysis of Reinforced Concrete Shells with Edge Beams. Report No. UCB/SESM - 82/08, Div. of Structural Eng. and Structural Mechanics, UC Berkeley, California, 1982.

[22] ZERNA, W., MUNGAN, I., STEFFEN, W.: Wind - Buckling Approach for RC Cooling Towers. J. Eng. Mech. Div., ASCE 109 (1983) 836 - 848.

[23] MANG, H.A.: Wind - Buckling Approach for RC Cooling Towers. Discussion to [22]. J. Eng. Mech. Div., ASCE 110 (1984) 1163 - 1168.

[24] MANG, H.A., FLOEGL, H., TRAPPEL, F., WALTER, H.: Wind - loaded Reinforced - concrete Cooling Towers: Buckling or Ultimate Load? Eng. Struct. 5 (1983) 163 - 180.

[25] MANG, H.A., TRAPPEL, F.: Physically Linear Buckling Analysis of Reinforced Concrete Cooling Towers - Design Necessity or Academic Exercise? Proc., 2nd Int. Symp. 'Natural Draught Cooling Towers' (eds. P.L. Gould et al.), Bochum, 1984, Springer-Verlag, 1984.

[26] MILFORD, R.V., SCHNOBRICH, W.C.: The Effect of Cracking on the Ultimate Load of Reinforced Concrete Cooling Towers. Proc., 2nd Int. Symp. 'Natural Draught Cooling Towers' (eds. P.L. Gould et al.), Bochum, 1984, Springer-Verlag, 1984.

[27] MILFORD, R.V.: Nonlinear Behavior of Reinforced Concrete Shells. Ph.D. thesis. University of Illinois, Urbana, Illinois, 1984.

[28] ARNESEN, A.: Analysis of Reinforced Concrete Shells Considering Material and Geometric Nonlinearities. Report No. 79-1, Div. Struct. Mech., Norwegian Institute of Technology, University of Trondheim, Norway, 1979.

[29] MANG, H.A., EBERHARDSTEINER, J.: Collapse Analysis of RC Shells Based on a New Fracture Criterion. Proc., Seminar 'Finite Element Analysis of Reinforced Concrete Structures', Tokyo, Japan, May 1985.

[30] KOMPFNER, T.A.: Ein finites Elementmodell für die geometrisch und physikalisch nichtlineare Berechnung von Stahlbetonschalen. Dissertation, Universität Stuttgart, 1983.

[31] RAMM, E., KOMPFNER, T.A.: Reinforced Concrete Shell Analysis Using an Inelastic Large Deformation Finite Element Formulation. Proc., Int. Conference 'Computer-aided Analysis and Design of Concrete Structures' (eds. F. Damjanič et al.), Split, 1984, Pineridge Press, Swansea, UK.

[32] FIGUEIRAS, J.A., OWEN, D.R.J.: Nonlinear Analysis of Reinforced Concrete Slab and Box-girder Bridge Decks. Proc., Int. Conference 'Computer Aided Analysis and Design of Concrete Structures' Split, 1985, Pineridge Press, Swansea, UK, 509 - 532.

[33] GHONEIM, G.A.-A.M.: Nonlinear Finite Element Analysis of Concrete Structures. Ph.D. thesis, University of Calgary, Canada, 1978.

[34] CERVERA, M., ABDEL RAHMAN, H.H., HINTON, E.: Material and Geometrical Nonlinear Analysis of Reinforced Concrete Plate and Shell Systems. Proc., Int. Conference 'Computer Aided Analysis and Design of Concrete Structures', Split, 1985, Pineridge Press, Swansea, UK, 547-564.

[35] RAMM, E., BURMEISTER, A., STEGMÜLLER, H.: Stabilitäts- und Traglastuntersuchungen der Hybridkühltürme Altbach und Neckarwestheim. To be published.

Leere Seite
Blank page
Page vide

Stability and Uniqueness in Numerical Modelling of Concrete Structures

Stabilité et unicité des modèles numériques dans les structures en béton

Stabilität und Eindeutigkeit numerischer Modelle im Stahlbeton

René de BORST
TNO-IBBC
Delft, The Netherlands

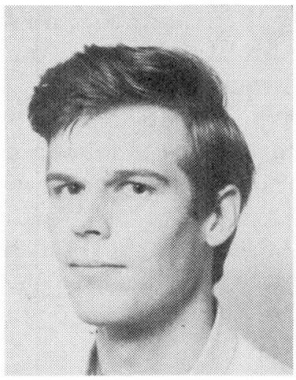

René de Borst, born 1958, earned his Ir. degree in civil engineering in 1982 and his Dr. degree in 1986, both from Delft University of Technology. He has been a member of the DIANA group of the TNO Institute for Building Materials and Structures since 1982.

SUMMARY
Recent advances in smeared crack modeling and computational techniques for concrete structures are reviewed. Special attention is given to the issue of stability and uniqueness in numerical computations of strain-softening concrete. Techniques for overcoming bifurcation and limit points are discussed whereby special attention is given to cases with highly localized failure modes. The techniques are applied to some reinforced and unreinforced concrete structures.

RÉSUMÉ
Les progrès récents dans la modélisation des fissures homogénéisées et les techniques de calcul à l'ordinateur pour les structures en béton sont passés en revue. Une attention particulière est portée au cas de la stabilité et de l'unicité, dans de nombreux calculs, du béton se plastifiant sous contrainte. Des techniques pour résoudre les problèmes de bifurcation et de points limites sont discutées et une attention particulière est portée aux cas de modes de rupture hautement localisés. Les techniques sont appliquées à certaines structures en béton armé et non-armé.

ZUSAMMENFASSUNG
In diesem Beitrag wird eine Übersicht über neue Entwicklungen der ausgeglichenen Rissbildung und Rechenverfahren für Betonkonstruktionen gegeben. Hauptaugenmerk wird gerichtet auf Stabilität und Eindeutigkeit in numerischen Berechnungen von entfestigendem Beton. Lösungsmethoden zur Vermeidung von Bifurkation und Grenzwerte werden diskutiert für höchstbelastete Bereiche. Die Methoden werden auf einige bewehrte und unbewehrte Betonkonstruktionen angewandt.

1. INTRODUCTION

Concrete is a very complicated material because of its heterogeneity, the presence of reinforcement, the low tensile strength, the change in properties when it matures, and so on. It is therefore not surprising that predictions of the mechanical behavior of concrete structures still suffer from a lack of reliability. Nevertheless, the discrepancy between analytical results and the real behavior is often greater than necessary when considering the current level of sophistication of testing procedures, constitutive models and computational techniques. Significant, and in some areas seemingly insurmountable difficulties persist, but progress has definitely been made in analyzing concrete structures with aid of finite elements.

It is the purpose of the present paper to give an overview of some recent achievements of the DIANA-group in constitutive modeling and the application of computational techniques to concrete structures. The review is by no means intended to be exhaustive, and important issues like for instance time-dependent behavior [11,13] or bond-slip behavior [27] will not be treated. The main topics which will be considered, are smeared crack modeling and issues regarding stability and uniqueness of computations for concrete structures. It is recognized that the crack model, which we will henceforth refer to as the DIANA-crack model, has been treated extensively in previous publications [7,8,10,13,26,29], but because crack formation plays such a pivotal role in the behavior of concrete structures, there may be some justification in briefly reviewing the main concepts of it before discussing issues regarding stability and uniqueness.

2. MODELING OF SMEARED CRACKING

The fundamental feature of the employed smeared crack model is a decomposition of the total strain rate into a concrete strain rate $\dot{\boldsymbol{\varepsilon}}^{co}$ and into a crack strain rate $\dot{\boldsymbol{\varepsilon}}^{cr}$ (e.g., also [4,22]):

$$\dot{\boldsymbol{\varepsilon}}=\dot{\boldsymbol{\varepsilon}}^{co}+\dot{\boldsymbol{\varepsilon}}^{cr} \tag{1}$$

The concrete strain rate itself may also be composed of several contributions e.g., an elastic part and a viscous part. Similarly, the crack strain rate $\dot{\boldsymbol{\varepsilon}}^{cr}$ may be decomposed into several contributions:

$$\dot{\boldsymbol{\varepsilon}}^{cr}=\dot{\boldsymbol{\varepsilon}}_1^{cr}+\dot{\boldsymbol{\varepsilon}}_2^{cr}+\ldots\ldots\ldots \tag{2}$$

where $\dot{\boldsymbol{\varepsilon}}_1^{cr}$ is the strain rate of a primary crack, $\dot{\boldsymbol{\varepsilon}}_2^{cr}$ is the strain rate of a secondary crack and so on. Combining eqs. (1) and (2), we obtain

$$\dot{\boldsymbol{\varepsilon}}=\dot{\boldsymbol{\varepsilon}}^{co}+\dot{\boldsymbol{\varepsilon}}_1^{cr}+\dot{\boldsymbol{\varepsilon}}_2^{cr}+\ldots\ldots\ldots\ldots \tag{3}$$

The relation between the strain rate of a particular crack (either primary or secondary) and the stress rate is most conveniently defined in the coordinate system which is aligned with the crack. This necessitates a transformation between the crack strain rate $\dot{\boldsymbol{\varepsilon}}_n^{cr}$ of crack n in the global x,y,z-coordinates and a crack strain rate $\dot{\boldsymbol{e}}_n^{cr}$ which is expressed in local coordinates. Restricting the treatment to a two-dimensional configuration (which is not essential), we observe that a crack only has a normal strain rate $\dot{e}_n^{cr}$ and a shear strain rate $\dot{\gamma}_n^{cr}$, so that

$$\dot{\boldsymbol{e}}_n^{cr}=(\dot{e}_n^{cr}\ \ \dot{\gamma}_n^{cr})^T \tag{4}$$

where the superscript T denotes a transpose. The relation between $\dot{\boldsymbol{\varepsilon}}_n^{cr}$ and $\dot{\boldsymbol{e}}_n^{cr}$ reads

$$\dot{\boldsymbol{\varepsilon}}_n^{cr}=\boldsymbol{N}_n\,\dot{\boldsymbol{e}}_n^{cr} \tag{5}$$

with

$$\boldsymbol{N}_n=\begin{bmatrix} \cos^2\vartheta_n & -\sin\vartheta_n\cos\vartheta_n \\ \sin^2\vartheta_n & \sin\vartheta_n\cos\vartheta_n \\ 2\sin\vartheta_n\cos\vartheta_n & \cos^2\vartheta_n-\sin^2\vartheta_n \end{bmatrix} \tag{6}$$

where ϑ_n is the inclination angle of the normal of crack n with the x-axis. Substitution of eq. (5) in eq. (2) gives for multiple cracks

$$\dot{\boldsymbol{\varepsilon}}^{cr}=\boldsymbol{N}_1\dot{\boldsymbol{e}}_1^{cr}+\boldsymbol{N}_2\dot{\boldsymbol{e}}_2^{cr}+\ldots\ldots\ldots \tag{7}$$

For the derivation of the stress-strain law of the system of cracks and concrete, it is convenient to assemble all the crack strain rates which are expressed in their own local coordinate system in a vector $\dot{\boldsymbol{e}}^{cr}$,

$$\dot{\boldsymbol{e}}^{cr}=(\dot{e}_1^{cr}\ \ \dot{\gamma}_1^{cr}\ \ \dot{e}_2^{cr}\ \ \dot{\gamma}_2^{cr}\ldots\ldots\ldots)^T \tag{8}$$

When we also introduce the matrix $\boldsymbol{N}$,

$$\boldsymbol{N}=\left[\boldsymbol{N}_1\ \boldsymbol{N}_2\ldots\ldots\ldots\ldots\right] \tag{9}$$

we observe that we can rewrite eq. (7) as

$$\dot{\boldsymbol{\varepsilon}}^{cr}=\boldsymbol{N}\dot{\boldsymbol{e}}^{cr} \tag{10}$$

In a similar way, we can define a vector $\dot{\boldsymbol{s}}_n$

$$\dot{\boldsymbol{s}}_n=(\dot{s}_1\ \ \dot{t}_1)^T \tag{11}$$

with $\dot{s}_n$ the normal and $\dot{t}_n$ the shear stress rate in crack n of the integration point. The vector $\dot{\boldsymbol{s}}$ which assembles all stress rates with respect to their own local coordinate system then reads:

$$\dot{\boldsymbol{s}}=(\dot{s}_1\ \ \dot{t}_1\ \ \dot{s}_2\ \ \dot{t}_2\ldots\ldots\ldots\ldots\ldots)^T \tag{12}$$

and the relation between the stress rate in the global coordinate system $\dot{\boldsymbol{\sigma}}$ and the stress vector $\dot{\boldsymbol{s}}$ can be derived to be

$$\dot{\boldsymbol{s}}=\boldsymbol{N}^T\dot{\boldsymbol{\sigma}} \tag{13}$$

To complete the system of equations, we need a constitutive model for the intact concrete and a stress-strain relation for the smeared cracks. For the concrete between the cracks we assume a relationship which has the following structure

$$\dot{\boldsymbol{\sigma}}=\boldsymbol{D}^{co}\dot{\boldsymbol{\varepsilon}}^{co} \tag{14}$$

where the matrix $\boldsymbol{D}^{co}$ contains the instantaneous moduli of the concrete. The formalism of eq. (14) can be extended to deal with phenomena like thermal dilatation, shrinkage and creep [11,13], but this will not be pursued in the present paper. In a similar way, we can define a relation between the crack strain rate $\dot{\boldsymbol{e}}_n^{cr}$ of crack n and the stress rate $\dot{\boldsymbol{s}}_n$ in that crack. In this paper, we will assume a relation which formally reads:

$$\dot{\boldsymbol{s}}_n=\boldsymbol{D}_n^{cr}\dot{\boldsymbol{e}}_n^{cr} \tag{15}$$

with $\boldsymbol{D}_n^{cr}$ a 2*2 matrix. For the derivation of the stress-strain relation of the cracked concrete, it is again convenient to assemble all the matrices $\boldsymbol{D}_n^{cr}$ in a matrix $\boldsymbol{D}^{cr}$,

$$\boldsymbol{D}^{cr}=\begin{bmatrix}\boldsymbol{D}_1^{cr} & \boldsymbol{0} & \ldots\ldots\\ \boldsymbol{0} & \boldsymbol{D}_2^{cr} & \ldots\ldots\\ \ldots\ldots & \ldots\ldots & \ldots\ldots\end{bmatrix} \tag{16}$$

so that the relation between $\dot{\boldsymbol{s}}$ and $\dot{\boldsymbol{e}}^{cr}$ reads

$$\dot{\boldsymbol{s}}=\boldsymbol{D}^{cr}\dot{\boldsymbol{e}}^{cr} \tag{17}$$

Using eqs. (1), (10), (13), (14) and (17) we can obtain the compliance relation for the cracked concrete:

$$\dot{\boldsymbol{\varepsilon}}=\left\{\boldsymbol{C}^{co}+\boldsymbol{N}\boldsymbol{C}^{cr}\boldsymbol{N}^T\right\}\dot{\boldsymbol{\sigma}} \tag{18}$$

with $\boldsymbol{C}^{co}=(\boldsymbol{D}^{co})^{-1}$ and $\boldsymbol{C}^{cr}=(\boldsymbol{D}^{cr})^{-1}$ the compliance matrices of the concrete and the cracks respectively. With aid of the Sherman-Morrison-Woodbury formula we can also obtain the

stiffness relation

$$\dot{\sigma}=\left\{\boldsymbol{D}^{co}-\boldsymbol{D}^{co}\boldsymbol{N}[\boldsymbol{D}^{cr}+\boldsymbol{N}^{T}\boldsymbol{D}^{co}\boldsymbol{N}]^{-1}\boldsymbol{N}^{T}\boldsymbol{D}^{co}\right\}\dot{\boldsymbol{\varepsilon}} \tag{19}$$

The success of this multiple crack model is contingent upon a proper formulation of the constitutive matrix

$$\boldsymbol{D}_{n}^{cr}=\begin{bmatrix} D_{11}^{cr} & D_{12}^{cr} \\ D_{21}^{cr} & D_{22}^{cr} \end{bmatrix} \tag{20}$$

for the smeared-out cracks. Fortunately, in many concrete structures the crack strains are so small that coupling effects between the normal crack strain and the shear stress, or between the shear crack strain and the normal stress can be disregarded, so that we may set the off-diagonal terms in eq. (20) equal to zero ($D_{12}^{cr}=0$ and $D_{21}^{cr}=0$). If, such as in crack-dilatancy models [4,32] or in jointed rock masses [2], D_{12}^{cr} and D_{21}^{cr} can not be assumed to vanish, we face significant additional difficulties, since the values for D_{12}^{cr} and D_{21}^{cr} generally differ considerably. This implies that $\boldsymbol{D}_{n}^{cr}$ becomes nonsymmetric, which also destroys the major symmetry of eq. (19). Apart from the fact, that this leads to significantly larger CPU-times, it also has consequences for the stability of the model, as will be briefly discussed in the sequel of this paper.

The tangent modulus D_{11}^{cr} represents the relation between the normal crack strain rate and the normal stress rate. In practice, D_{11}^{cr} is negative as we normally have a descending relation between $\dot{s}_n$ and $\dot{e}_n^{cr}$. However, the evaluation of D_{11}^{cr} from test data entails a complication, as recent research [5,21] indicates that a straightforward translation from experimental data in a value for D_{11}^{cr} leads to results which are not objective with regard to mesh refinement. To overcome this problem, it has been proposed to consider the fracture energy G_f [5,21] as the fundamental parameter which governs crack propagation. It is beginning to emerge gradually that this so-called "tension-softening" model is not free from deficiencies. This is particularly so when we allow for the possibility of multiple cracks. Suppose that a primary crack has been created with a D_{11}^{cr} determined from the fracture energy G_f. If upon formation of a secondary crack the same crack stress-strain relation is adopted for the second crack, the fracture energy will be consumed twice. If both cracks are orthogonal to each other, this is not unrealistic, but for any other inclination angle it seems incorrect. Hence, the concept of a fracture energy as outlined above does not seem to suffice for multiple crack formation. Indeed, a solution in which the fracture energy is distributed over both cracks is not correct as the fracture energy G_f is not a scalar, but a vector although this does not seem to have been recognized widely.

The shear modulus D_{22}^{cr} of the crack is usually assigned a constant value. This leads to the anomaly that for very large crack strains we continue to compute an increase of the shear stresses transferred across a crack, which may result in shear stresses of more than 15 N/mm^2. A shear-softening model, quite similar to the tension-softening model, has recently been proposed to remedy this anomaly [29]. Deployment of this model resulted in a major improvement for some unreinforced shear beams, especially in the post-peak regime.

It is finally noted that the structure of eq. (19) is quite similar to the structure of an elastoplastic stiffness tensor at a yield vertex. Indeed, any constitutive law in which a decomposition in the sense of eq. (1) is assumed, will lead to an equation with a similar structure. This holds true for a yield vertex in which two yield surfaces are active, but for instance also for the intersection of a yield surface and a fracture surface [13,14].

3. STABILITY AND UNIQUENESS OF DISCRETE MECHANICAL SYSTEMS

A body is said to be in a state of stable equilibrium if the response on a vanishingly small disturbance also remains vanishingly small [20]. This condition is usually replaced by the condition that

$$U=\int_V \dot{\boldsymbol{\varepsilon}}^T \dot{\boldsymbol{\sigma}}\, dV \tag{21}$$

is positive for all kinematically admissible strain rate fields $\dot{\boldsymbol{\varepsilon}}$, while the equilibrium is unstable under dead loading if U becomes negative for at least one kinematically admissible strain rate field. Although it has not been proved rigorously for all classes of constitutive models that the criterion that the second-order work (eq. 21) is positive, is indeed equivalent to the abovementioned definition, it seems to be a reasonable hypothesis.

For an incrementally-linear constitutive model,

$$\dot{\boldsymbol{\sigma}}=\boldsymbol{D}\dot{\boldsymbol{\varepsilon}} \tag{22}$$

with $\boldsymbol{D}$ the matrix which contains the stiffness moduli, eq. (21) can be replaced by

$$U=\int_V \dot{\boldsymbol{\varepsilon}}^T \boldsymbol{D}\dot{\boldsymbol{\varepsilon}}\, dV \tag{23}$$

Since we have, for the skew-symmetric part of $\boldsymbol{D}$, $\dot{\boldsymbol{\varepsilon}}^T[\boldsymbol{D}-\boldsymbol{D}^T]\dot{\boldsymbol{\varepsilon}}=0$, we can write eq. (23) also as

$$U=\tfrac{1}{2}\int_V \dot{\boldsymbol{\varepsilon}}^T[\boldsymbol{D}+\boldsymbol{D}^T]\dot{\boldsymbol{\varepsilon}}\, dV \tag{24}$$

Consequently, stability under dead loading is no longer assured if

$$\int_V \dot{\boldsymbol{\varepsilon}}^T[\boldsymbol{D}+\boldsymbol{D}^T]\dot{\boldsymbol{\varepsilon}}\, dV=0 \tag{25}$$

for at least one kinematically admissible $\dot{\boldsymbol{\varepsilon}}$.

To investigate the implications of the stability requirement $U>0$ for discrete mechanical systems such as arise in finite element applications, we divide the continuum in an arbitrary number of finite elements, and we interpolate the continuous velocity field $\boldsymbol{v}$ as follows:

$$\boldsymbol{v}=\boldsymbol{H}\dot{\boldsymbol{a}} \tag{26}$$

in which the matrix $\boldsymbol{H}$ contains the interpolation polynomials and $\boldsymbol{a}$ is a vector which contains the nodal displacements (e.g., [3]). The relation between the velocity field $\boldsymbol{v}$ and the strain rate $\dot{\boldsymbol{\varepsilon}}$ can formally be written as

$$\dot{\boldsymbol{\varepsilon}}=\boldsymbol{L}\boldsymbol{v} \tag{27}$$

with $\boldsymbol{L}$ a matrix which contains differential operators. The relation between the nodal velocities and the strain rate then becomes

$$\dot{\boldsymbol{\varepsilon}}=\boldsymbol{B}\dot{\boldsymbol{a}} \tag{28}$$

where the notation $\boldsymbol{B}=\boldsymbol{L}\boldsymbol{H}$ has been introduced.

With the notations and the definitions of the preceding, we can rewrite the stability condition (23) as

$$\int_V \dot{\boldsymbol{a}}^T \boldsymbol{B}^T \boldsymbol{D}\, \boldsymbol{B}\dot{\boldsymbol{a}}\, dV>0 \tag{29}$$

for all kinematically admissible velocity fields $\dot{\boldsymbol{a}}$. With the notation

$$\boldsymbol{K}=\int_V \boldsymbol{B}^T \boldsymbol{D}\, \boldsymbol{B} dV \tag{30}$$

for the tangent stiffness matrix of the underlying system, we obtain that the stability of the equilibrium of a discrete mechanical system becomes critical if

$$\dot{\boldsymbol{a}}^T\boldsymbol{K}\dot{\boldsymbol{a}}=0 \tag{31}$$

for at least one kinematically admissible vector $\dot{\boldsymbol{a}}$. This condition is satisfied if

$$\det(\boldsymbol{K})=0 \tag{32}$$

which according to Vieta's rule,

$$\det(K)=\prod_{i=1}^{n}\lambda_i \tag{33}$$

with λ_i the eigenvalues of $\boldsymbol{K}$, implies that at least one eigenvalue vanishes. For symmetric systems, eq. (32) is not only a sufficient, but also a necessary condition for eq. (31) to hold. However, for nonsymmetric matrices $\boldsymbol{K}$ eq. (31) may also be satisfied when $\dot{\boldsymbol{a}}$ is orthogonal to $\boldsymbol{K}\dot{\boldsymbol{a}}$. Hence, the vanishing of $\det(\boldsymbol{K})$ or alternatively, the vanishing of at least one eigenvalue of $\boldsymbol{K}$ implies that the equilibrium is in a critical state, but for nonsymmetric systems this critical state can also be attained when all eigenvalues of the tangent stiffness matrix of the underlying solid are non-zero. Put differently, *the positiveness of the eigenvalues of $\boldsymbol{K}$ is a necessary, but not a sufficient condition for stability of a mechanical system which is governed by a nonsymmetric matrix $\boldsymbol{K}$.*

Let us next consider eq. (25), i.e., the case that we have removed the skew-symmetric part from the functional of eq. (23). Then, we obtain that the equilibrium of a discrete mechanical system becomes neutrally stable if

$$\dot{\boldsymbol{a}}^T\left[\boldsymbol{K}+\boldsymbol{K}^T\right]\dot{\boldsymbol{a}}=0 \tag{34}$$

for at least one kinematically admissible velocity field. Since $\boldsymbol{K}+\boldsymbol{K}^T$ is symmetric, this condition is satisfied if and only if

$$\det(\boldsymbol{K}+\boldsymbol{K}^T)=0 \tag{35}$$

or equivalently, U vanishes if and only if an eigenvalue of $\boldsymbol{K}+\boldsymbol{K}^T$ vanishes. Consequently, *the positiveness of the eigenvalues of the matrix $\boldsymbol{K}+\boldsymbol{K}^T$ is a sufficient and necessary condition for the stability of a discrete mechanical system which is governed by a nonsymmetric tangent stiffness matrix $\boldsymbol{K}$*. For the limiting case of a symmetric stiffness matrix we recover the classical notion that we have stability when all eigenvalues of the tangent stiffness matrix $\boldsymbol{K}$ of the underlying solid are positive.

With regard to uniqueness of solution, we observe that incremental equilibrium must be complied with at each instant in the loading process

$$\int_V \boldsymbol{B}^T\dot{\boldsymbol{\sigma}}dV=\dot{\mu}\boldsymbol{q}^* \tag{36}$$

In it, $\dot{\mu}$ is the loading rate, and $\boldsymbol{q}^*$ is a normalized load vector. Suppose that there would be another stress rate distribution, which would result from the loading rate $\dot{\mu}$ and which would also satisfy incremental equilibrium. The *difference* $\Delta\dot{\boldsymbol{\sigma}}$ of both stress rate distributions would then satisfy the condition that

$$\int_V \boldsymbol{B}^T\Delta\dot{\boldsymbol{\sigma}}dV=\boldsymbol{0} \tag{37}$$

With eqs. (22), (28) and (30), we can rewrite eq. (37) as

$$\boldsymbol{K}\Delta\dot{\boldsymbol{a}}=\boldsymbol{0} \tag{38}$$

with $\Delta\dot{\boldsymbol{a}}$ the difference between both velocity fields. A non-trivial solution may then exists if and only if

$$\det(\boldsymbol{K})=0 \tag{39}$$

or equivalently, if at least one eigenvalue of $\boldsymbol{K}$ vanishes. If a non-trivial solution indeed exists, such a point is commonly named a bifurcation point. Several equilibrium branches emanate from such a point. There is yet another possibility that $\det(\boldsymbol{K})$ vanishes. If the load reaches a maximum, $\dot{\mu}$ vanishes, and eq. (36) reduces to

$$\boldsymbol{K}\dot{\boldsymbol{a}}=\boldsymbol{0} \tag{40}$$

so that for a non-zero vector $\dot{\boldsymbol{a}}$ we also find that eq. (39) must be fulfilled. The latter possibility is called a limit point.

In passing from eq. (37) to eq. (38) it has been tacitly assumed that both strain rates are related to stress rates by the same matrix of (tangential) moduli $\boldsymbol{D}$. For elastic-plastic or elastic-fracturing solids, where we have different behavior in loading and unloading, this is not necessary. Strictly speaking, we have to investigate all possible combinations of loading and unloading for such a multi-valued constitutive law in order to determine whether eq. (37) holds true for some $\Delta\dot{\boldsymbol{a}}$.

For nonsymmetric stress-strain laws, the situation is even more complicated, since $\det(\boldsymbol{K}+\boldsymbol{K}^T)$ may vanish prior to the vanishing of $\det(\boldsymbol{K})$. Hence, loss of stability may precede loss of uniqueness of solution for solids with a nonsymmetric stress-strain relation.

Although there seems no convenient procedure available to determine whether a solution is unique or not, the presence of negative eigenvalues of the tangent stiffness matrix $\boldsymbol{K}$ conversely clearly indicates the existence of alternative equilibrium branches or the fact that we have passed a limit point. In the case that we have passed a limit point, which implies that the load is descending, we find one negative eigenvalue which is associated with the descending branch. The other possibility is that the negative eigenvalues belong to alternative equilibrium states so that we have passed a bifurcation point. Again, two possibilities arise, since the basic path after bifurcation may be ascending or descending. If it is still ascending, all the, say m negative eigenvalues can be associated with m alternative equilibrium states which can in principle be reached via a suitable combination of the incremental displacement vector of the basic path and the corresponding eigenvector, as detailed in the next section. If the basic path is descending after passing a bifurcation point, one negative eigenvalue is associated with the descending basic path, while the remaining negative eigenvalues correspond to m-1 alternative equilibrium states.

A final remark addresses the question whether the alternative equilibrium states are indeed accessible. If a mechanical system is undergoing a continuous process, such an alternative equilibrium state can only be reached via an equilibrium path. If a bifurcation point has been passed and the system is on a path of unstable equilibrium thereafter, it will continue on this unstable path because other equilibrium states cannot be reached under dead loading conditions. If a *temporal* discretization of the loading process is employed, i.e. if the loading program is subdivided into a number of finite intervals, alternative equilibrium states can also be reached via non-equilibrium paths, because we then essentially deal with equilibrium states and not with equilibrium paths. In fact, we obtain a sequence of non-equilibrium states when iterating to a converged solution. An example of reaching a new equilibrium state via a number of non-converged states will be given at the end of this paper.

4. NUMERICAL APPROACH FOR POST-BIFURCATION AND POST-FAILURE BEHAVIOR

In numerical applications, the lowest eigenvalue will never become exactly zero because of round-off errors. Rather, we monitor the sign of the eigenvalues of the tangent stiffness matrix and when we encounter a negative eigenvalue while the load is rising, or when we compute more than one negative eigenvalue while the load is descending, we conclude that we have passed a bifurcation point.

Continuation on an alternative equilibrium branch can then be forced by adding a part of the eigenmode $\boldsymbol{v}_1$, which belongs to the vanishing eigenvalue, to the incremental displacement field of the fundamental path $\Delta\boldsymbol{a}^*$ [8,12,24]

$$\Delta\boldsymbol{a}=\Delta\boldsymbol{a}^*+\beta\boldsymbol{v}_1 \tag{41}$$

with β a scalar. The magnitude of β is fixed by second-order terms or by switch conditions for elastoplasticity or for plastic-fracturing materials. The most simple way to determine β numerically is to construct a trial displacement increment $\Delta\boldsymbol{a}$ such that it is orthogonal to the basic path:

$$\Delta\boldsymbol{a}^T\Delta\boldsymbol{a}^*=0 \tag{42}$$

Substituting eq. (41) in this expression yields for $\Delta\boldsymbol{a}$

$$\Delta \boldsymbol{a} = \Delta \boldsymbol{a}^* - \frac{(\Delta \boldsymbol{a}^*)^T \Delta \boldsymbol{a}^*}{(\Delta \boldsymbol{a}^*)^T \boldsymbol{v}_1} \boldsymbol{v}_1 \tag{43}$$

Eq. (43) fails when $(\Delta \boldsymbol{a}^*)^T \boldsymbol{v}_1 = 0$, i.e., when the eigenmode is orthogonal to the basic path. A simple remedy is to normalize $\Delta \boldsymbol{a}$ such that [8,12],

$$(\Delta \boldsymbol{a}^*)^T \Delta \boldsymbol{a}^* = \Delta \boldsymbol{a}^T \Delta \boldsymbol{a} \tag{44}$$

or to put

$$\Delta \boldsymbol{a}^* = \sqrt{\Delta \boldsymbol{a}^T \Delta \boldsymbol{a}}\, \boldsymbol{v}_1 \tag{45}$$

in such cases.

In general, the bifurcation path will not be orthogonal to the fundamental path, but when we add equilibrium iterations, the orthogonality condition (42) will maximize the possibility that we converge to a bifurcation branch and not to the basic path, although this is not necessarily the lowest bifurcation path when there emanate several equilibrium branches from the bifurcation point. When we do not converge on the lowest bifurcation path, this will be revealed by negative eigenvalues of the stiffness matrix of the bifurcated solution. The above described procedure can then be repeated until we ultimately arrive at the lowest bifurcation path.

The procedure described in the preceding is well suited for assessing post-bifurcation behavior. Bifurcations however are rather rare in normal structures owing to imperfections, and even if a bifurcation point exists, numerical round-off errors and spatial discretization usually transfer the bifurcation point into a limit point unless we have a homogeneous stress field.This observation does not render the approach to bifurcation problems worthless as it provides a thorough insight which is of importance for the associated limit problems, but it is obvious that numerical procedures must also be capable of locating limit points and tracing post-limit behavior.

In a nonlinear finite element analysis, the load is applied in a number of small increments (e.g., [3]). Within each load increment, equilibrium iterations are applied and the iterative improvement $\delta \boldsymbol{a}_i$ in iteration number i to the displacement increment $\Delta \boldsymbol{a}_{i-1}$ is given by

$$\delta \boldsymbol{a}_i = \boldsymbol{K}_{i-1}^{-1} \left[\boldsymbol{p}_{i-1} + \Delta \mu_i \boldsymbol{q}^* \right] \tag{46}$$

$\boldsymbol{K}_{i-1}$ is the possibly updated stiffness matrix, $\Delta \mu_i$ is the value of the load increment which may change from iteration to iteration and $\boldsymbol{p}_{i-1}$ is defined by

$$\boldsymbol{p}_{i-1} = \mu_0 \boldsymbol{q}^* - \int_V \boldsymbol{B}^T \boldsymbol{\sigma}_{i-1} dV \tag{47}$$

In (47), the symbols μ_0 and $\boldsymbol{\sigma}_{i-1}$ have been introduced for the value of the scalar load parameter at the beginning of the current increment and the stress vector at iteration number $i-1$.

The essence of controlling the iterative solution procedure indirectly by displacements, is that $\delta \boldsymbol{a}_i$ is conceived to be composed of two contributions

$$\delta \boldsymbol{a}_i = \delta \boldsymbol{a}_i^I + \Delta \mu_i \, \delta \boldsymbol{a}_i^{II} \tag{48}$$

with

$$\delta \boldsymbol{a}_i^I = \boldsymbol{K}_{i-1}^{-1} \, \boldsymbol{p}_{i-1} \tag{49}$$

and

$$\delta \boldsymbol{a}_i^{II} = \boldsymbol{K}_{i-1}^{-1} \, \boldsymbol{q}^* \tag{50}$$

After calculating the displacement vectors $\delta \boldsymbol{a}_i^I$ and $\delta \boldsymbol{a}_i^{II}$, $\Delta \mu_i$ is determined from some constraint equation on the displacement increments and $\Delta \boldsymbol{a}_i$ is subsequently calculated from

$$\Delta \boldsymbol{a}_i = \Delta \boldsymbol{a}_{i-1} + \delta \boldsymbol{a}_i \tag{51}$$

Crisfield [15] for instance uses the norm of the incremental displacements as constraint

equation

$$\Delta \boldsymbol{a}_i^T \Delta \boldsymbol{a}_i = \Delta l^2 \tag{52}$$

where Δl is the arc-length of the equilibrium path in the n-dimensional displacement space. The drawback of this so-called spherical arc-length method is that it yields a quadratic equation for the load increment. To circumvent this problem, we may linearize eq. (52), yielding [23]:

$$\Delta \boldsymbol{a}_i^T \Delta \boldsymbol{a}_{i-1} = \Delta l^2 \tag{53}$$

This method, known as the updated normal path method, results in a linear equation for the load increment. With the additional approximation [8,12]

$$\delta \boldsymbol{a}_i \approx 2(\Delta \boldsymbol{a}_i - \Delta \boldsymbol{a}_{i-2}) \tag{54}$$

we obtain for $\Delta\mu_i$:

$$\Delta\mu_i = -\frac{\Delta \boldsymbol{a}_{i-1}^T \delta \boldsymbol{a}_i^I}{\Delta \boldsymbol{a}_{i-1}^T \delta \boldsymbol{a}_i^{II}} \tag{55}$$

Both eqs. (52) and (53) have been employed successfully within the realm of geometrically nonlinear problems, where snapping and buckling of thin shells can be traced quite elegantly. Nevertheless, for materially nonlinear problems the method sometimes fails, which may be explained by considering that for materially nonlinear problems, failure or bifurcation modes are often highly localized. Hence, *only a few nodes contribute to the norm of displacement increments, and failure is not sensed accurately by such a global norm.* As straightforward application of eqs. (52) or (53) is not always successful, we may amend these constraint equations by applying weights to the different degrees of freedom or omitting some of them from the constraint equation. The constraint equation (53) then changes into

$$\Delta \boldsymbol{u}_i^T \Delta \boldsymbol{u}_{i-1} = \Delta l^2 \tag{56}$$

where $\Delta \boldsymbol{u}_i$ contains only a limited number of the degrees of freedom of those of $\Delta \boldsymbol{a}_i$, and eq. (55) changes in a similar fashion. The term "arc-length" control now no longer seems very appropriate, and the term "indirect displacement control" is probably more suitable. The disadvantage of modifying the constraint equation is that the constraint equation becomes problem dependent. As a consequence, the method loses some of its generality and elegance.

5. EXAMPLES

We will now illustrate some of the procedures discussed in the preceding by a few examples and we will begin with the simple case of an unreinforced bar loaded in pure tension. This example has been used before by other researchers [16], but so much insight can be gained from it, both in a theoretical and in a numerical sense, that we will again resort to it. The bar is modeled with m elements and is composed of an elastic-softening material with an ultimate strain ε_u at which the tensile strength has vanished completely. ε_u is assumed to be equal to n times the strain at the tensile strength. A perfect bar would deform uniformly throughout the loading process and the load-deflection curve is simply a copy of the imposed stress-strain law. However, if one element has a slight imperfection, only this element will show loading while the other elements will show unloading. Then, the imposed stress-strain law at a local level is not reproduced. Instead, an average strain is calculated in the post-peak regime which is smaller than the strain of the stress-strain law since the element which shows loading, will follow the path A-B in Fig. 1, while the other elements will follow the path A-C. This implies that when all elements have the same dimensions, we have for the average strain increment $\Delta\bar{\varepsilon}$

$$\Delta\bar{\varepsilon} = \left(\frac{n}{m} - 1\right)\frac{\Delta\sigma}{E} \tag{57}$$

Consequently, when we increase the number of elements while keeping the length of the bar fixed, the average strain in the post-peak regime gradually becomes smaller and for $m > n$ the

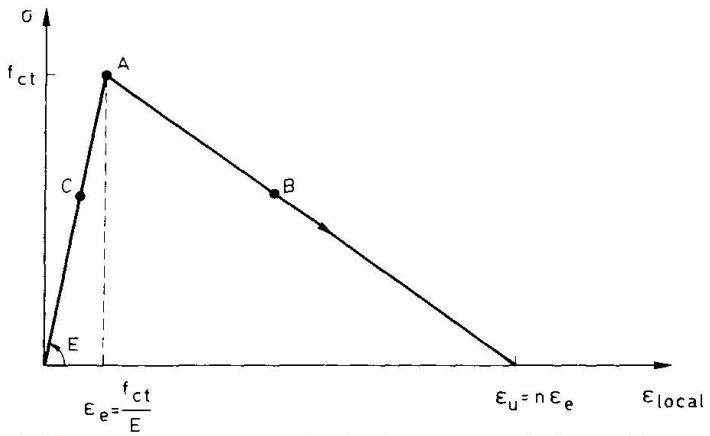

Fig. 1. Stress vs. average strain for an unreinforced bar.

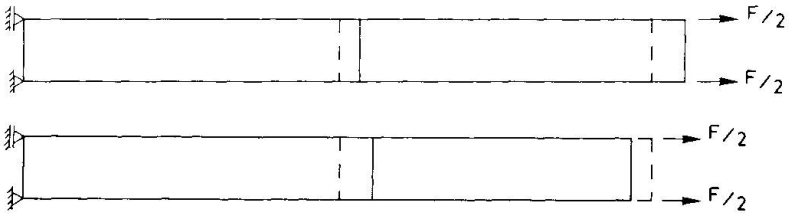

Fig. 2. Eigenmodes for two-element bar just beyond the limit point.

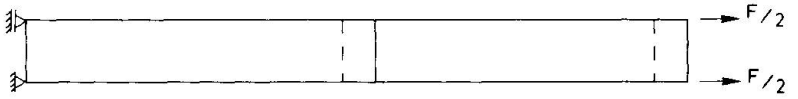

Fig. 3. Total displacements at zero load level.

average strain in the post-peak regime even becomes *smaller* than the strain at peak load. This implies that for $m > n$, the load-deflection curve shows a *snap-back* [8,12,17,29,30]. Obviously, "*snap-back*" *behavior cannot be analyzed under direct displacement control, but only with indirect displacement control*. Yet, the possibility of this phenomenon has been ignored frequently in the past, and many analyses have been terminated at such a point because of divergence of the iterative procedure. A further parallel can be drawn with experiments which can not be carried out properly under displacement control, e.g., with shear or other brittle failures. The observed explosive failure is then simply the result of an attempt to traverse an equilibrium path under improper static loading conditions.

A numerical simulation of this problem is shown in Figs. 2 and 3 for the case that the bar is divided in two elements and that the length of the softening branch is equal to ten times the strain at the tensile strength ($m=2$ and $n=10$). In this case a perfect bar is loaded just beyond the limit load, using indirect displacement control (eq. 56). If the solution is continued the solid post-peak line of Fig. 1 is obtained. However, when we carry out an eigenvalue analysis of the tangent stiffness matrix just beyond peak strength (Fig. 2) and perturb the fundamental solution using eq. (41), we obtain the localization of Fig. 3. Continuing the solution then results in an ultimate average strain $\bar{\varepsilon} = \frac{1}{2}\varepsilon_u$.

From the preceding discussion it will be clear that the response of an imperfect bar in the post-failure regime will depend upon the number of elements and the degree of interpolation within the elements. It has been attempted to control this mesh-dependence in the softening regime using energy approaches [5,25,26,28,33]. Such approaches can only be partially successful since the spread of the softening region is not known in advance. Consequently, the observation that use of a local softening law may involve snap-back behavior on structural level and to a strongly mesh-dependent and a non-unique post-peak response may hold even when such an energy approach is adopted. This is exemplified by the beam of Figs. 4 and 5, which exhibits a violent snap-back behavior in spite of the fact that the length of the softening branch had been adapted to some structural size. Also, the mesh-dependence of the calculated failure

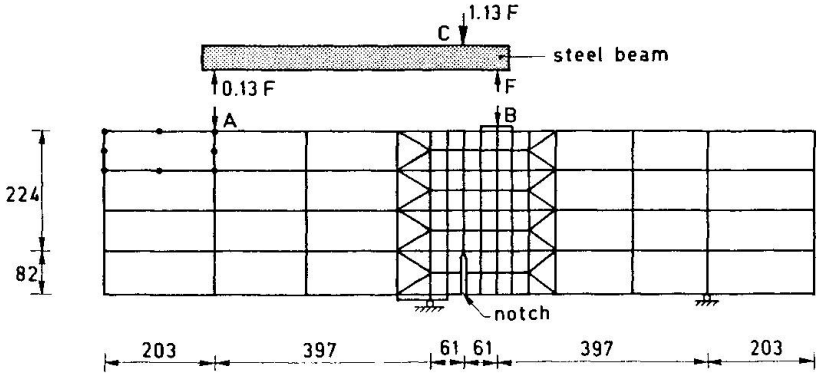

Fig. 4. Element mesh and dimension for unreinforced beam [1].

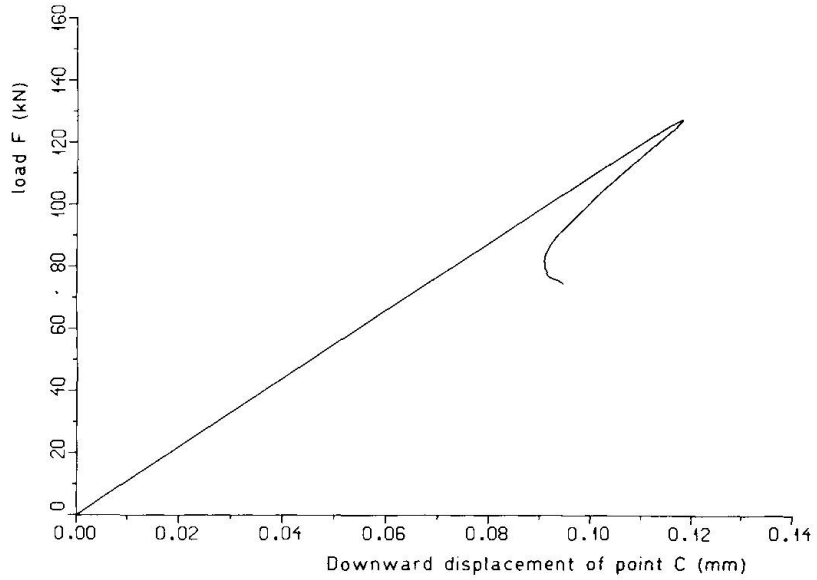

Fig. 5. Load-deflection curve for point C.

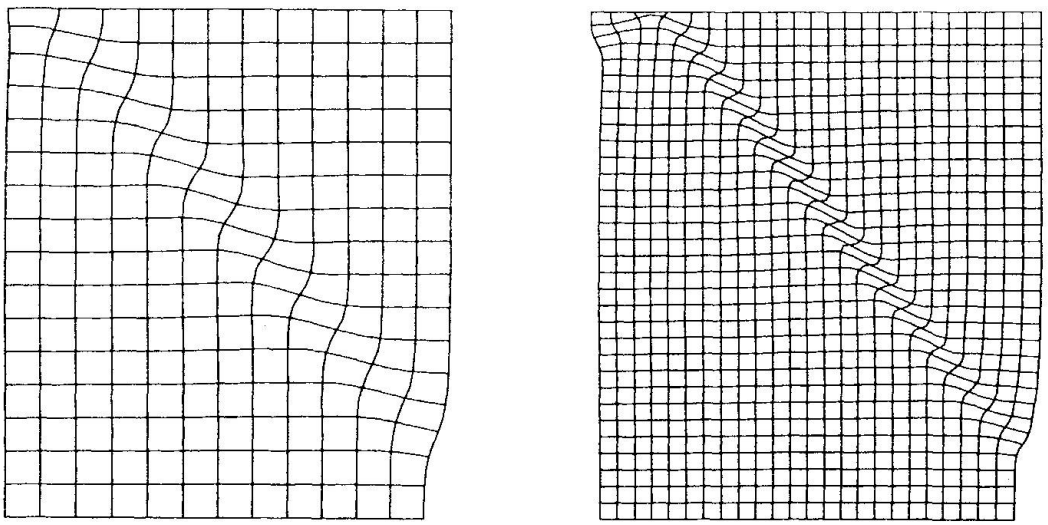

Fig. 6. Incremental displacements for a biaxial test on a sand sample. The failure state shows a strong mesh-dependence.

mode persists. This is demonstrated by the example of Fig. 6, which is a bifurcation analysis for a (plane-strain) biaxal test on sand. We observe that the width of the shear band which develops, is highly dependent on the fineness of the grid [8,9]. A possible solution to these basic deficiencies might be the use of non-local constitutive laws in the softening regime [6,31].

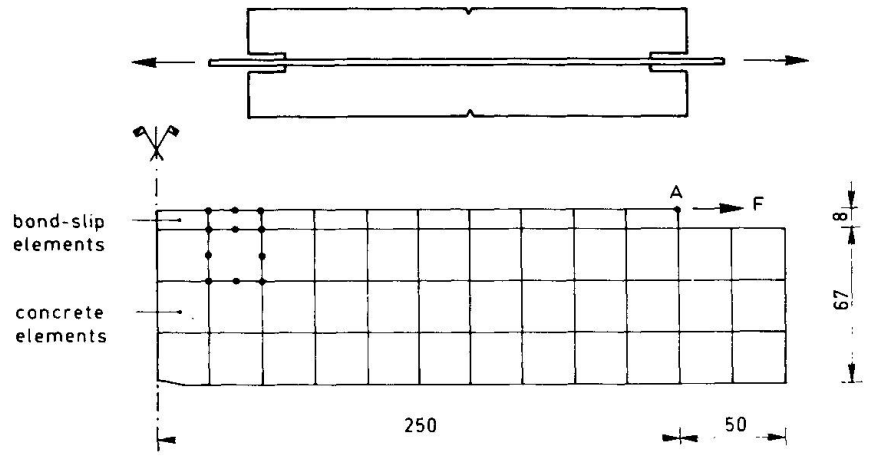

Fig. 7. Element mesh and dimensions for tension-pull specimen [19].

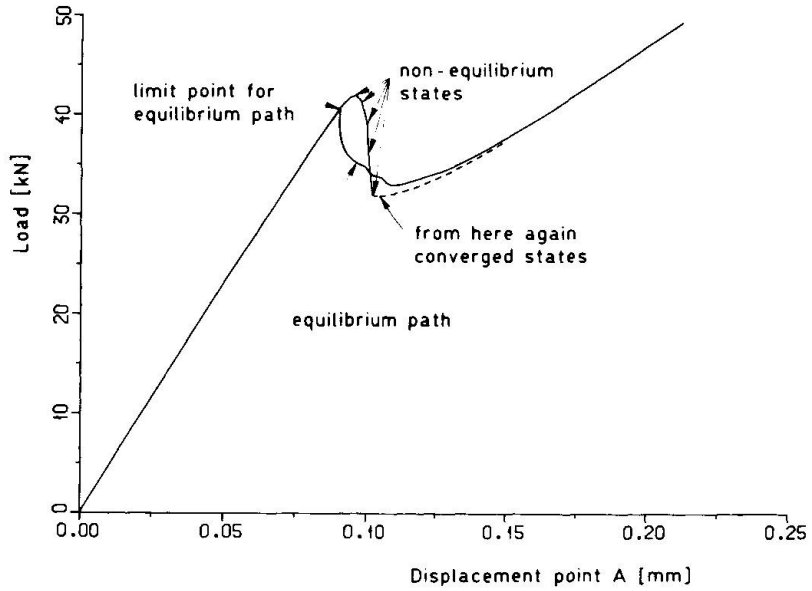

Fig. 8. Load-deflection curve for point A.

Addition of reinforcement not always improves the behavior described in the preceding. When the reinforcement is densely distributed, we mostly obtain a rather ductile response and we seldom encounter numerical difficulties, but when we have a dominant, concentrated reinforcing bar, the presence of reinforcement only adds to the possibility that spurious alternative equilibrium states and snap-back behavior occur [12,17]. We will demonstrate this by the simple tension-pull specimen of Fig. 7 [19]. The reinforcing bar is given by the line AB and a linear bond-slip law is assumed between the concrete and the reinforcement. For the concrete, steel and interface properties the reader is referred to Rots [27].

The loading is applied to point A (Fig. 7) in the form of a concentrated load and the ensuing load-displacement diagram is given in Fig. 8. The present problem is well suited for demonstrating that straightforward application of a norm of incremental displacements to control the solution process often does not work effectively for localized failures. To this end we consider the incremental displacement fields just prior to and just beyond the limit point (Figs. 9 and 10). Prior to the limit point, the elastic deformations of the bar are relatively so great, that they dominate the norm of incremental displacements. Just beyond the peak, when the crack near the center-line has localized, the incremental deformations of the reinforcing bar nearly vanish (they even change sign, so that we again have a snap-back) and the concrete is the prime contributor to the total norm of incremental displacements. However, because of the relatively great magnitudes of the steel deformations just prior to the limit point, the arc-length in the displacement space is not influenced significantly. In this case, the degrees of

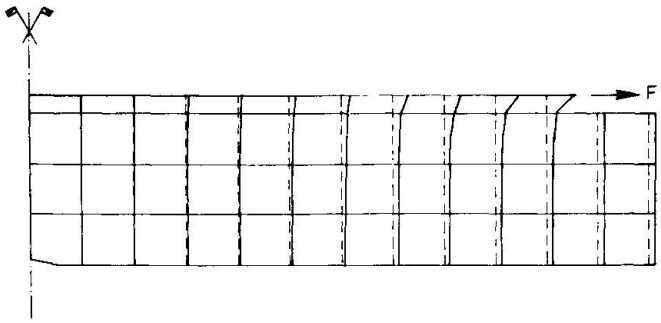

Fig. 9. Incremental displacements just prior to the limit point.

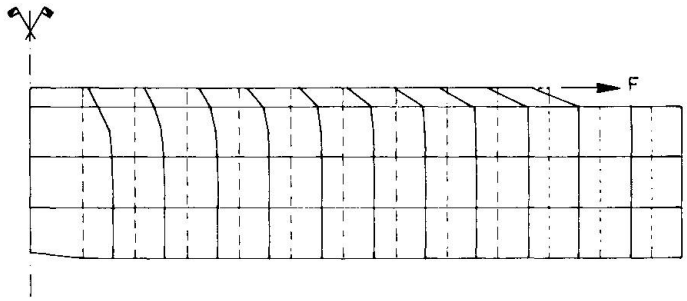

Fig. 10. Incremental displacements just beyond the limit point.

freedom belonging to the steel have therefore been omitted from the norm of incremental displacements for overcoming the limit point. For traversing the valley in the load-displacement curve of Fig. 8 on the other hand, the solution process has been controlled by the displacements of the steel, as then these displacements increase monotonically.

The present example is also well suited for assessing the question whether an equilibrium state can be reached via a non-equilibrium path. It is the Author's experience that this is often possible when we adopt direct displacement control and if there exists another equilibrium state which is located "not too far away" from the current state. Indeed, when we attempted to analyze the present problem by prescribing the displacement of point A, we obtained a number of non-converged states just after the limit point. This non-equilibrium path is indicated by the dotted line in Fig. 8. However, after the crack had localized, we again obtained converged equilibrium states (dashed line in Fig. 8), which indicated that we had arrived on a new equilibrium path. This illustrates that reaching another part of the equilibrium path via a number of non-equilibrium states is sometimes possible, provided that there exists a new equilibrium state which is "sufficiently close" to the previous equilibrium state. Here, the tension-pull specimen contrasts with the example of Figs. 4 and 5, as in the latter case equilibrium could not be restored using direct displacement control.

6. STRAIN-SOFTENING AND SPURIOUS ZERO-ENERGY MODES

A major problem which presently hampers finite element calculations of material models in which use is made of strain-softening (like for instance crack models), is the fact that strain-softening triggers spurious zero-energy modes. This has been recognized by Dodds et al. [18], de Borst and Nauta [7] and Crisfield [17] for the case of underintegrated elements, but Rots and de Borst [29] have recently demonstrated that it may also happen for e.g., eight-noded elements with nine-point integration or four-noded elements with four-point integration. In fact, the analysis of the beam of Fig. 4 had to be terminated because of the occurrence of such a zero-energy mode which was triggered by strain-softening. A converged solution could no longer be obtained at the point where the load-displacement curve of Fig. 5 is terminated. An eigenvalue analysis of the tangent stiffness matrix revealed two negative eigenvalues. The eigenmode of Fig. 11 has a clear physical meaning, since it represents the localization which has by then progressed through the depth of the beam. The eigenmode of Fig. 12 is due to pathological behavior of one element at the top of the beam. It is emphasized that this behavior occurred in spite of the fact that nine-point Gaussian quadrature had been used. Later

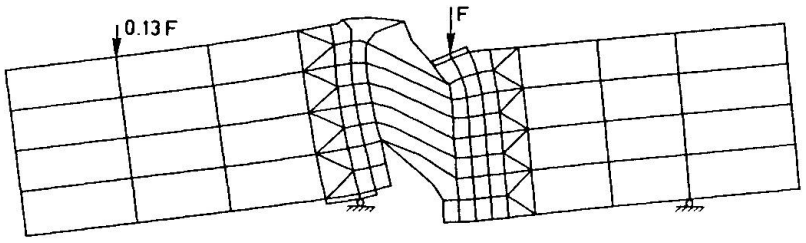

Fig. 11. First eigenmode at residual load of the unreinforced beam of Fig. 4.

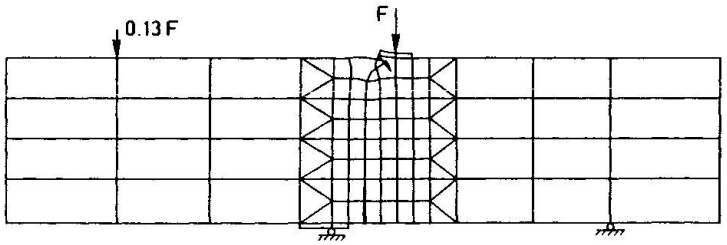

Fig. 12. Second eigenmode at residual load of the unreinforced beam of Fig. 4.

investigations also revealed that groups of four elements displayed spurious zero-energy modes when four-noded elements with four-point integration were employed [29].

7. CONCLUDING REMARKS

The essential features of the DIANA-crack model have been described. By dividing the total strain rate rigorously into a concrete and a crack strain rate, and by subdividing these strain rates again into a number of distinct contributions each of which is associated with a clearly defined physical phenomenon, it is possible to simultaneously analyze non-orthogonal cracks, creep, shrinkage, thermal dilatation and plasticity within a smeared context.

The incorporation of strain-softening models on integration point level may lead to unexpected behavior on structural level. An example is snap-back behavior. This phenomenon cannot be analyzed under direct displacement control, but only using indirect displacement control. Another consequence of deployment of strain-softening models is the possibility that bifurcations occur even under the assumption of small displacement gradients. Techniques have been discussed which permit tracing snap-back and post-bifurcation behavior. Some examples have been included to demonstrate that such techniques broaden the class of concrete structures which can be analyzed numerically.

On the other hand, it is not justified to state that any concrete structure can now easily be analyzed. A major problem which still hampers finite element analyses is the fact that strain-softening triggers the formation of spurious zero-energy modes. Techniques to control such modes in strain-softening materials must be developed before the limits of the class of problems which can be solved properly can be pushed further away.

Considering nonsymmetric stress-strain laws, we observe that little numerical work has been done. This is partly due to the fact that only a few finite element codes have been adapted for nonsymmetric solvers. But even if a finite element code with a nonsymmetric solver is available to the analyst, he faces the problem that the issues of stability and uniqueness of solution are much less clear-cut than for symmetric problems. This is particularly relevant when an analysis diverges, since in such a case it is much more difficult to trace whether the divergence is caused by failure or bifurcation phenomena in the model of the structure, or is simply caused by e.g., a trivial programming error. Yet, as soon as frictional processes take place, which is the case for concrete, stress-strain laws necessarily become nonsymmetric, which calls for an enhanced research effort to develop numerical procedures for such models.

ACKNOWLEDGEMENTS

Major parts of the research reported in this paper have been supported financially by CUR-Committee A26 "Concrete Mechanics". The examples shown in this paper have been obtained using the DIANA finite element code. I am indebted to my colleagues of the DIANA-group for their continuous support and pleasant collaboration, in particular Mr. Jan G. Rots, Mr. Pier Nauta, Mr. Ger M.A. Kusters and Mr. Frits C. de Witte. This paper was written during a leave at the University of New Mexico, Department of Mechanical Engineering.

REFERENCES

1. ARREA M. & INGRAFFEA A.R., Mixed-mode crack propagation in mortar and concrete. Report No. 81-13, Department of Structural Engineering, Cornell University, Ithaca, New York, 1981.
2. BARTON N., Deformation phenomena in jointed rock. Géotechnique 36, 1986, pp. 147-167.
3. BATHE K.-J., Finite element procedures in engineering analysis. Prentice-Hall, New Jersey, 1982.
4. BAZANT Z.P. & GAMBAROVA P., Rough cracks in reinforced concrete. ASCE J. Struct. Div. 106, 1980, pp. 819-842.
5. BAZANT Z.P. & OH B., Crack band theory for fracture of concrete. RILEM Materials and Structures 16, 1983, pp. 155-177.
6. BAZANT Z.P., BELYTSCHKO T. & CHANG T.-P., Continuum theory for strain softening. ASCE J. Eng. Mech. 110, 1984, pp. 1666-1692.
7. De BORST R. & NAUTA P., Non-orthogonal cracks in a smeared finite element model. Eng. Comput. 2, 1985, pp. 35-46.
8. De BORST R., Non-linear analysis of frictional materials. Dissertation, Delft University of Technology, Delft, 1986.
9. De BORST R., Numerical simulation of shear-band bifurcation in sand bodies. Numerical Models in Geomechanics (eds. G.N. Pande & W.F. van Impe), M. Jackson & Sons, Redrudth, 1986, pp. 91-98.
10. De BORST R., Computational aspects of smeared crack analysis. Computational Modelling of Reinforced Concrete Structures (eds. E. Hinton & D.R.J. Owen), Pineridge Press, Swansea, 1986, Ch. 2, pp. 44-83.
11. De BORST R. & Van Den BERG P., Analysis of creep and cracking in concrete members. Preprints RILEM Symp. on Creep and Shrinkage of Concrete: Mathematical Modeling (ed. Z.P. Bažant), Northwestern University, Evanston, Ill., 1986, pp. 527-538.
12. De BORST R., Computation of post-bifurcation and post-failure behavior of strain-softening solids. Comput. Struct. 25, 1987, pp. 211-224.
13. De BORST R., Smeared cracking, plasticity, creep and thermal loading - a unified approach. Comp. Meth. Appl. Mech. Eng., 1987.
14. De BORST R., Integration of plasticity equations for singular yield functions. Comput. Struct., 1987.
15. CRISFIELD M.A., A fast incremental/iterative procedure that handles snap-through. Comput. Struct. 13, 1981, pp. 55-62.
16. CRISFIELD M.A., Local instabilities in the non-linear analysis of reinforced concrete beams and slabs. Proc. Instn. Civ. Engrs. 73, 1982, pp. 135-145.
17. CRISFIELD M.A., Snap-through and snap-back response in concrete structures and the dangers of underintegration, Int. J. Num. Meth. Eng. 22, 1986, pp. 751-768.
18. DODDS R.H., DARWIN D., SMITH J.L. & LEIBENGOOD L.D., Grid size effects with smeared cracking in finite element analysis of reinforced concrete. SM Report No. 6, University of Kansas, Lawrence, Kansas, 1982.
19. DORR K., Kraft- und Dehnungsverlauf von in Betonzylindern zentrisch einbetonierten Bewehrungsstaben under Querdruck. Forschungsbericht No. 30, Institut für Massivbau der Technischen Hochschule Darmstadt, 1975.

20. HILL R., Some basic principles in the mechanics of solids without a natural time. J. Mech. Phys. Solids 7, 1959, pp. 209-225.
21. HILLERBORG A., MODEER M. & PETERSSON P.E., Analysis of crack formation and crack growth in concrete by means of fracture mechanics and finite elements. Cement and Concrete Research 6, 1976, pp. 773-782.
22. LITTON R.W., A contribution to the analysis of concrete structures under cyclic loading. Ph.D. Thesis, University of California, Berkeley, Calif., 1974,
23. RAMM E., Strategies for tracing the nonlinear response near limit points. Nonlinear Finite Element Analysis in Structural Mechanics, (Eds. W. Wunderlich, E. Stein & K.-J. Bathe), Springer Verlag, Berlin, 1981, pp. 63-83.
24. RIKS E., An incremental approach to the solution of snapping and buckling problems. Int. J. Solids Structures 15, 1979, pp. 529-551.
25. ROTS J.G., KUSTERS G.M.A. & BLAAUWENDRAAD J., The need for fracture mechanics options in finite element models for concrete structures. Proc. Int. Conf. Computer Aided Analysis and Design of Concrete Structures, Part 1, (eds. F. Damjanić et al.), Pineridge Press, Swansea, 1984, pp. 19-32.
26. ROTS J.G., NAUTA P., KUSTERS G.M.A. & BLAAUWENDRAAD J., Smeared crack approach and fracture localization in concrete. Heron 30, No. 1, 1985.
27. ROTS J.G., Bond-slip simulations using smeared cracks and/or interface elements. Research Report, Structural Mechanics Group, Department of Civil Engineering, Delft University of Technology, 1985.
28. ROTS J.G., Strain-softening analysis of concrete fracture specimens. Fracture Toughness and Fracture Energy of Concrete (Ed. F.H. Wittmann), Elsevier Science Publ., Amsterdam, 1986, pp. 137-148.
29. ROTS J.G. & De BORST R., Analysis of mixed-mode fracture in concrete. ASCE J. Eng. Mech., 1987.
30. ROTS J.G., HORDIJK D.A. & De BORST R., Numerical simulation of concrete fracture in 'direct' tension. Numerical Methods in Fracture Mechanics (eds. A.R. Luxmoore et al.), Pineridge Press, Swansea, 1987, pp. 457-471.
31. SCHREYER H.L. & CHEN Z., One-dimensional softening with localization. J. Appl. Mech., 1986, pp. 791-797.
32. WALRAVEN J.C. & REINHARDT H.W., Theory and experiments on the mechanical behavior of cracks in plain and reinforced concrete subjected to shear loading. Heron 26, No. 1A, 1981.
33. WILLAM K.J., Experimental and computational aspects of concrete fracture. Proc. Int. Conf. Computer Aided Analysis and Design of Concrete Structures, Part 1, (Eds. F. Damjanić et al.), Pineridge Press, Swansea, 1984, pp. 33-70.

Numerical Comparisons Involving Different 'Concrete-Models'

Comparaisons numériques sur la base de différents modèles de béton

Numerische Vergleiche verschiedener Beton-Modelle

Michael A. CRISFIELD
Transp. and Road Res. Lab.
Crowthorne, Berkshire
England

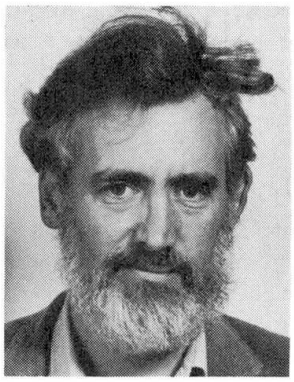

Michael Crisfield obtained both his B.Sc. and Ph.D. at the Queen's University of Belfast. Since that time he has mainly worked at the Transport and Road Research Laboratory on the application of non-linear finite element methods to bridge structures.

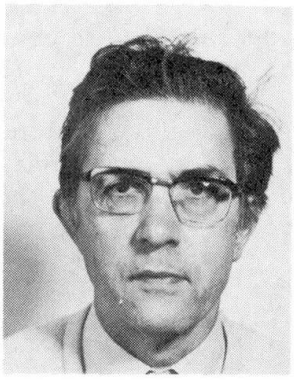

John Wills graduated from Cambridge University in 1955 with a First Class Honours Degree in Mechanical Sciences. He worked for ten years in the gas-turbine research field before joining the Transport and Road Research Laboratory where he is working on the numerical analysis of bridge structures.

John WILLS
Transp. and Road Res. Lab.
Crowthorne, Berkshire
England

SUMMARY

The paper applies different concrete models to the finite element analysis of simple reinforced-concrete panels subject to monotonically increasing states of uniform stress. The panels involve: a) a hypothetical model designed to test the limit-loads when idealised material properties are assumed and b) Vecchio and Collins' experimental panels. The different 'concrete models' involve: 1) fixed orthogonal-cracks, 2) 'swinging cracks' in which the directions of principal stress and principal strain are assumed to coincide, 3) a modification to the previous model whereby the stress in one swinging direction is influenced by the strain in the swinging direction, 4) simple plasticity-models involving both flow and deformation theory which assume no-tension and a 'square yield-criterion'.

RÉSUMÉ

La contribution applique différents modèles de béton pour l'analyse par éléments finis de panneaux simples en béton armé soumis à des contraintes uniformes croissant de façon monotonique. Les panneaux sont définis dans un cas par un modèle théorique analysant les charges limites pour des matériaux idéaux; dans l'autre cas, il s'agit des panneaux expérimentaux de Vecchio et Collins. Les différents modèles de béton prennent en considération les fissures fixes orthogonales; les fissures mouvantes dans lesquelles la direction des contraintes principales et des déformations principales sont les mêmes par hypothèse; une modification du modèle précédent dans lequel la contrainte dans une direction mouvante est influencée par la déformation dans une autre direction; enfin les modèles plastiques simple basés sur la théorie d'écoulement et de déformation, en considèrant qu'il n'y a pas de tension et qu'il y a un critère d'écoulement.

ZUSAMMENFASSUNG

Der Beitrag verwendet verschiedene Werkstoffmodelle für Beton bei der Anwendung auf statisch belastete Scheiben. Die Scheiben betreffen einen hypothetischen Fall und die Experimente von Vecchio/Collins. Die Werkstoffmodelle sind: festgelegte orthonogale Risse, Risse in der Richtung der Hauptspannungen bzw. -Dehnungen, Interaktion zwischen Spannung und Dehnung in Rissrichtung und schliesslich ein einfaches Plastizitätsmodell.

1. INTRODUCTION

Most current finite element programs adopt the fixed-orthogonal crack model [1] to treat the cracking of concrete. In this approach, the direction of cracking is governed by the direction of the first principal tensile stress that exceeds the cracking stress. The major drawback of this model involves the development of principal tensile stresses greater than the cracking stress at angles that differ from those of the original two fixed-orthogonal directions. This deficiency arises when the straining is "non-proportional". Even for monotonic, proportional loading, such non-proportional straining is often experienced at the local, Gauss-point level as the adjacent stresses and stiffnesses change. Consequently, the fixed-crack model can give solutions that are far too stiff and collapse loads that are significantly too high [2-4].

Various attempts have been made to allow for non-orthogonal cracks [5-6]. (They are surprisingly few. Non-orthogonal cracks are hardly mentioned in the ASCE review [1]). Of these formulations, the authors considered de Borst's model [5], in which the effect of cracking and plasticity are superimposed, to be most hopeful. However, in attempting to implement this model, the authors encountered significant numerical difficulties when "state changes" occurred within an increment. Difficulties are also associated with discontinuities involving the "threshold angle" [5] beyond which the second non-orthogonal crack is activated.

For these reasons, the authors have, for the time-being, reverted to a simple swinging-crack model [2,4] in which the directions of principal stress and principal strain are assumed to coincide. These models can be criticised [7] for being "un-physical" in that the properties originally relating to a crack, or series of cracks, in one direction are assumed to rotate and relate to a new direction. However, the direction of the principal strain can be considered as relating to the currently-most-active crack for which the properties are influenced by previous adjacent cracks.

Much previous work on reinforced concrete has employed limit-analysis and plasticity with the square yield-criterion [8,9]. The authors have therefore introduced such a yield-criterion into a finite element computer program and have established a close relationship with the simple swinging-crack model. Finally, the basic swinging-crack model has been improved by incorporating the ideas of Vecchio and Collins [10] to degrade the compressive strength as a function of the tensile strain in the orthogonal direction.

2. THE FIXED-CRACK MODEL

Once cracking has occurred, the fixed-crack model is based on the incremental stiffness relationship:

$$\Delta\sigma_{xy} = \begin{bmatrix} \Delta\sigma_x \\ \Delta\sigma_y \\ \Delta\tau_{xy} \end{bmatrix} = \begin{bmatrix} c^2 & s^2 & -2sc \\ s^2 & c^2 & 2sc \\ sc & -sc & c^2-s^2 \end{bmatrix} \begin{bmatrix} \Delta\sigma_1 \\ \Delta\sigma_2 \\ \Delta\tau_{12} \end{bmatrix} = T(\theta)^T \Delta\sigma_{12} \quad \ldots\ldots\ldots (1)$$

$$\text{or:} \qquad \Delta\sigma_{xy} = T(\theta)^T \begin{bmatrix} E_{t1} & 0 & 0 \\ 0 & E_{t2} & 0 \\ 0 & 0 & \beta G \end{bmatrix} \Delta\epsilon_{12} = T(\theta)^T E_{t12}\, T(\theta)\, \Delta\epsilon_{xy} \quad \ldots (2)$$

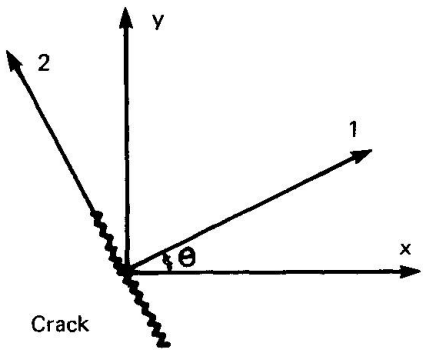

Fig. 1 1–2 and x–y coordinate system

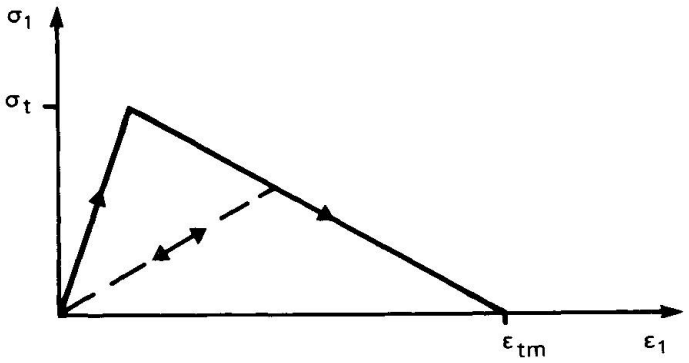

Fig. 2 Concrete softening (tension stiffening)

where c = cosθ and s = sin(θ) and θ (Fig. 1) is fixed as the direction of the principal stress (σ_1) at first cracking. The terms E_{t1} and E_{t2} in the matrix E_{t12} of (2) are the slopes of the uniaxial stress-strain curves. Immediately after cracking, E_{t1} will be negative to allow for the softening (or tension-stiffening) in tension (Fig. 2). When an incremental step moves from an uncracked to a cracked state, the strain ratio r is computed whereby the old stresses, σ_o, are augmented by $rE\Delta\epsilon$ such that the resulting stresses:

$$\sigma_r = \sigma_o + rE\Delta\epsilon \qquad \ldots\ldots\ldots\ldots\ldots\ldots\ldots\ldots\ldots\ldots (3)$$

have a principal tensile stress that just reaches the cracking strength. Assuming no plasticity prior to cracking, the matrix E in (4) is the elastic isotropic modular matrix. The remaining strain step $(1-r)\Delta\epsilon$ is applied using equation (2).

3. THE SWINGING-CRACK MODEL

The simplest swinging-crack model assumes that the principal stresses and strains coincide and that:

$$\sigma_{xy} = \begin{bmatrix} \sigma_x \\ \sigma_y \\ \tau_{xy} \end{bmatrix} = T(\theta)^T \begin{bmatrix} \sigma_1(\epsilon_1(\theta)) \\ \sigma_2(\epsilon_2(\theta)) \\ 0 \end{bmatrix} = T'(\theta)^T \begin{bmatrix} \sigma_1 \\ \sigma_2 \end{bmatrix} = T'(\theta)^T \sigma'_{12} \quad .(4)$$

where $T'(\theta)^T$ contains the first two columns of the matrix $T(\theta)$ given in (1) with θ relating to the direction of the continuously varying principal strain. Equation (4) can be differentiated to give:

$$\delta\sigma_{xy} = \left[T'(\theta)^T \begin{bmatrix} \frac{\partial\sigma_1}{\partial\epsilon_1} & \frac{\partial\sigma_1}{\partial\epsilon_2} \\ \frac{\partial\sigma_2}{\partial\epsilon_1} & \frac{\partial\sigma_2}{\partial\epsilon_2} \end{bmatrix} T'(\theta) + \frac{0.5\gamma_{xy}\sin 2\theta(\sigma_1-\sigma_2)}{(\epsilon_x-\epsilon_y)^2+\gamma_{xy}^2} \begin{bmatrix} 1 & -1 & -\omega \\ -1 & 1 & \omega \\ -\omega & \omega & \omega^2 \end{bmatrix} \right] \delta\epsilon_{xy} \quad .(5)$$

where $\omega = \cot 2\theta$. The $\frac{\partial\sigma_1}{\partial\epsilon_2}$ and $\frac{\partial\sigma_2}{\partial\epsilon_1}$ terms in (5) are zero if,as here, (4) is adopted for the total stress-strain relationships. They are included in (5) in order to allow for extensions in the next section. The special form of (5) involving a no-tension material with zero Poisson's ratio and an elastic compressive response was derived by Guptal et al [4]. The tangent modular matrix in (5) follows directly from equation (4) and does not involve the shear-retention factor, β, that is used in (2) for the fixed-crack model.

4. A SIMPLE PLASTICITY MODEL

The square yield criterion of Fig. 3(a) has often been used for "limit-load plasticity computations" [8,9] involving reinforced concrete. In its basic form, no tension is allowed and a perfectly plastic response is assumed in compression (Fig. 3(b)) once the compressive strength (say the cylinder strength, f_c') is reached. Limit-load calculations also consider the elastic strains to be negligible in comparison to the plastic strains but this assumption will not be adopted here. From Fig. 3(a), the yield functions are given by:

$$f = \sigma_1(\theta)\sigma_2(\theta) = (\sigma_1(\theta) - f_c')(\sigma_2(\theta) - f_c') = 0 \quad \ldots\ldots\ldots\ldots(6)$$

The principal stresses $\sigma_1(\theta)$ and $\sigma_2(\theta)$ can be related to σ_{xy} using standard transformations and equations (6) become:

$$f = \sigma_x\sigma_y - \tau_{xy}^2 = (\sigma_x - f_c')(\sigma_y - f_c') - \tau_{xy}^2 = 0 \quad \ldots\ldots\ldots(7)$$

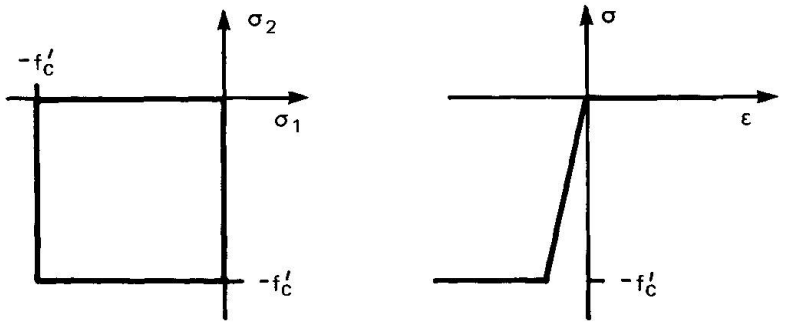

(a) Square yield criterion (b) Idealised stress-strain curve

Fig. 3 Yield criterion and stress-strain relationship for plasticity model

If we consider a deformation theory with Poisson's ratio as zero, application of normality to (7) leads to:

$$\sigma_x = E\left[\epsilon_x - \lambda(\sigma_y - \{f_c'\})\right]$$

$$\sigma_y = E\left[\epsilon_y - \lambda(\sigma_x - \{f_c'\})\right] \qquad \ldots\ldots\ldots\ldots\ldots(8)$$

$$\tau_{xy} = \frac{E}{2}(\gamma_{xy} + 2\lambda\tau_{xy})$$

where λ is a "plastic-strain multiplier". Depending on the particular part of the yield surface on which the stresses lie, the $\{f_c'\}$ term may or may not be included. Equations (8) can be used to show that:

$$\tan 2\theta = \frac{\gamma_{xy}}{\epsilon_x - \epsilon_y} = \frac{2\tau_{xy}}{\sigma_x - \sigma_y} \qquad \ldots\ldots\ldots\ldots\ldots(9)$$

and hence, as with the previous swinging-crack model, the principal stresses and principal strains coincide. Following this observation, it can be shown that, if both formulations adopt the stress/strain curves of Fig. 3(b), solutions obtained with the swinging-crack equations (4) will coincide with those obtained from the plasticity equations (6)-(8). The authors' computer program adopts an incremental flow-rule so that the σ_x, σ_y, τ_{xy} terms on the left-hand-side of (8) and the ϵ_x, ϵ_y, γ_{xy} terms on the right-hand-side of (8) are replaced by $\Delta\sigma_x$, ... and $\Delta\epsilon_x$, ... respectively. In these circumstances, the directions of the principal stresses and principal strains will only coincide when "proportional straining" has been applied. Consequently, there is no longer a direct relationship with the swinging-crack model. Solutions using deformation rather than flow theory can be obtained numerically by applying the complete load in a single step.

5.0 THE MODIFIED SWINGING-CRACK MODEL

Numerical results have shown that the basic swinging-crack formulation (Section 3.0) leads to overestimates of the strength of panels failing by shear/compression. This finding is consistent with the relationship that has been demonstrated between the basic swinging-crack model and simple plasticity-theory. For, it is well established that an "effectiveness factor" [9] is required to reduce the compressive strengths when applying the latter theory to the limit-analysis of beams failing in shear [9].

The previous swinging-crack model involves no Poisson or biaxial effects. Milford and Schnobrich [3] have introduced these effects into a swinging-crack formulation by adopting the orthotropic stress-strain relationships of Liu et al [11] and a "failure criterion" relating closely to the experimental results of Kupfer et al [12]. For the present we will ignore any enhanced strength in biaxial compression but are concerned to allow for the reduced compressive strength under tension/compression. To this end, we could have followed Milford and Schnobrick and used failure criteria, involving stresses, that are related to the experimental results of Kupfer et al. However, as the concrete softens, the tensile strain will reach ϵ_{tm} in Fig. 2 and the orthogonal tensile stress will be zero. Hence no strength degradation will be introduced. Consequently,

we have followed Vecchio and Collins [10] in adopting a degradation involving the orthogonal tensile strain rather than the orthogonal tensile stress.

The strength degradations have been incorporated into the swinging-crack model by modifying the simple relationship of (4) to:

$$\sigma_{xy} = T'(\theta)^T \begin{bmatrix} \sigma_1(\epsilon_1(\theta),\epsilon_2(\theta)) \\ \sigma_2(\epsilon_1(\theta),\epsilon_2(\theta)) \end{bmatrix} \qquad \ldots\ldots\ldots\ldots\ldots\ldots(10)$$

Following from their experimental results on a series of reinforced concrete panels [10], Vecchio and Collins modified the standard compressive parabola to take the form:

$$\sigma_2 = f'_c\left[2\left(\frac{\epsilon_2}{\epsilon_o}\right) - \mu\left(\frac{\epsilon_2}{\epsilon_o}\right)^2\right] \text{ or } \sigma_2 = \frac{f'_c}{\mu}\left[1 - \frac{(\epsilon_2 - \epsilon_{2p})^2}{(2\epsilon_0 - \epsilon_{2p})^2}\right] \qquad \ldots(11)$$

depending on whether the compressive strain ϵ_2 is less or greater than the strain $\epsilon_{2p} = \epsilon_o/\mu$ at which the peak stress f'_c/μ occurs. The term ϵ_o in (11) is the strain corresponding under uniaxial conditions to f'_c. The "reduction factor" $1/\mu$ caused by the orthogonal tensile strains, ϵ_1, is given by:

$$\mu = 0.85 + 0.27\epsilon_1/\epsilon_2 \qquad \ldots\ldots\ldots\ldots\ldots\ldots\ldots\ldots(12)$$

These formulae have been incorporated into a modified swinging-crack model and the derivatives $\frac{\partial\sigma_1}{\partial\epsilon_1}$, $\frac{\partial\sigma_2}{\partial\epsilon_2}$ have been used in the tangent stiffness of (5). However, the terms $\frac{\partial\sigma_1}{\partial\epsilon_2}$, $\frac{\partial\sigma_2}{\partial\epsilon_1}$ have been neglected since they introduce non-symmetry. In order to make valid comparisons with the fixed and simple swinging-crack models, the first part of eqn. (11) with $\mu = 1$ has been adopted in these models for the stress/strain relationship in compression.

6.0 IDEALISED PANELS

Gupta and Akbar [4] analysed a set of panels of unit dimensions, subject to uniform stress states involving various combinations of N_x, N_y and N_{xy} (Fig. 4(a)). The latter were proportionally increased until failure occurred by yielding of both sets of reinforcement. The computations assumed that the concrete had no tensile strength and behaved elastically in compression while the steel was assumed to act in an elastic/ perfectly-plastic manner.

The non-linear finite element program has been used to analyse one of Gupta and Akbar's panels (Case 4 of [4]). The adopted properties and loadings were:

Percentage of steel, $\rho_x = 4.232$, $\rho_y = 0.768$:

$\upsilon = 0$, $E_c = 20{,}000$ N/mm^2, $E_s = 200{,}000$ N/mm^2, $\sigma_{ys} = 500$ N/mm^2:

$N_x = N_y = 2.5\lambda$ N/mm, $N_{xy} = 5.0\lambda$ N/mm.

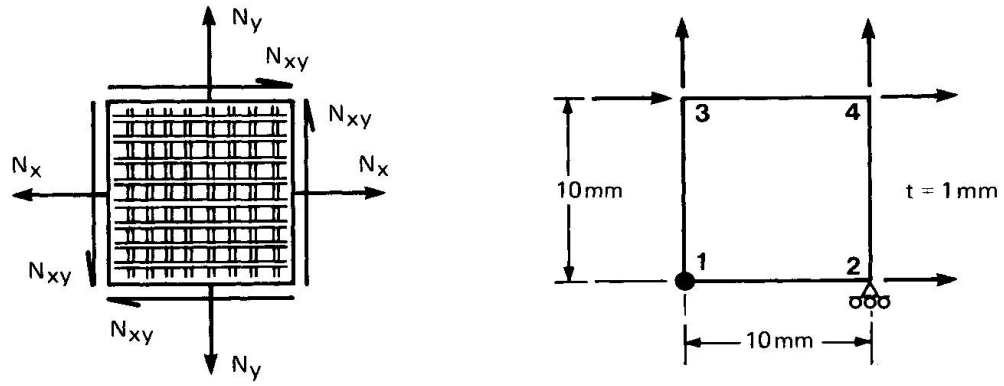

(a) Panel of unit dimensions (b) Finite element configuration

Fig. 4 Idealised panel

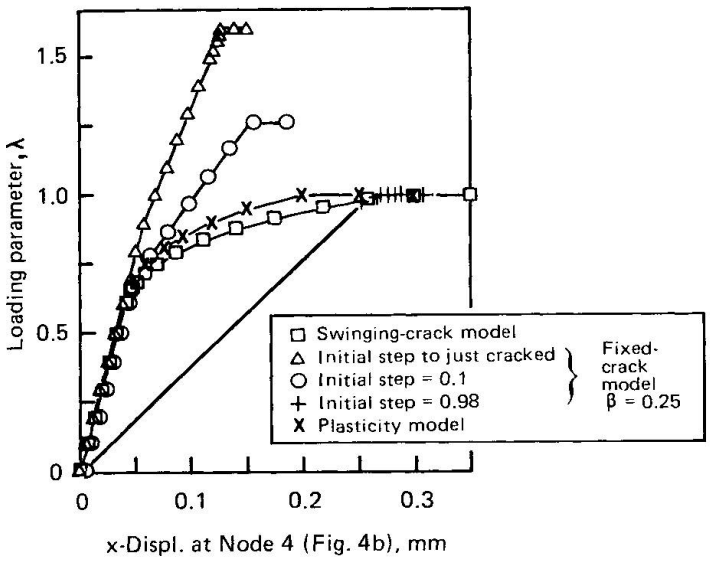

Fig. 5 Load/Deflection relationship for idealised model

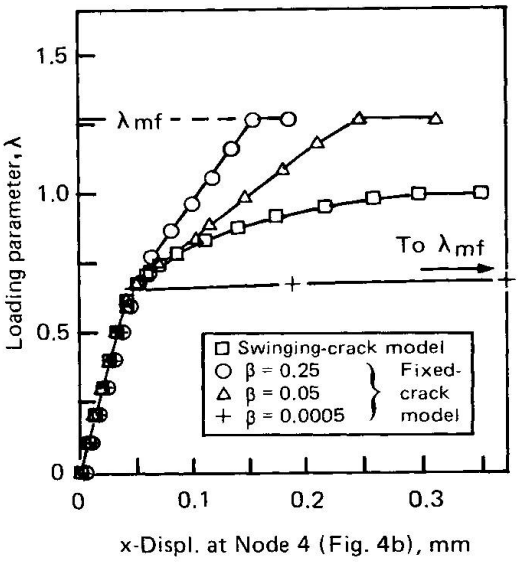

Fig. 6 Influence of shear retention factor, β

where λ is the loading parameter that is unity for the "exact collapse load" [4] obtained from equilibrium and the assumption of no-tension in the concrete. This no-tension condition was approximated by providing a very small tensile strength. In order to produce the simplest possible idealisation and yet use a standard non-linear finite element program, the panel was analysed using a single element with a single Gauss point. The two "mechanisms" were removed via constraint equations.

Fig. 5 plots the loading parameter, λ against the x displacement at node 4 (Fig. 4(b)). It can be seen that both the swinging-crack and plasticity models give the correct collapse load and very similar load/deflection relationships. When the plasticity solutions were obtained in single steps, thus simulating deformation theory, the resulting solutions coincided with the swinging-crack results. For these models, the angle θ (Fig. 1) of the principal tensile stress was 75^{o} when the limit-load was reached. The solutions that were obtained with

the fixed-crack model depended heavily on the initial step-sizes (Fig. 5). For example, when a very small first step was applied, the finite element model provided a crack orthogonal to the principal tensile stress at θ (Fig. 1) = 46.7^{o}. This angle is very close to the angle of the maximum principal stress before cracking. In total contrast, when one single-step was applied almost to the limit-load (using the arc-length method [13]), the fixed-crack model gave a crack orthogonal to $\theta = 75^{o}$ and a solution that lay on the load/deflection curve given by the swinging-crack model. This occurred because, in the limit as the ratio, r, to give first cracking (eqn. (3)) tends to zero, the fixed-crack model (see Section 2) gives:

$$\sigma_{xy} = T(\theta)^{T} \begin{bmatrix} 0 \\ E\epsilon_{2}(\theta) \\ \beta G\gamma_{12}(\theta) \end{bmatrix} \qquad \ldots\ldots\ldots\ldots\ldots\ldots\ldots\ldots (13)$$

But θ is given by the principal tensile stress direction of $rE\epsilon_{xy}$ or, equivalently, of ϵ_{xy}. Hence, $\gamma_{12} = 0$ and (13) coincides with (4) which governs the swinging-crack model.

All the fixed-crack solutions obtained in Fig. 5 involved a shear-retention factor, β, of 0.25. Fig. 6. illustrates the effect of varying this factor. It can be seen that, although this parameter affects the load/deflection response, the final collapse load does not depend on β.

7.0 THE PANELS OF VECCHIO AND COLLINS

Numerical analyses have been carried out on five of the thirty panels tested by Vecchio and Collins [10]. These five were chosen with a view to producing a range of failure modes. The adopted compressive stress/strain laws have already been discussed (Section 5). In tension, we normally introduce a simple softening relationship of the form illustrated in Fig. 2. For the current problems, this softening relates to the "tension stiffening" [1,14] which compensates for the inadequacy of the mesh and modelling to capture the shear transfer from the steel to the concrete. Vecchio and Collins have plotted the experimental relationship between the principal tensile stresses and principal tensile strains. From these plots, we have derived a simple relationship of the form of Fig. 2 with $\epsilon_{tm} = 0.004$. This strain is approximately twice the yield strain of the reinforcement.

For the finite element analyses, the panels were idealised using a similar procedure to that described in Section 6 for the "idealised panel". The following models were adopted:

F-CT: the fixed crack model (Section 2) with tensile strength and tension-stiffening and the parabolic compressive stress-strain relationship given by the first part of (11) with $\mu = 1$. The shear-retention factor, β, of (2) is set to 0.25

F-CNT: The fixed-crack model (Section 2) with no tensile strength and a stress/strain relationship as in Fig. 3(b) with an E value of $0.75f'_{c}/\epsilon_{o}$ and a maximum stress of $0.975f'_{c}$.

S-CT: As F-CT but using the swinging-crack model of Section 3

S-CNT: As F-CNT but using the swinging-crack model of Section 3
MS-CT As S-CT but using the modified swinging-crack model of Section 5 with compressive stress-strain relationsips as in (11)
MS-CNT As MS-CT but with no tensile strength
PNT: The plasticity model of Section 4 with no-tension and the idealised compressive stress-strain relationship of model F-CNT

For each analysis, the recorded collapse "loads" are specified (see Table) by means of the maximum shear stress (N/mm^2) applied to the panel. The ratio of $N_x:N_y:N_{xy}$ is given in the Table.

Table: Computed and experimental collapse "loads" (N/mm^2) for the panels of Vecchio and Collins

	PV11	PV19	PV22	PV25	PV27
$N_x:N_y:N_{xy}$	0:0:1	0:0:1	0:0:1	0.69:0.69:1	0:0:1
$\rho_x\sigma_{ysx}/\rho_y\sigma_{ysy}$	1.37	3.83	1.28	1.0	1.0
angles	45^o-49.5^o	45^o-63^o	45^o-48.5^o	45^o-45^o	45^o-45^o
Experimental	3.56(Y2)	3.95(S/C+Y1)	6.07(S/C)	9.12(S/C)	6.35(S/C)
F-CT	3.84(Y1) before 3.63(Y2)	5.12(Y2)	7.29(S/C+Y2)	9.72(S/C)	7.89(Y2)
F-CNT	3.61(Y2)	4.67(Y2)	7.27(Y2)	9.28(S/C)	7.89(Y2)
S-CT	3.78(Y1) before 3.59(Y2)	4.18(Y2)	7.24(Y2)	9.72(S/C)	7.89(Y2)
S-CNT	3.59(Y2)	4.18(Y2)	7.24(Y2)	9.28(S/C)	7.89(Y2)
MS-CT	3.69(Y1) before 3.59(Y2)	3.40(S/C+Y1)	5.71(S/C)	7.65(S/C)	5.96(S/C)
MS-CNT	3.59(Y2)	3.39(S/C+Y1)	5.69(S/C)	7.15(S/C)	5.95(S/C)
PNT	3.59(Y2)	4.18(Y2)	7.24(Y2)	9.28(S/C)	7.89(Y2)

S/C = shear/compression failure in concrete
S/C + Y1 = shear/compression failure in concrete + yielding of one set of steel
Y1 = failure by yielding of one set of steel
Y2 = failure by yielding of both sets of steel

In producing these results, an arc-length solution procedure [13] was adopted and hence the limit-loads could be well established without any failure in the iterative solution technique. Also, local limit-loads could be overcome. This is apparent from the numerical results given in the Table for panel PV11 which was the only one to fail exclusively by steel yielding. These local

limit-points could have been removed by reducing the tension-stiffening.

Of all the methods tested, only the modified S-C models (MS-CT and MS-CNT) consistently gave the same collapse modes as those observed in the experiments. These models also gave good or conservative predictions for the collapse strength. The more basic swinging-crack models (S-CT and S-CNT) overestimated the collapse load by about twenty per cent for two of the panels (PV22 and PV27). The fixed-crack models were equally bad in these instances and additionally gave an overestimate of thirty per cent for panel PV19 in which, because the ratio $\rho_x\sigma_{ysx}/\rho_y\sigma_{ysy}$ was high, there was a significant change in the angle of the principal strains.

For every panel, the simple plasticity-model, PNT, gave collapse loads that, as anticipated, coincided with those given by the simple S-C model with no-tension (S-CNT) although, for PV19, in which a significant "swing" occurred, there was some difference in the computed load/deflection" response. However, as predicted, these differences were eliminated when single large-steps were used for the model PNT.

Milford and Schnobrich [3] rejected the use of Vecchio and Collin's strain-related compressive strength degradations because "predicting compression related failures is very sensitive to the tension-stiffening". However, the present results indicate that even the use of a no-tension model in conjunction with the "degraded compression curves" gives reasonable, safe solutions.

8. CONCLUSIONS

The following tentative conclusions have been derived from the numerical tests that have been described. More tests will be required to substantiate these findings.

1. When the straining is non-proportional, the fixed-crack model may give excessively high collapse loads because the crack directions are totally governed by the early straining. However, in some circumstances, the introduction of large step-sizes will reduce the stiffness so that the solutions tend towards those of the swinging-crack model.
2 For steel-dominated ductile failures, the computed load/deflection response, but not the final collapse load, will depend on the shear-retention factor, β, if the fixed-crack model is adopted.
3. If deformation-theory is combined with plastic approach involving the square yield-criterion, the results will coincide with those obtained from an equivalent swinging-crack model. If flow-theory is adopted, the results will often be very similar.
4. A tangent stiffness matrix that is consistent with the swinging-crack model does not require the provision of a shear-retention factor, β.
5. The simple swinging-crack model may overestimate the strength and incorrectly assesses the failure modes of panels failing due to shear/compression.
6. This deficiency can be overcome by providing a compressive stress-strain relationsip, similar to that proposed by Vecchio and Collins [10], whereby the compressive strength is reduced by the presence of orthogonal tensile strains (not stresses). Unfortunately this leads to a non-symmetric tangent stiffness matrix that must be symmetrically approximated if efficient solutions are to be obtained. It is probable that an equivalent plasticity-model would involve a non-associative flow-rule.
6. Depending on the choice of tension-stiffening, local limit-points may well be encountered and it is essential to use a numerical solution procedure that will handle these phenomena.

7. In the absence of a simple, but effective fixed-crack model that allows for multiple and non-orthogonal cracks, the modified swinging-crack model appears to offer many advantages. Much further theoretical and experimental work is required on the development of effective stress/strain relationships in both tension and compression. These will need to be functions of both the mesh size and the vicinity and nature of the reinforcement.

9. ACKNOWLEDGEMENTS

The work descibed in this paper forms part of the programme of the Transport and Road Research Laboratory and is published by permission of the Director.

10. REFERENCES

1. ASCE, Finite element analysis of renforced concrete: state-of-the-art report, Struct. Div., Committee on Conc. & Masonry Structs., ASCE, New York, 1982.
2. COPE, R.J., RAO, P.V., CLARK, L.A. & NORRIS, P., Modelling of reinforced concrete behaviour for finite element analysis of bridge slabs, in: Numerical Methods for Nonlinear Problems, ed. C. Taylor et al, Pineridge Press, Swansea, Vol. 1, 1980, pp.457-470.
3. MILFORD, R.V., & SCHNOBRICH, Nonlinear behaviour of reinforced concrete cooling towers, Report ISSN: 0069-4274, University of Illinois, May 1984.
4. GUPTA, A.K. & AKBAR, A., Cracking in reinforced concrete analysis, J.of Struct. Div., ASCE, 110, 1984, pp.1735-1746
5. DE BORST, R. & NAUTA, P., Non-orthogonal cracks in a smeared finite element model, Engineering Computations, 2, 1985, pp.35-46
6. ONATE, E, OLIVER, J., & BUGEDA, G., Finite element analysis of the response of concrete dams subjected to internal loads, Finite Element Methods for Nonlinear Problems, ed. P.G. Bergan et al., Springer-Verlag, Berlin, 1985, pp. 653-672.
7. BAZANT, Z.P., Comment on orthotropic models for concrete and geomaterials, J. of Eng. Mech. Div., ASCE, 109, 1983, pp.849-865.
8. NEILSON, M.P., Yield conditions for reinforced concrete shells in the membrane state, Non-classical Shell Problems, Proc. IASS Symp., North-Holland, Amsterdam, 1963, pp.1030-1040.
9. MARTI, P., Plastic analysis of reinforced concrete shear walls, Introductory Report of IABSE Colloq. on Plasticity in Concrete, Zurich, 1979, pp.51-69.
10. VECCHIO, F. & COLLINS, M.P., The response of reinforced concrete to in-plane shear and normal stresses, ISBN 0-7727-7029-8, Pub. No. 82-03, University of Toronto, 1982.
11. LIU, T.C.Y., NILSON, A.H. & SLATE, F.O., Biaxial stress-strain relations for concrete, J. Struct. Div., ASCE, 98, 1972, pp.1025-1034.
12. KUPFER, H. & GERSTLE, K.N., Behaviour of concrete under biaxial stresses, J. Engng. Mech. Div., ASCE, 99, 1973, pp.852-866.
13. CRISFIELD, M.A., A fast incremental/iterative solution procedure that handles snap-through, Comp. & Structs., 13, 1981, pp.55-62.
14. SCANLON, A. & MURRAY, D.W., Time dependant reinforced concrete slab deflectins, J. Struct. Div., ASCE, 100, 1974, pp.1911-1924

Leere Seite
Blank page
Page vide

Finite Element Supported Fracture Testing of Concrete

Essai de rupture du béton appuyé par un calcul par éléments finis

Rechnergestützte Bruchuntersuchungen an Beton

Dirk A. HORDIJK
Research Engineer
Delft Univ. of Techn.
Delft, The Netherlands

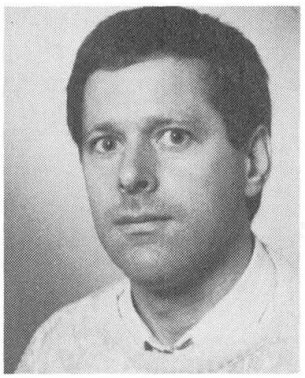

Dirk A. Hordijk, born in 1957, received his master of science degree at the Delft University of Technology in 1985. Presently he is working as a research engineer at the Stevin Laboratory of the Delft University of Technology.

Jan G. ROTS
Research Engineer
Delft Univ. of Techn.
Delft, The Netherlands

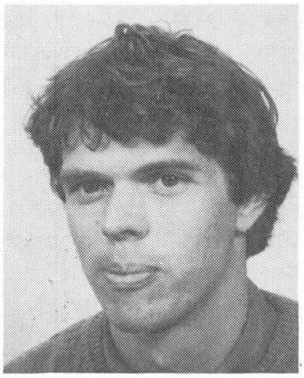

Jan Rots, born 1958, graduated from Delft University of Technology in 1983. Since 1983 he has been involved in a research project in the field of concrete mechanics.

Hans W. REINHARDT
Prof.Dr.-Ing.
Delft Univ. of Techn.
Delft, The Netherlands

Hans W. Reinhardt graduated from Stuttgart University in 1964. He joined Delft University in 1975 as head of the concrete section of the Stevin Laboratory. In 1986 he accepted a position at Darmstadt University.

SUMMARY

This paper discusses the uniaxial tensile test on a concrete specimen. Two phenomena, i.e. non-symmetric crack opening and irregular descending branch as sometimes observed in this fracture test, were investigated by a numerical analysis. 'Structural behaviour' as already inferred from experimental results was confirmed by this analysis. It also showed how this behaviour influences the measured stress-deformation diagram. The paper demonstrates how experimental and numerical research can support each other when they encounter similar problems.

RÉSUMÉ

Cet article décrit l'essai de traction uni-axiale d'une éprouvette en béton. Deux phénomènes ont été examinés à l'aide d'une analyse numérique, notamment: l'ouverture de fissures non-symétriques et une courbe descendante irrégulière, telle qu'observée parfois dans de tels essais. Un 'comportement structural', expliqué par les résultats expérimentaux, a été confirmé par cette analyse. Il a également montré comment ce comportement influence le diagramme tension-déformation mesuré. L'article montre comment des recherches expérimentales et numériques peuvent se compléter lorsqu'elles rencontrent les mêmes problèmes.

ZUSAMMENFASSUNG

In diesem Beitrag wird der zentrische Zugversuch an Beton kritisch beleuchtet. Zwei Erscheinungen, nämlich die unsymmetrische Rissöffnung und ein unregelmässig fallender Ast der Spannungs-Rissöffnungs-Linie, wie sie manchmal in diesem Versuch wahrgenommen werden, wurden in einer FE-Rechnung untersucht. Das 'Struktur-Verhalten', das schon früher aus Versuchsresultaten abgeleitet wurde, konnte durch diese Berechnung bestätigt werden. Es wurde auch deutlich, wie dieses Verhalten die Spannungs-Rissöffnungs-Linie beeinflusst. Der Beitrag zeigt, wie sich experimentelle und numerische Forschung ergänzen, wenn ähnliche Probleme angetroffen werden.

1. INTRODUCTION

Due to developments in finite element techniques, research activities in laboratories for concrete structures are being more and more devoted to determining the material properties. Since the results of FE computations strongly depend on the correct input parameters it is very important to ascertain the actual material properties. One of these properties is the behaviour of concrete under tensile loading. The fact that concrete is a tension-softening material, which means that the stress beyond the peak load decreases with increasing deformation, makes investigation of concrete fracture rather difficult. Nevertheless, new achievements in the electro-hydraulic control of testing machines now enable complete stress-deformation curves to be determined. In addition, computational techniques have evolved so far that tracing the post-peak softening behaviour is no longer a problem.

The uniaxial tensile test is probably the most fundamental fracture test. It has been supposed that this test yields a stress-deformation diagram that includes all the fracture mechanics parameters, i.e. the tensile strength f_t, Young's modulus E_o, the fracture energy G_f, the shape of the descending branch and the maximum crack opening δ_o at which stress can no longer be transferred [1]. Therefore, sometimes the name 'direct' tension test is used. Recently, however, some doubts have been raised about this assumption [2,3]. Due to a particular 'structural behaviour' as will be discussed in the next chapter, the crack opening in a uniaxial tensile test is non-symmetrically distributed over the specimen cross-section in some part of the loading path. As a result, the shape of the descending branch will be affected.

In this paper it is investigated whether this 'structural behaviour' can also be determined by means of a numerical analysis. Details of this analysis have been given before by Rots, Hordijk and de Borst [4]. The purpose of this paper is to discuss these numerical results in close relation to the experimental results. Therefore, the underlying computational and constitutive aspects will not be discussed in detail here. For more information on these aspects the reader is referred to de Borst [5] and Rots et al. [6] respectively.

2. THE BEHAVIOUR OF CONCRETE IN A UNIAXIAL TENSILE TEST

2.1 General

Concrete is an elastic-softening material (Fig. 1a). Straining concrete in uniaxial tension displays a linear stress-strain relation almost up to the peak. Then, beyond the peak a steep decay occurs which gradually evolves into a long tail. This decay is due to the development of one single crack in the specimen. The intention of a uniaxial tensile test is to create a crack, while the crack surfaces remain parallel to each other from the instant at which the first micro cracks are initiated until a crack opening δ_o is reached at which no more stress can be transferred. In that case we assume the σ-δ_{tot} relation to be a material property. It should be noted, however, that a visible crack starts as a cluster of micro cracks which coalesce during further deformation. The deformation measurement is taken over a specimen slice which contains the softening zone. Consequently the measured σ-δ_{tot} relation is linked up with the applied measuring length of the gauges. Subtracting the

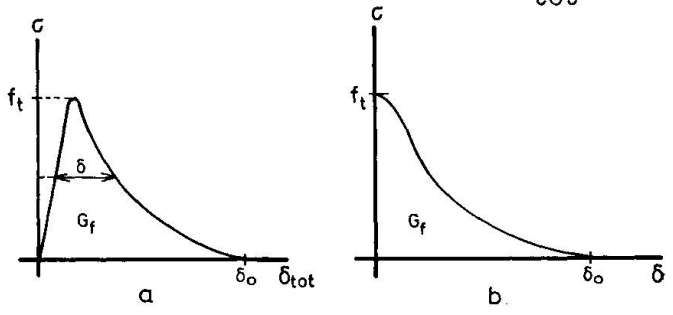

Fig. 1a a) Stress-deformation diagram.
b) Stress-crack opening diagram.

elastic deformation over the gauge length yields the stress-crack opening displacement (Fig. 1b) which may serve as a basis for a crack model.

2.2 Non-symmetric crack openings and 'bump' in the descending branch

Two peculiar aspects have sometimes been observed in uniaxial tensile tests. First, a non-symmetric crack opening may occur in some part of the loading path. Fig. 2b shows a typical test result obtained on a lightweight concrete [2]. In this test a prismatic specimen 250 mm long, 60 mm wide and 50 mm thick was used. Two saw cuts 5 mm x 5 mm reduced the critical cross-sectional area to 50 mm x 50 mm.

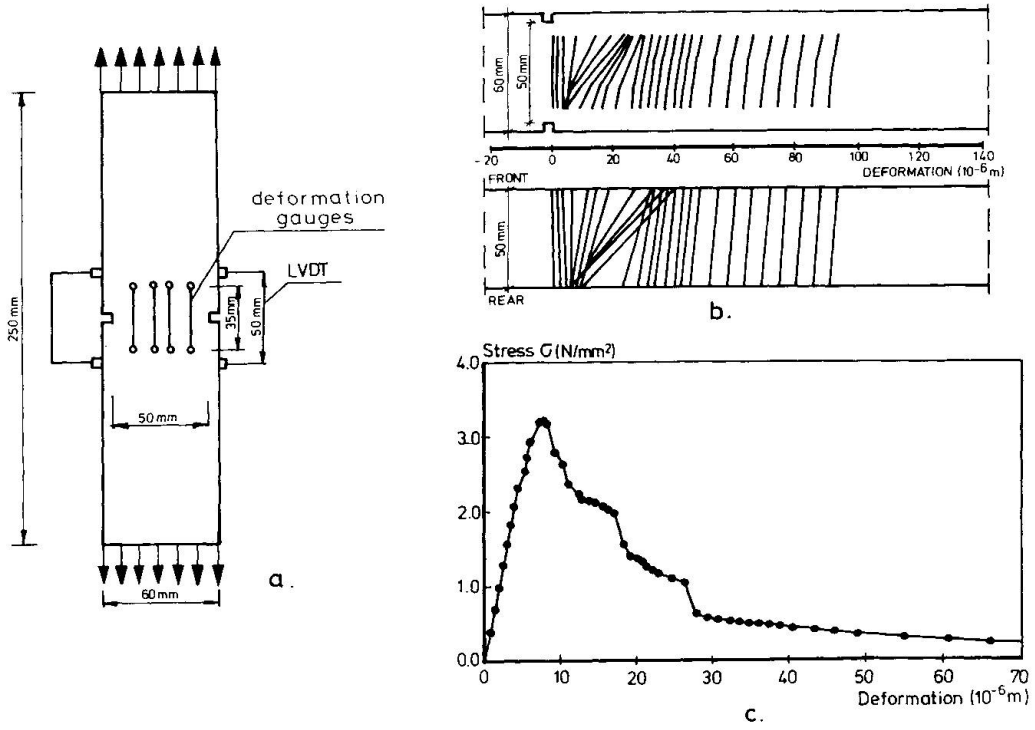

Fig. 2 Experimental result; a) specimen, b) deformation distribution and c) stress-deformation diagram.

For the deformation distribution eight deformation gauges with a gauge length of 35 mm were used, four on the front and four on the rear side of the specimen. It can be seen in Fig. 2b that in some part of the loading history the deformation distribution is non-symmetric even though rotation of the loading platens was prevented by a stiff guiding system. Such non-symmetric tensile fracture modes have also been reported by other investigators [3,7,8,9]. Gopalaratnam and Shah [10], however, reported symmetric modes.

The second peculiar aspect is that sometimes a 'bump' can be observed in the descending branch. As an example Fig. 2c displays two of these bumps. Similar results of bumps in the descending branch of stress-deformation diagrams have been reported by, for example, van Mier [3], Willam et al. [11] and Budnik [12].

2.3 Explanation of the observed phenomena

In [2] a qualitative model has been given that can possibly explain the phenomena described above. The basic idea of that model will be briefly summarized. Suppose that the stress-deformation relation for a small slice of concrete comprising the critical cross-section is as shown in Fig. 3a. In Fig. 3b it can

be observed that, for an average deformation δ_{peak}, the applied force must be larger in case of a symmetric deformation distribution (solid line) than in case of a non-symmetric one (dashed line). Nevertheless a non-symmetric deformation as indicated by an angle ϕ is limited by the rotational stiffness of the remaining part of the specimen in combination with the rotational stiffness of the loading platens.

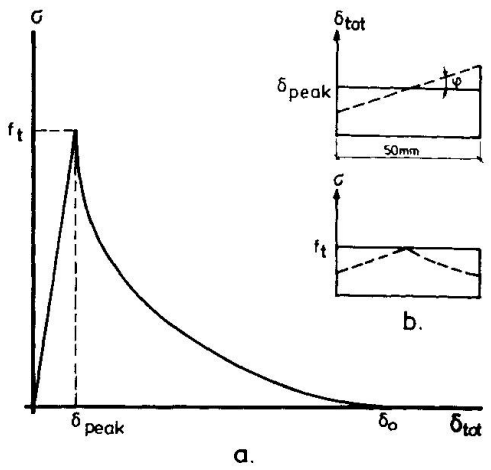

Fig. 3 a) Assumed σ-δ_{tot} relation.
b) Deformation and stress distributions.

In an experimental programme this model was verified by varying the specimen length [2]. It was concluded that there is a direct relation between the non-symmetric crack opening and the bump in the descending branch, on the one hand, and between the degree of non-symmetric crack opening and the rotational stiffness of the surrounding of the softening zone, on the other hand. Furthermore it became clear that the deformations must be studied three-dimensionally as appears also from Fig. 2b, in which deformation distributions projected on two perpendicular planes were plotted. By using very short specimens symmetric crack openings and a smooth descending branch were obtained.

The said phenomena were also observed by van Mier [3]. He explains them by the growth of a crack from one side of the specimen to the other. In his opinion the crack-arresting effect of large inclusions may cause a pronounced plateau (bump) in the descending branch. In addition, he suggests that the boundary condition is responsible for it because non-rotatable end-platens compel the crack, starting from one side, to jump to the other side.

3. FINITE ELEMENT ANALYSIS OF A UNIAXIAL TENSILE TEST

3.1 General

A numerical analysis of a uniaxial tensile test may shed some new light on the response of concrete in such a test. Therefore a test performed in the Stevin Laboratory was simulated by Rots, Hordijk and de Borst [4]. Some typical results of their study will be discussed here in relation to the experimental observations. It was intended to investigate the observed phenomena rather than to fit an experimental result exactly. This would not even have been possible, since a two-dimensional analysis was performed, while the specimen in an experiment reacted three-dimensionally.

3.2 Constitutive modelling

A smeared crack model as proposed by Rots et al. [6] has been used with a linearly elastic model for the concrete and a softening model for the crack. For the tensile softening a bilinear diagram was adopted as shown in Fig. 4. The fracture energy G_f was assumed to be a fixed material constant. As a smeared crack model was employed this energy is related to a certain crack band width, which in turn is related to the element configuration. The

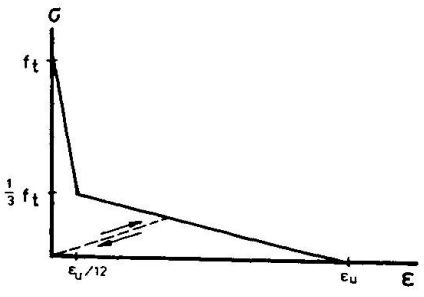

Fig. 4 Bilinear softening diagram.

necessary provisions were included to correctly release the fracture energy over the crack band width [13]. For the unloading and reloading a secant approach was used (Fig. 4).

3.3 Finite element idealization and material properties

The finite element mesh of the specimen as shown in Fig. 2a is given in Fig. 5. Four noded bilinear elements were used which were integrated using four-point Gauss quadrature. For the centre elements, where the fracture was expected to occur, a reduced centre-point integration scheme was used [6]. The lower boundary was assumed to be fixed, whereas the upper boundary was provided with a translational spring (k_t=148000 N/mm) and a rotational spring (k_r=10^9 Nmm/rad) in order to simulate the experimental conditions. Dependence relations were used to prevent distortion of the upper boundary which is in agreement with a rigid loading platen in an experiment.

In the experiment the load was applied at the upper boundary and was servo-controlled by a feed-back signal from two LVDTs mounted on the sides of the specimen (measuring length 50 mm). In the analysis this control mechanism was simulated by using the averaged crack opening displacement as a control parameter. This procedure of 'indirect displacement control' has recently been proposed by de Borst [5]. Further, a full Newton Raphson iterative procedure was employed with the tangent matrix being updated before each iteration.

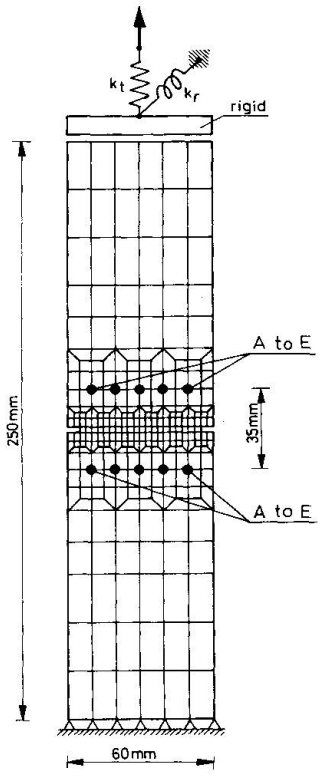

Fig. 5 Finite element mesh.

The elastic concrete properties were assumed to be: Young's modulus E=18000 N/mm² and Poisson's ratio ν=0.2, corresponding to a lightweight concrete. The softening properties were taken as: tensile strength f_t=3.4 N/mm², fracture energy G_f=59.3 N/m and crack band width h=2.5 mm. One element in front of the righthand notch was given a material imperfection by means of 1 percent reduction of G_f. The importance of this will become clear from the sequel of this paper.

3.4 Computational results

In conformity with the experiments, stress is given as the applied force divided by the central cross-sectional area, whereas deformation is the mean of five values measured between points A to E (Fig. 5). In previous experiments five instead of four deformation gauges were used on each side of the specimen. In Fig. 6 the incremental deformations are shown which refer to key events in the fracture localization process. Pre-peak deformations appeared to be symmetric (Fig. 6a). At an average stress σ=2.856 N/mm² a limit point was encountered. For this point a negative eigenvalue was calculated for the tangent stiffness matrix. In the corresponding eigenmode (Fig. 6b), which is identical to the incremental deformation field, a non-symmetric behaviour can be observed. Obviously, the side with the small imperfection opens, while the other side unloads. Upon further increase of the control parameter the load was decremented and a genuine equilibrium path was obtained. The fracture localization was propagated to the other side of the specimen (Fig. 6c) till the left side of the specimen tended to open suddenly, which resulted in a temporarily unloading of the right side (Fig. 6d). Subsequently, after a slight increase the load could decrease to zero while further the deformations were symmetric (Fig. 6e).

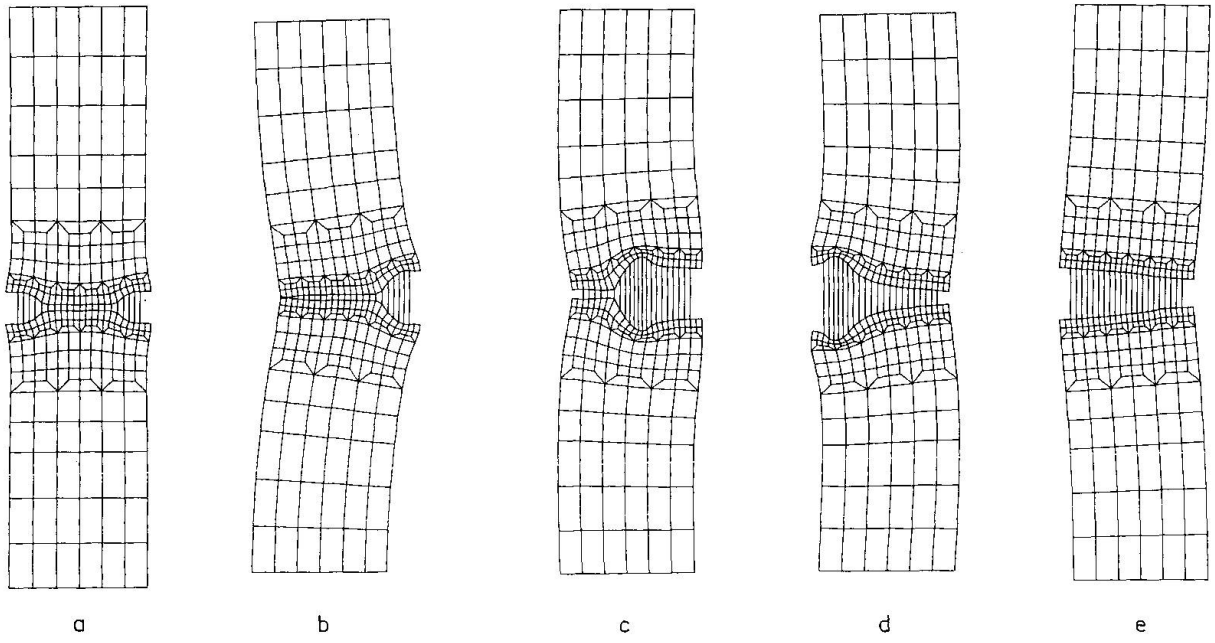

Fig. 6 Eigenmodes for different loading points.
a) pre-peak , σ=2.837 N/mm^2 b) at peak , σ=2.856 N/mm^2
c) post-peak, σ=1.865 N/mm^2 d) post-peak, σ=1.101 N/mm^2
e) post-peak, σ=1.026 N/mm^2

A stress-deformation diagram of two analyses has been plotted in Fig. 7. The first refers to the analysis with the imperfect material, the second belongs to an analysis with symmetric deformations. In the latter case the material imperfection was omitted. It appears that as a result of the non-symmetric deformations the peak load is reduced. More interesting, however, is the consequence for the shape of the descending branch which seems to be drastically affected. The resemblance with the experiment is evident. The 'bump' in the descending branch is now proven to be merely the result of the non-symmetric deformations.

In Fig. 7 an interesting phenomenon can be observed in the stress-deformation diagram for the non-symmetric solution. Beyond point A the deformation as well as the stress decreased. This phenomenon is called 'snap-back'. The importance of snap-back behaviour in elastic-softening materials was recognized before by, for example, Carpinteri [14] and de Borst [5]. It should be noted that the snap-back in the descending branch was found because the pure crack opening displacement was controlled. In the experiments the deformation was controlled by the average signal of the LVDTs ($l_{meas.}$=50 mm). Therefore a sudden drop as indicated by the dashed line A-B is mostly observed in the experiments (see Fig. 2). From the results of a post-peak cyclic test a snap-back as in Fig. 7 was already inferred [2].

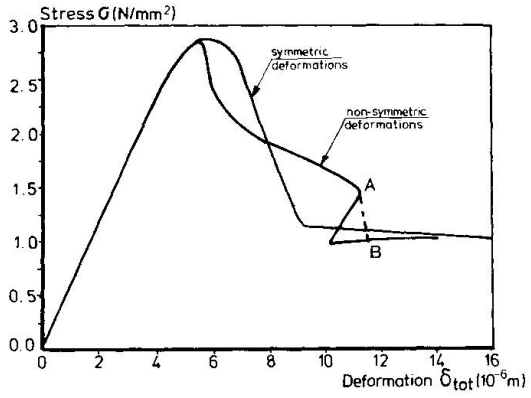

Fig. 7 Stress-deformation diagrams.

4. DISCUSSION

In the numerical analysis for the non-symmetric solution a small imperfection was given to one of the elements. Of course concrete is a heterogeneous material containing a lot of imperfections and it is therefore concluded that the response of concrete in a tension test will always be associated with a non-symmetric state of deformations. The numerical analysis clearly demonstrates that the stress-deformation relation from a uniaxial tensile test can strongly be influenced by these non-symmetric deformations. The tensile strength and the shape of the descending branch no longer necessarily represent the actual material behaviour. In the event of sudden jumps, due to snap-back behaviour, also the area under the stress-deformation relation may be measured incorrectly. If this is so, the fracture energy G_f is incorrect.

In the numerical analysis with the imperfection non-symmetric deformations could be observed between $\delta_{tot} \approx 5\mu m$ and $\delta_{tot} \approx 14\mu m$. For other values of δ_{tot} the deformation distribution as well as the stress was equal to that in the symmetric solution (Fig. 7). Therefore we still assume that for crack openings in which these openings are symmetric the σ-δ_{tot} relation can be regarded as a material property. In this respect it can be mentioned that it is known from experiments [2] that the non-symmetric crack openings can be restricted to a small part of the loading history by means of a high rotational stiffness of the boundary of the softening zone. With very short specimens it was even possible to obtain symmetric crack openings in every loading stage. Further research activities should clarify whether the σ-δ_{tot} relation obtained on such short specimens can be regarded as a material property.

It has been shown that the observed 'bump' is caused by the boundary conditions, as suggested by van Mier [3]. In the case of hinges instead of non-rotatable end-platens the crack will probably continue to open from one side, resulting in a smooth descending branch, as has been discussed by van Mier [3]. It should not be difficult to check this numerically.

5. CONCLUSIONS

- In a uniaxial tensile test on an elastic-softening material like concrete the crack opening will be non-symmetric in some part of the loading history.
- The phenomenon of non-symmetric crack openings can be regarded as 'structural behaviour'.
- Due to the structural behaviour in a uniaxial tensile test the measured stress-deformation relation cannot directly be regarded as a material property.
- A numerical analysis simulate the behaviour of concrete in a uniaxial tensile test, including the structural behaviour. Such an analysis can be used to investigate the influence of this structural behaviour on the material models derived from such a fracture test. Furthermore it can be used to improve the fracture test.
- In order to obtain post-peak stable softening behaviour in a displacement controlled uniaxial tensile test, very short gauge lengths have to be used.
- In numerical and experimental research the same types of problem can be encountered. Therefore the co-operation of these research fields should be stimulated.

ACKNOWLEDGEMENTS

The calculations reported in this paper have been performed with the DIANA finite element code of the TNO Institute for Building Materials and Structures (TNO-IBBC). Support of the DIANA-group of TNO-IBBC is gratefully acknowledged. The authors are indebted to Dr. R. de Borst for his share in the numerical part of this study. This investigation was partly supported by the Netherlands Technology Foundation (STW). The second author's contribution is part of a STW research project under supervision of Prof. J. Blaauwendraad of Delft University of Technology.

REFERENCES

1. HILLERBORG A., The theoretical basis of a method to determine the fracture energy G_F of concrete. Matériaux et Constructions, July-August 1985, pp 291-296.

2. HORDIJK D.A., REINHARDT H.W. and CORNELISSEN H.A.W., Fracture mechanics parameters of concrete from uniaxial tensile tests as influenced by specimen length. Proc. Int. Conf. on Fracture Mechanics of Concrete and Rock, Houston, U.S.A., June 1987.

3. VAN MIER J.G.M., Fracture of concrete under complex stress. HERON, No. 3, 1986, 90 pp.

4. ROTS J.G., HORDIJK D.A. and DE BORST R., Numerical simulation of concrete fracture in 'direct' tension. Proc. Fourth Int. Conf. on Numerical Methods in Fracture Mechanics, San Antonio, U.S.A., March 1987.

5. DE BORST R., Non-linear analysis of frictional materials. Dissertation, Delft University of Technology, Delft 1986, 140 pp.

6. ROTS J.G., NAUTA P., KUSTERS G.M.A. and BLAAUWENDRAAD J., Smeared crack approach and fracture localization in concrete, HERON, No. 1, 1985, 48 pp.

7. LABUZ J.F., SHAH S.P. and DOWDING C.H., Experimental analysis of crack propagation in granite. Int. J. Rock Mech. Min. Sci. & Geomech. Abstr., No. 2, 1985, pp 85-98.

8. SCHEIDLER D., Experimentelle und analytische Untersuchungen zur wirklichkeitsnahen Bestimmung der Bruchschnittgrössen unbewehrter Betonbauteile unter Zugbeanspruchung. Dissertation, Darmstadt 1985.

9. NOTTER R., Schallemissionsanalyse für Beton im dehnungsgesteuerten Zugversuch. Dissertation, Zürich 1982.

10. GOPALARATNAM V.S. and SHAH S.P., Softening response of plain concrete in direct tension. ACI Journal, May-June 1985, pp 310-324.

11. WILLAM K., HURLBUT B. and STURE S., Experimental, constitutive and computational aspects of concrete failure. Preprints US-Japan Seminar on Finite Element Analysis of Reinforced Concrete Structures, Tokyo 1985, pp 149-171.

12. BUDNIK J., Bruch- und Verformungsverhalten harzmodifizierter und faserverstärkter Betone bei einachsiger Zugbeanspruchung. Dissertation, Ruhr-Universität, Bochum 1985.

13. BAZANT Z.P. and OH B.H., Crack band theory for fracture of concrete. Matériaux et Constructions, May-June 1983, pp 155-177.

14. CARPINTERI A., DI TOMASSO A. and FANELLI M., Influence of material parameters and geometry on cohesive crack propagation. Fracture Toughness and Fracture Energy of Concrete, F.H. Wittmann Ed., Amsterdam 1986, pp 117-135.

Comparison of Constitutive Models for Triaxially Loaded Concrete

Comparaison de modèles de comportement du béton sous charge triaxiale

Vergleich konstitutiver Modelle für Beton unter dreiachsialer Belastung

J. EBERHARDSTEINER
University Assistant
Technical Univ.
Vienna, Austria

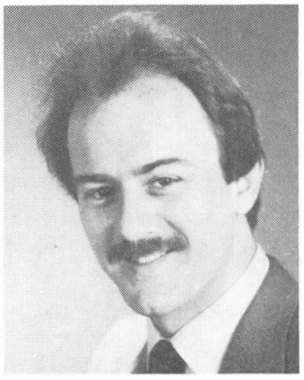

Josef Eberhardsteiner, born 1957, graduated as Dipl.-Ing. (Civil Engineer) from TU-Vienna in 1983. Since then he has been a University Assistant at the Institute of Strength of Materials at TU-Vienna.

G. MESCHKE
Research Assistant
Technical Univ.
Vienna, Austria

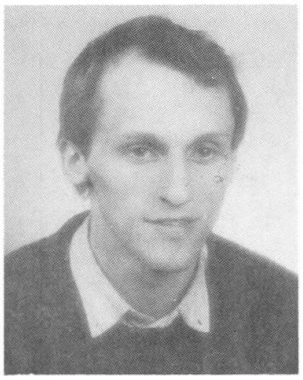

Günther Meschke, born 1958, graduated as Dipl.-Ing. (Civil Engineer) from TU-Vienna in 1983. Since then he has been a Research Assistant at the Institute of Strength of Materials at TU-Vienna.

H.A. MANG
Professor
Technical Univ.
Vienna, Austria

Herbert A. Mang, born 1942, graduated as Dr.techn. (1970), from TU-Vienna, Ph.D. (1974) from Texas Tech. University; University Assistant (1967), Professor (1983), both at TU-Vienna; Corresponding Member of the Austrian Academy of Sciences (1985).

SUMMARY
After a description of four triaxial constitutive models for concrete, based on different mechanical concepts, a comparative evaluation is carried out. One of the models is a new hypoplastic model. Shortcomings of some models, occurring in case of non-monotonic load histories, are eliminated by adequate modifications. Generally, there is a good agreement between model predictions and test results.

RÉSUMÉ
Une présentation de quatre modèles triaxiaux de comportement du béton sur la base des différentes théories mécaniques est suivie d'une évaluation comparative. Un des modèles est une nouvelle formulation hypoplastique. Quelques modèles présentent des défauts – lors de cas de charges non-monotones – lesquels sont éliminés par des modifications appropriées. Généralement, les résultats du modèle correspondent bien avec des résultats expérimentaux.

ZUSAMMENFASSUNG
Vier auf verschiedenen mechanischen Konzepten beruhenden dreiachsiale konstitutive Modelle für Beton werden beschrieben und einer vergleichenden Wertung unterzogen. Eines dieser Modelle ist ein neues hypoplastisches Modell. Mängel einzelner Modelle, die bei nichtmonotonen Lastgeschichten auftreten, werden durch geeignete Modifikationen beseitigt. Im allgemeinen liegt eine gute Übereinstimmung zwischen Modellvoraussagen und Versuchsergebnissen vor.

1. INTRODUCTION

Knowledge of suitable constitutive equations is a necessary prerequisite for finite element ultimate load analysis of thick-walled structures made of reinforced concrete. During the last years a number of triaxial constitutive models, based on different mechanical concepts, have been proposed. So far, a comparative evaluation of their potential for modelling the behavior of concrete under multi-axial states of stress does not seem to exist in the open literature. This was the motivation for a comprehensive comparative study of a relatively large number of material laws proposed by several investigators to describe the mechanical behavior of concrete subjected to triaxial non-monotonic loading up to material failure [1].

The present paper is based on the mentioned investigation. It consists of a report on four constitutive models, selected from [1], representing four different mechanical concepts. The purpose of the paper is to provide information about the capability of typical representatives of different classes of constitutive models for description of the material behavior of multiaxially loaded concrete.

The chosen models are the Cauchy (nonlinear elastic) model by Kotsovos and Newman [2], the hypoelastic material law by Stankowski and Gerstle [3], an elasto-plastic constitutive model by Han and Chen [4] and a bounding surface model developed by the second author, reported in [1]. After description of these models a comparative evaluation is carried out. It is based on a comparison of results from selected load paths with corresponding test results.

2. CONSTITUTIVE MODELS

2.1 Cauchy (Nonlinear Elastic) Model by Kotsovos and Newman

This constitutive model is characterized by a total (secant) formulation. Introducing the octahedral strains, $\varepsilon_o = I_1'/3$ and $\gamma_o = \sqrt{2J_2'/3}$, and stresses, $\sigma_o = I_1/3$ and $\tau_o = \sqrt{2J_2/3}$, where I_1 is the first invariant of the stress tensor, I_1' is the first invariant of the strain tensor, J_2 is the second invariant of the stress deviation tensor and J_2' is the second invariant of the strain deviation tensor, the constitutive equations are given as [2]:

$$\varepsilon_o = (\sigma_o+\sigma_o')/(3K_S) \quad , \qquad \gamma_o = \tau_o/(2G_S) \quad . \tag{1}$$

The two secant material moduli, K_S (bulk modulus) and G_S (shear modulus), depend on the uniaxial compressive strength of concrete, f_{cu}. They are obtained by means of curve fitting, using experimental results. An essential feature of this constitutive model is the quantity [2]

$$\sigma_o' = f(\sigma_o,\tau_o) = \{a(\tau_o/f_{cu})^b\}/\{1+c(\sigma_o/f_{cu})^d\} \tag{2}$$

where a,b,c and d are regression coefficients. The purpose of adding σ_o' to σ_o in the expression for ε_o is consideration of the fact that deviatoric loading yields deviatoric as well as volumetric deformations.

Recomputations of several experiments have shown that for the case of nonproportional loading the constitutive model by Kotsovos and Newman is deficient. The shortcomings are caused by (a) the lack of a parameter considering the load history (introduction of such a quantity, however, would be beyond the scope of a classical Cauchy model) and (b) the loading criterion based on the octahedral stresses. The second deficiency was eliminated by introducing a loading criterion proposed by Stankowski and Gerstle [3], which is based on the principal normal stresses. According to this criterion, loading in the direction of a principal normal stress σ_i is characterized by exceeding the previously reached maximum

value of the respective principal normal stress.

Fig.1 illustrates the difference between the two criteria. For the considered stress path the first criterion indicates triaxial loading up to point 0 followed by hydrostatic unloading and deviatoric loading (Fig.1(a)). According to the second criterion, unloading in the directions of σ_2 and σ_3 begins already at point P (Fig.1(b)). This criterion agrees very well with test results.

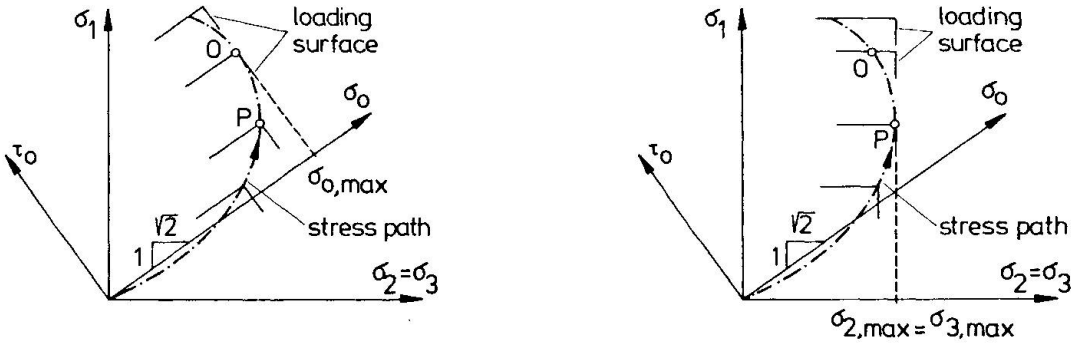

(a) octahedral stress criterion (b) principal normal stress criterion

Fig.1 Loading Surfaces in the Stress Space for Two Different Loading Criteria

Determination of deformations resulting from nonmonotonic loading requires formulation of an incremental relationship $\Delta\boldsymbol{\varepsilon} = \mathbf{D}_T\Delta\boldsymbol{\sigma}$, where $\mathbf{D}_T$ is a tangent material matrix relating increments of principal normal stresses to increments of principal normal strains. For a situation characterized by loading in the direction of σ_1 and unloading in the directions of σ_2 and σ_3, this relationship is given as

$$\begin{Bmatrix} \Delta\varepsilon_1 \\ \Delta\varepsilon_2 \\ \Delta\varepsilon_3 \end{Bmatrix} = \begin{bmatrix} \alpha_1 & \beta & \beta \\ \beta & \alpha' & \beta' \\ \beta & \beta' & \alpha' \end{bmatrix} \begin{Bmatrix} \Delta\sigma_1 \\ \Delta\sigma_2 \\ \Delta\sigma_3 \end{Bmatrix}, \tag{3}$$

where

$$\begin{aligned} \alpha' &= 1/(9K_0)+1/(3G_0) , & \alpha_1 &= 1/(9K_T)+1/(3G_T)+\Delta\sigma_o'/(3K_T\Delta\sigma_1) \\ \beta' &= 1/(9K_0)-1/(6G_0) , & \beta &= 1/(9K_T)-1/(6G_T) \end{aligned} \tag{4}$$

The tangent material moduli K_T and G_T are obtained through differentiation of K_S and G_S. The material behavior described by the Eqs.3 and 4 is called "transversely isotropic" [5]. It is characterized by material properties in the direction of σ_1 which are different from the ones in a plane normal to this direction, representing a plane of isotropy.

2.2 Hypoelastic Model by Stankowski and Gerstle

This nonlinear material model is characterized by an incremental (tangent) formulation. The respective constitutive equations are given as [3]

$$\begin{Bmatrix} \Delta\varepsilon_o \\ \Delta\gamma_o \end{Bmatrix} = \begin{bmatrix} 1/(3K_T) & 1/H_T \\ 1/Y_T & 1/(2G_T) \end{bmatrix} \begin{Bmatrix} \Delta\sigma_o \\ \Delta\tau_o \end{Bmatrix} , \tag{5}$$

where $K_T = f(\sigma_o)$ and $G_T = f(\sigma_o,\tau_o)$ are obtained through curve fitting, using experimental results. The coupling tangent material moduli H_T and Y_T permit consideration of the influence of $\Delta\tau_o$ on $\Delta\varepsilon_o$ and of $\Delta\sigma_o$ on $\Delta\gamma_o$, respectively. With regards to constitutive modelling of these interactions, Stankowski and Gerstle were influenced by results obtained by Scavuzzo et al. [6] from comprehensive test series.

For the current state of stress, characterized by point P on the stress path shown in Fig.2(a), $\Delta\varepsilon_o^{pl}/\Delta\gamma_o^{pl} = 1/\sqrt{2}$ where $\Delta\varepsilon_o^{pl}$ and $\Delta\gamma_o^{pl}$ are increments of the

plastic octahedral strains. Using the following relationships for a purely deviatoric load increment:

$$\Delta\varepsilon_o = \Delta\varepsilon_o^{el} + \Delta\varepsilon_o^{pl} = 0 + \Delta\varepsilon_o^{pl} = \Delta\tau_o/H_T \quad \text{and} \tag{6}$$

$$\Delta\gamma_o = \Delta\gamma_o^{el} + \Delta\gamma_o^{pl} = \Delta\tau_o/(2G_0) + \Delta\gamma_o^{pl} = \Delta\tau_o/(2G_T) \tag{7}$$

where $\Delta\varepsilon_o$ ($\Delta\varepsilon_o^{el}$) and $\Delta\gamma$ ($\Delta\gamma_o^{el}$) are increments of the (elastic) octahedral strains, in order to express $\Delta\varepsilon_o^{pl}/\Delta\gamma_o^{pl}$ in terms of H_T, G_T and G_0, where G_0 is the initial value of G, and setting this expression equal to $1/\sqrt{2}$, yields

$$H_T = 2\sqrt{2}G_T/(1-G_T/G_0). \tag{8}$$

Considering a purely volumetric load increment, by analogy to determination of H_T, Y_T is obtained as

$$Y_T = 3K_T/\{\sqrt{2}(1-K_T/K_0)\} \tag{9}$$

where K_0 is the initial value of K.

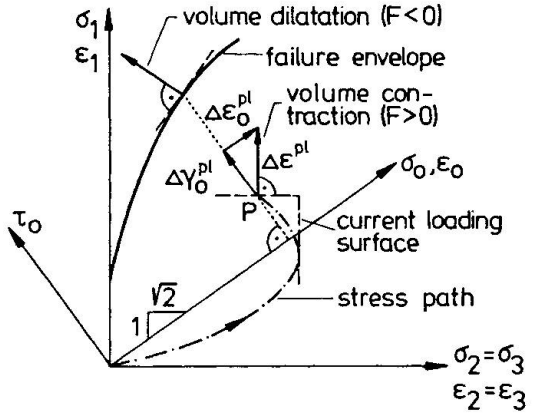

(a) increments of plastic strains

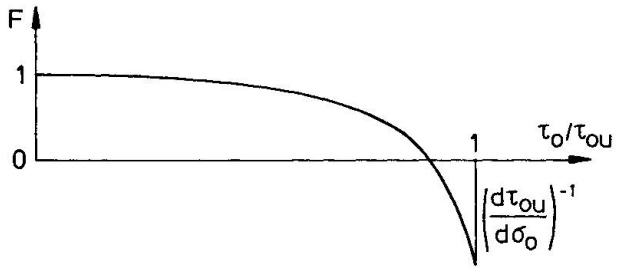

(b) corrective factor $F = f(\tau_o/\tau_{ou})$

Fig.2 Rotation of Vector $\Delta\varepsilon^{pl}$ for Consideration of Volume Dilatation

According to the loading criterion based on the principal normal stresses, for purely deviatoric loading the loading surfaces are normal to the direction of σ_1. Thus, $\Delta\varepsilon_o^{pl} > 0$ (Fig.2(a)), indicating volume contraction irrespective of the magnitude of τ_o. By contrast to this analytical result, it is known from experiments that a change from volume contraction to dilatation occurs when τ_o exceeds a value of approximately $0.9\tau_{ou}$ where τ_{ou} is the octahedral shear strength. In order to consider this fact, Stankowski and Gerstle have redefined the ratio $\Delta\varepsilon_o^{pl}/\Delta\gamma_o^{pl}$ as $\Delta\varepsilon_o^{pl}/\Delta\gamma_o^{pl} = F/\sqrt{2}$ where F is a corrective factor depending on τ_o/τ_{ou} as shown in Fig.2(b). This factor results in a rotation of the vector $\Delta\varepsilon^{pl}$ such that for $\tau_o = \tau_{ou}$ it is normal to the failure envelope. For negative values of F, $\Delta\varepsilon_o^{pl} < 0$, indicating volume dilatation.

For axisymmetric states of stress, the two quantities $\Delta\varepsilon_o$ and $\Delta\gamma_o$ are sufficient for determination of $\Delta\varepsilon_1$ and $\Delta\varepsilon_2 = \Delta\varepsilon_3$. For general triaxial states of stress, however, an additional condition is necessary to determine $\Delta\varepsilon_1$, $\Delta\varepsilon_2$ and $\Delta\varepsilon_3$ from $\Delta\varepsilon_o$ and $\Delta\gamma_o$. It is assumed that the directions of the increments of the stress deviation vector coincide with the directions of the corresponding increments of the strain deviation vector. In general, however, this assumption does not agree with reality.

2.3 Elasto-Plastic Model by Han and Chen

The hardening characteristics of this constitutive model account for the ductility of concrete under compression and for its brittleness under tension. The loading surface expands from the (initial) yield surface to the failure surface (Fig.3(a)). It is described by the relationship [4]

$$f = r - kr_f(\sigma_m,\theta) = 0 \tag{10}$$

where $r = \sqrt{2J_2}/f_{cu}$ is the deviatoric length normalized with respect to f_{cu}, $\sigma_m = \sigma_o/f_{cu}$, $\theta = (1/3)\arccos\left((3\sqrt{3}/2)(J_3 J_2^{(3/2)})\right)$ is the Lode angle with J_3 as the third invariant of the stress deviation tensor, k is a form factor depending on σ_m and on the hardening parameter k_o characterized by $k_y \le k_o \le 1$, with $k_o = k_y$ and $k_o = 1$ referring to the yield surface and to the failure surface $r = r_f$, respectively. Results presented in this paper, which are based on the constitutive model by Han and Chen, were obtained by means of the failure surface by Willam and Warnke [7].

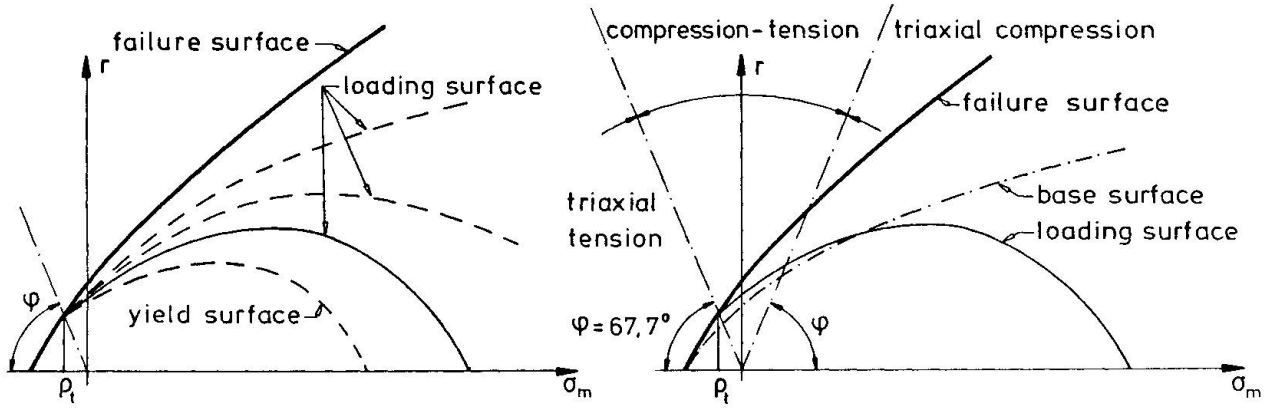

(a) expansion of the yield surface (b) construction of a loading surface

Fig.3 Expansion of the Yield Surface and Construction of a Loading Surface

The starting point for the construction of a loading surface is the base surface (Fig.3(b)), representing an affine contraction of the failure surface. It is described by the relationship

$$f_b = r - k_o r_f = 0. \tag{11}$$

The shape function $k = k(\sigma_m,k_o)$, defining the corresponding loading surface, is determined such that for triaxial tension ($\sigma_m \ge \rho_t$) there is no hardening zone (Fig.3). Additional aspects for determination of k are the increase of the hardening zone with increasing hydrostatic compression and the close up of the loading surface at the hydrostatic axis in the region of triaxial compression, indicating a large hardening zone.

The hardening parameter k_o is determined with the help of a σ-ε^{pl} diagram where σ and ε^{pl} are the stress and the plastic strain, respectively, obtained from a uniaxial compression test, and of the condition

$$dW^{pl} = \sigma_{ij} d\varepsilon^{pl}_{ij} = \sigma d\varepsilon^{pl} \tag{12}$$

where dW^{pl} is a differential of the specific plastic work and $d\varepsilon^{pl}_{ij}$ is a differential of the plastic strains ε^{pl}_{ij}. Thus, each loading surface is associated with a so-called base plastic modulus $H^{pl}_b = d\sigma/d\varepsilon^{pl}$, resulting from the uniaxial compression test [4].

In order to consider the ductile material behavior of concrete under triaxial

compression, H_b^{pl} was replaced by a modified plastic modulus $H^{pl} = M(\sigma_m,\theta).H_b^{pl}$ where M is a modification factor. For large compressive stresses the form of M suggested by Han and Chen [4] yields a physically unrealistic restiffening of the material.

For the purpose of an adequate description of volume contraction and dilatancy, the direction of the vector of plastic flow is defined by a nonassociated flow rule which can be written formally as

$$d\varepsilon_{ij}^{pl} = d\lambda \partial g/\partial \sigma_{ij} \tag{13}$$

where $d\lambda$ is a positive scalar factor of proportionality and g is the plastic potential given as [4]

$$g = \alpha I_1 + \sqrt{J_2} - k^* = 0 \tag{14}$$

where α represents the plastic dilatancy factor, proposed in [4] as a linear function of k_o, and k^* is a constant which does not appear in the flow rule. The dilatancy factor controls the description of the $\tau_o - \varepsilon_o^{pl}$ relationship. It also has an influence on the stiffness modulus h, appearing in the expression for the plastic material stiffness tensor (Eq.16).

A shortcoming of the original form of $\alpha = \alpha(k_o)$, which occurs when leaving the hydrostatic axis after a significant elasto-plastic hydrostatic preloading, is the strong rotation of the vector of plastic flow $d\varepsilon_{ij}^{pl}$ in the direction of the τ_o-axis, connected with a considerable decrease of $(\partial g/\partial \sigma_{ij})\sigma_{ij}$ and, thus, of h (Eq.17). Thus, a modified dilatancy factor $\alpha(k,k_o,k_y,f_{cu},\theta,\sigma_o)$ was used in the numerical investigation for the present paper. This factor is based on test results showing the dependence of the $\tau_o - \varepsilon_o^{pl}$ relationship on f_{cu}, θ, and σ_m and on the type of loading.

The incremental stress-strain equations can be written formally as

$$d\sigma_{ij} = (D_{ijkl}^{el} + D_{ijkl}^{pl})\, d\varepsilon_{kl} \tag{15}$$

where D_{ijkl}^{el} is the elastic and D_{ijkl}^{pl} is the (unsymmetric) plastic material stiffness tensor, given as [4]

$$D_{ijkl}^{pl} = -(1/h)\left(D_{ijmn}^{el}(\partial g/\partial \sigma_{mn})(\partial f/\partial \sigma_{pq})D_{pqkl}^{el}\right) \tag{16}$$

with

$$h = (\partial f/\partial \sigma_{mn})D_{mnpq}^{el}(\partial g/\partial \sigma_{pq}) - H^{pl}(\partial f/\partial \sigma)(1/\sigma)(\partial g/\partial \sigma_{ij})\sigma_{ij}. \tag{17}$$

2.4 Bounding Surface Model by Meschke

This constitutive model belongs to a special category of bounding surface models, characterized by the vanishing of the elastic range. The mathematical formulation of such bounding surface models was introduced first by Dafalias and Popov [8]. The constitutive model proposed by Meschke [1] is based on the concept of hypoplasticity. According to Dafalias [9], the main distinguishing factor of hypoplasticity from ordinary plasticity is the dependence of the plastic strain rate and of the rate of the internal variables on the stress rate direction, in addition to the overall dependence on the stress state. Thus, for nonproportional loading hypoplasticity is incrementally nonlinear.

The basic relationship of the bounding surface model by Meschke is the equation

$$d\varepsilon^{pl} = (1/H^{pl})\langle L\rangle \rho \tag{18}$$

where ϵ^{pl} is the vector of plastic flow, $H^{pl} = H^{pl}(\sigma,k,\epsilon^{pl})$ is a generalized plastic modulus, <L> is a loading function defined as <L> = L = $d\sigma.\mathbf{n}$ for $d\sigma.\mathbf{n} > 0$ and as <L> = 0 for $d\sigma.\mathbf{n} \leq 0$ with $\mathbf{n}$ representing the normal vector at the image stress point σ_b on the loading surface (Fig.4), and ρ is a direction vector given as $\rho = d\epsilon^{pl}/|d\epsilon^{pl}|$. H^{pl} depends on the stress vector σ, defining a point in the space of principal stresses σ_i, on the normalized distance parameter $k = k(r,r_f,\xi)$, where ξ is a discrete internal variable representing a jump parameter which accounts for abrupt changes of the loading direction, and on the accumulated effective plastic strain ϵ^{pl}, representing an internal variable, given as

$$\epsilon^{pl} = \int d\epsilon^{pl} = \int (d\epsilon^{pl}.d\epsilon^{pl})^{1/2}. \tag{19}$$

With the help of Eq.(18) and of the relationship $d\epsilon = d\epsilon^{el} + d\epsilon^{pl}$ where $d\epsilon$ and $d\epsilon^{el}$ correspond to $d\varepsilon_{ij}$ and $d\varepsilon^{el}_{ij}$, respectively, the bounding surface model by Meschke can be formulated mathematically as follows:

$$d\sigma = \mathbf{D}^{ep} d\epsilon = \left[\mathbf{D}^{el} - (\mathbf{D}^{el}\rho\ \mathbf{D}^{el}\mathbf{n})/(\mathbf{n}\ \mathbf{D}^{el}\rho + H^{pl})\right] d\epsilon \tag{20}$$

where $\mathbf{D}^{ep} = \mathbf{D}^{el} + \mathbf{D}^{pl}$ is the elasto-plastic material stiffness matrix with $\mathbf{D}^{el}$ as the elastic and $\mathbf{D}^{pl}$ as the plastic material stiffness matrix.

Fig.4 illustrates a meridional section of the bounding surface, which is identical to the failure envelope, at two different levels of deviatoric loading, indicated by the stress point σ. A comparison of the two illustrations shows the rotation of the direction vector during deviatoric loading. The point designated as $\sigma_{2,max} = \sigma_{3,max}$ refers to the maximum value of the respective principal normal stress.

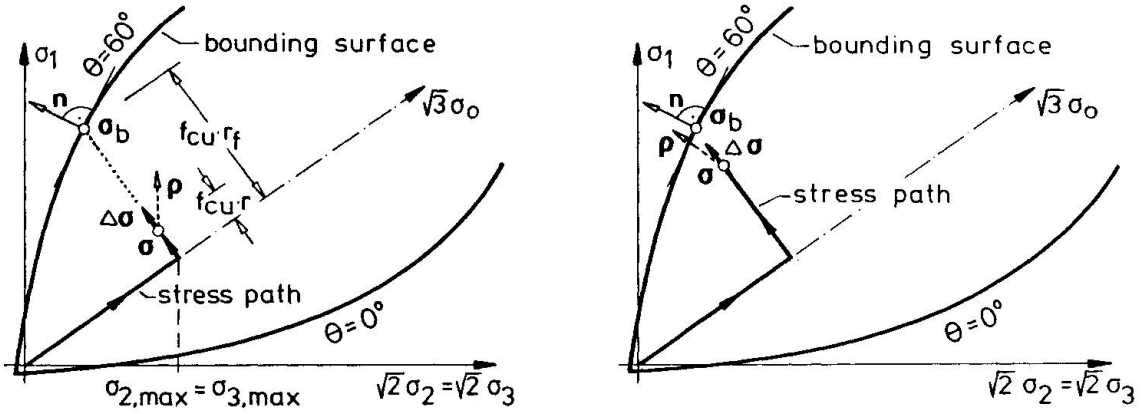

Fig.4 Rotation of the Direction Vector ρ in the Course of Deviatoric Loading

The following list refers to characteristics of the proposed bounding surface model:

(a) The loading surface degenerates to the actual stress point.

(b) Using the projection rule by Mróz [8], the gradient of the loading surface is replaced by the gradient $\mathbf{n}$ of the bounding surface $F(\sigma) = r - r_f = 0$ at the stress image point σ_b (Fig.4). In the pre-failure material regime the bounding surface is fixed in the stress space. At present, the post-failure behavior of the material is not considered.

(c) The direction vector ρ which controls the direction of the vector $d\epsilon^{pl}$ is determined on the basis of experimental results reported by Scavuzzo et al. [6]. For a stress point at a sufficiently large distance from the failure envelope, the direction of the largest principal stress reached so far in the

process of loading controls the direction of $\boldsymbol{\rho}$. (With regards to Fig.4, this is the σ_1-direction). As the stress point approaches the failure surface, the direction vector $\boldsymbol{\rho}$ rotates towards the direction of the gradient vector $\mathbf{n}$. This rotation is controlled by the distance parameter k. Abrupt changes of the direction of $\Delta\boldsymbol{\sigma}$, as occur, e.g., for unloading, are considered by means of the jump parameter ξ. For proportional loading, $\xi = 0$ and $k = r/r_f$.

(d) With increasing tension the rotation of $\boldsymbol{\rho}$ becomes slower.

(e) The value of the generalized plastic modulus H^{pl} is controlled by $\boldsymbol{\sigma}$, k, $\boldsymbol{\varepsilon}^{pl}$ and, because of $k = k(\xi)$, by the jump parameter ξ. Based on the stability criterion by Drucker, a lower bound of H^{pl} is obtained as

$$H_S^{pl} = -(1/2)\mathbf{n}\,\mathbf{D}^{el}\boldsymbol{\rho} + (1/2)\{(\boldsymbol{\rho}\,\mathbf{D}^{el}\boldsymbol{\rho})(\mathbf{n}\,\mathbf{D}\mathbf{n})\}^{1/2}. \qquad (21)$$

H_S^{pl} depends on the amount of the rotation of $d\boldsymbol{\varepsilon}^{pl}$ in the course of loading up to failure. The effectiveness of this bound depends on the stress path.

(f) The loading criterion by Stankowski and Gerstle [3] is used.

3. COMPARATIVE EVALUATION OF THE SELECTED CONSTITUTIVE MODELS

The following comparative evaluation is based on four different loading paths. They were chosen such that the capability of the different formulations to describe specific characteristics of concrete subjected to nonproportional and nonmonotonic loading can be investigated.

Fig.5 shows τ_o/f_{cu}-ε_o diagrams for purely deviatoric loading at two different hydrostatic load levels. The symbol "x" in Fig.5 refers to material failure. The test results illustrate the characteristic volumetric deformational behavior of concrete. Fig.5 elucidates that the nonlinear elastic constitutive model by Kotsovos and Newman does not account for dilatancy. The results obtained by the hypoelastic constitutive model of Stankowski and Gerstle are reasonably good. However, for loading path (b), this model underestimates the ultimate strength of the material by approximately 10 %. With regards to the elasto-plastic constitutive model by Han and Chen, for high hydrostatic load levels such as for loading path (b), the slope of the τ_o/f_{cu}-ε_o diagram at the beginning of deviatoric loading is too small. The reason for this shortcoming is the acute angle enclosed by the hydrostatic axis and the loading surface at the apex of the latter. The good correlation of the compaction/dilatancy characteristics is the result of the previously mentioned modification of the original dilatancy factor α. The constitutive model by Meschke yields results which agree reasonably well with the test results.

Fig.6 shows σ_o/f_{cu}-γ_o diagrams for hydrostatic loading and unloading at different deviatoric load levels. The analytical results in Fig.6 obtained by the two nonlinear elastic constitutive models and by the hypoplastic material model by Meschke, respectively, satisfy the principal stress loading criterion. At point A of loading path (a) at which the principal stress σ_1 exceeds the largest previously obtained value, the beginning of virgin loading is signalled. For this loading path and for the chosen loading surface the loading criterion of the theory of plasticity, used by Han and Chen for their elasto-plastic constitutive model, happens to be equally good as the principal stress loading criterion. For loading path (b), however, the loading criterion of the theory of plasticity results in a delayed beginning of the deviatoric plastic deformations. For this loading path all constitutive models underestimate the octahedral shear strain γ_o. As far as the nonlinear elastic material models are concerned, disregard of the dependence of the tangent bulk modulus K_T on τ_o appears to be the reason for this underestimation. The hypoplastic formulation by Meschke is found to be cap-

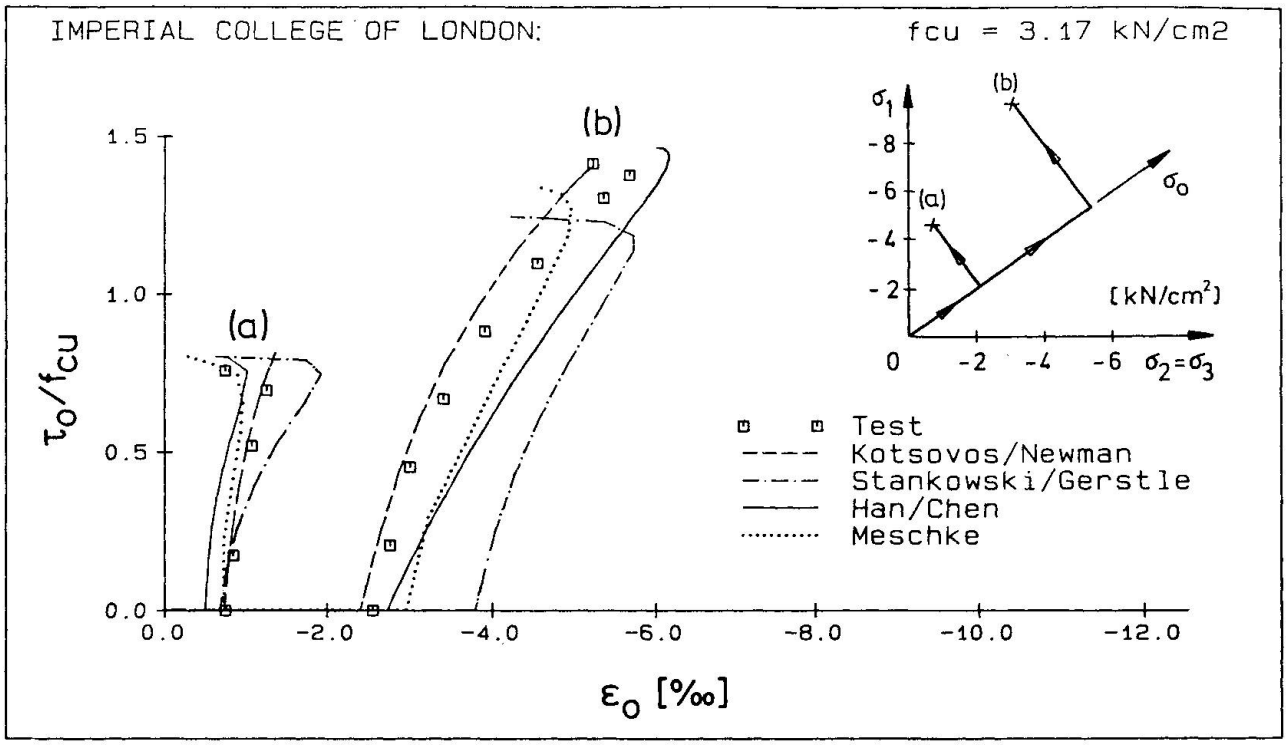

Fig.5 Deviatoric Loading at Two Different Hydrostatic Load Levels

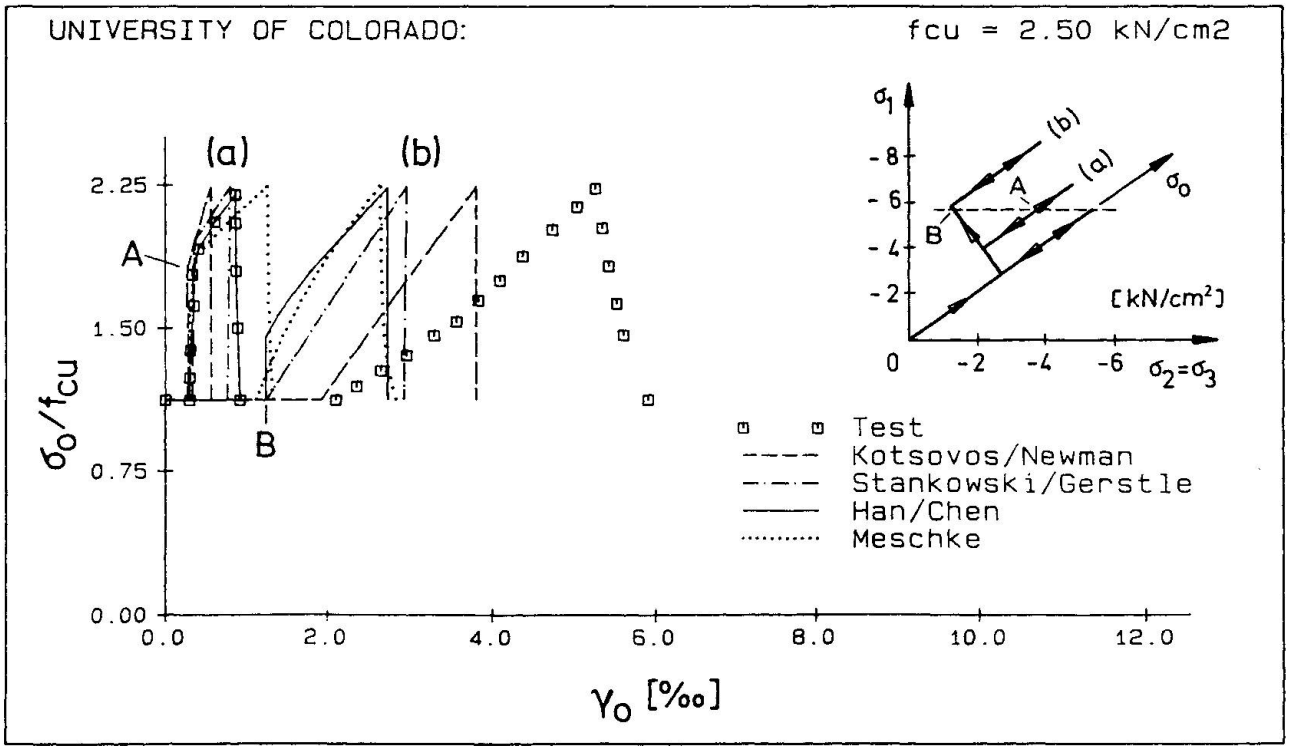

Fig.6 Hydrostatic Loading and Unloading at Different Deviatoric Load Levels

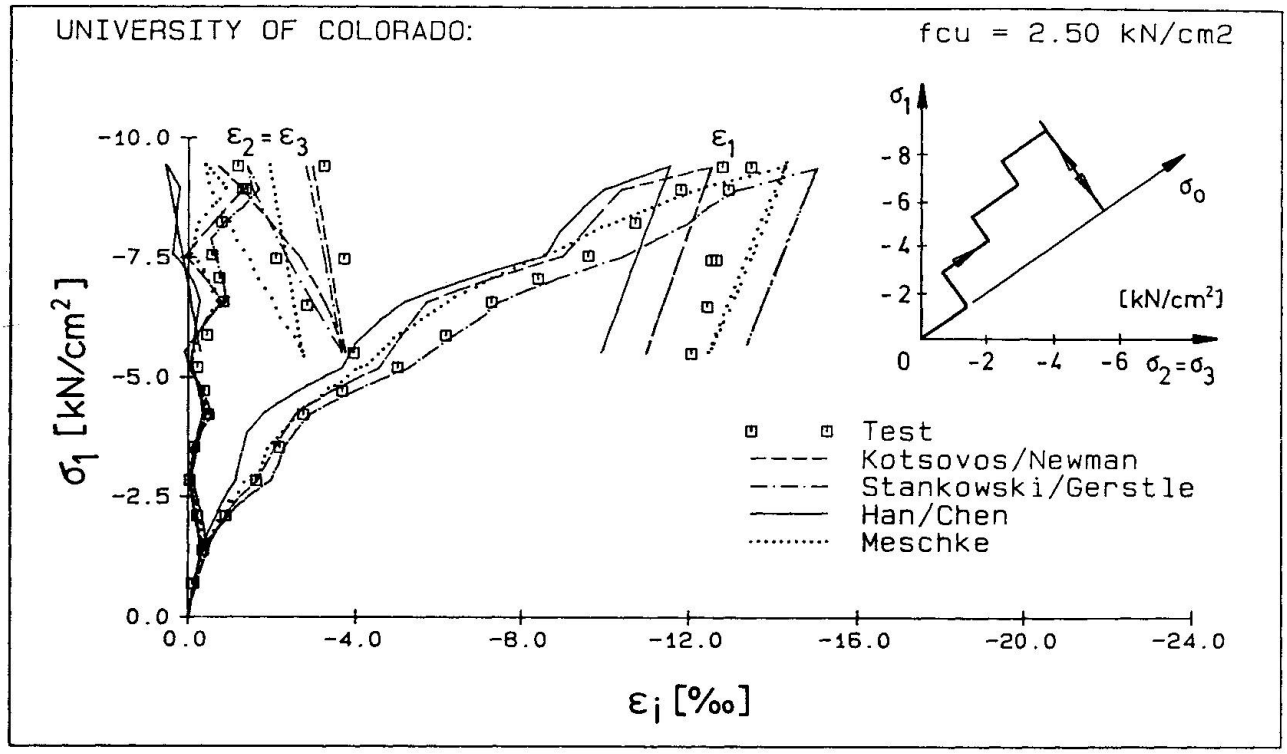

Fig.7 Alternating Hydrostatic and Deviatoric Load Steps Followed by Deviatoric Unloading and Reloading

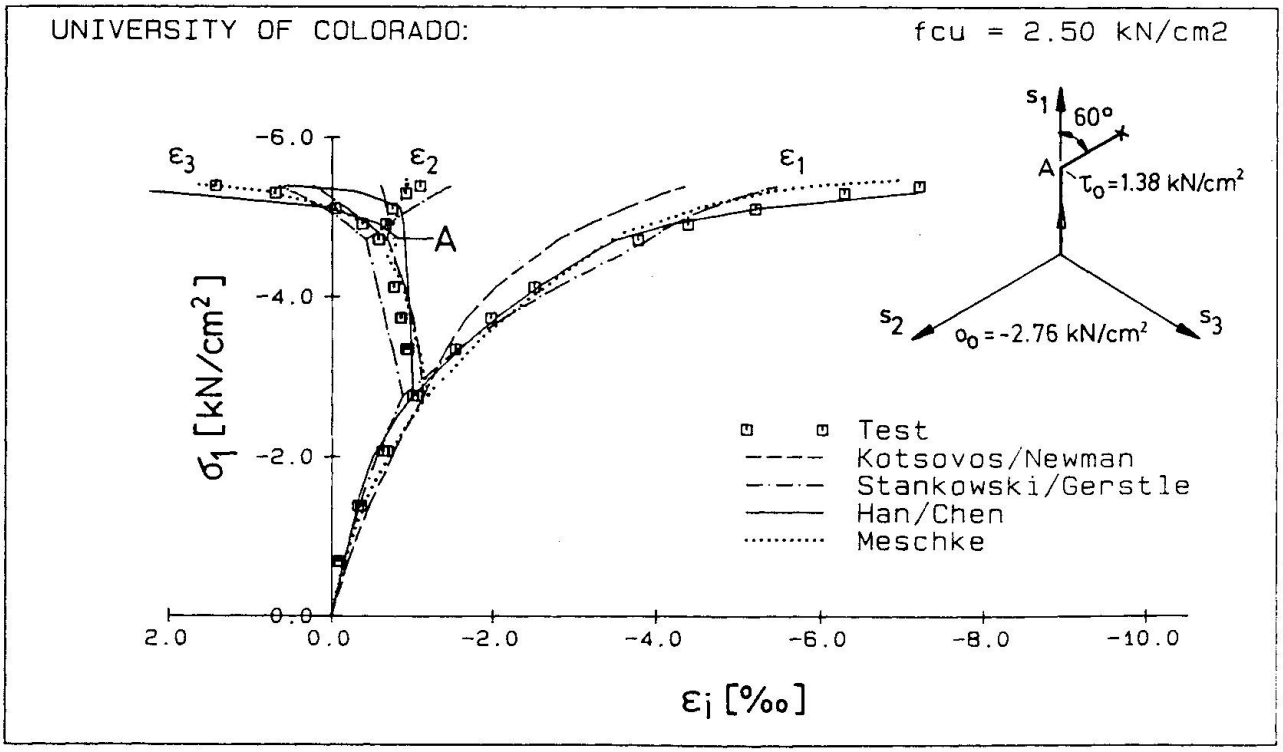

Fig.8 Nonproportional Deviatoric Load Path after Hydrostatic Preloading

able of modelling the remarkable increase of γ_o during hydrostatic unloading.

Fig.7 shows σ_1-ε_i diagrams for a load history characterized by alternating hydrostatic and deviatoric load steps followed by deviatoric unloading and reloading. At points referring to changes from one of these two kinds of load steps to the other one the curves obtained by the constitutive model by Han and Chen are not smooth which is typical for elasto-plastic formulations. The linear elastic unloading predicted by the constitutive model by Han and Chen does not agree with the test results which show a considerable increase of plastic strains ε_2^{pl} and ε_3^{pl}. This shortcoming of the material model by Han and Chen is attributed to the use of the loading criterion of the theory of plasticity. This underlines the importance of the principal normal stress criterion.

Fig.8 shows σ_1-ε_i diagrams for a load history characterized by a nonproportional deviatoric load path after hydrostatic preloading. The symbol "x" in Fig.8 refers to material failure. The reason for the difference between the test results and the analytical results obtained from the formulation of Kotsovos and Newman is disregard of the dependence of the tangent bulk modulus K_T on τ_o. For the section of the deviatoric load path beginning at point A (σ_o = -2.76 kN/cm^2, τ_o = 1.38 kN/cm^2) on the projection s_1 of the σ_1-axis onto the deviatoric plane, the elasto-plastic material model by Han and Chen yields incorrect strains ε_2. The reason for this shortcoming is the assumption of a circular shape of the section of the plastic potential surface by the considered deviatoric plane. For the hypoplastic constitutive model by Meschke good agreement between analytic and test results is observed.

4. CONCLUSIONS

Despite different mechanical concepts of the selected constitutive models and the fact that not all shortcomings inherent in some of these models could be eliminated, generally, good agreement between the model predictions of the deformational behavior and the ultimate strength of concrete and the test results was found. This also refers to results for the tension-compression material regime, which were not presented in this paper. At present, these material models are implemented in a multi-purpose finite element program.

Stress paths associated with characteristic points of thick-walled structures made of reinforced concrete, subjected to static loading, usually are less complex than the ones investigated in this paper. Therefore, for identical constitutive modelling of the post-failure behavior of concrete, it is expected that the chosen constitutive models for triaxially loaded concrete do not have much influence on the results of finite element ultimate load analysis of such structures.

ACKNOWLEDGEMENT

Financial support of the second author by the Austrian Foundation for the Promotion of Scientific Research is gratefully acknowledged.

REFERENCES

1. EBERHARDSTEINER J., MESCHKE G. and MANG H.A., Triaxiales konstitutives Modellieren von Beton zum Zwecke der Durchführung vergleichender Traglastanalysen dickwandiger Stahlbetonkonstruktionen mittels der Methode der Finiten Elemente, Report, Institute for Strength of Materials, Technical University of Vienna, Vienna, 1987.

2. KOTSOVOS M.D., Concrete. A Brittle Fracturing Material, Material and Structures, RILEM, Vol.17, No.98, 1984.

3. STANKOWSKI T. and GERSTLE K.H., Simple Formulation of Concrete Behavior under Multiaxial Load Histories, Journal of the American Concrete Institute, Vol.82, No.2, 1985.

4. HAN D.J., CHEN W.F., A Nonuniform Hardening Plasticity Model for Concrete Materials, Mechanics of Materials, No.4, 1985.

5. CHEN W.F. and SALEEB A.F., Constitutive Equations for Engineering Materials, Vol.1, Elasticity and Modeling, Wiley, New York, 1981.

6. SCAVUZZO R., STANKOWSKI T., GERSTLE K.H. and KO H.Y., Stress-Strain Curves under Multiaxial Load Histories, Report, Dept. of Civil, Environmental and Architectural Engineering, University of Colorado, Boulder, USA, August 1983.

7. WILLAM K.J. and WARNKE E.P., Constitutive Model for the Triaxial Behavior of Concrete, International Association for Bridge and Structural Engineering, Seminar on Concrete Structures Subjected to Triaxial Stresses, No.III-1, Bergamo, Italy, 1974.

8. DAFALIAS Y.F, POPOV E.P., Cyclic Loading for Materials with a Vanishing Elastic Region, Nuclear Engineering and Design, Vol.41, 1977.

9. DAFALIAS Y.F., Bounding Surface Plasticity. I: Mathematical Foundation and Hypoplasticity, Proceedings of the ASCE, Journal of the Engineering Mechanics Division, Vol.112, EM9, 1986.

A Finite Element Simulation Model for Cracks in Reinforced Concrete

Modèle de simulation par éléments finis pour des fissures dans le béton armé

Finite Element Simulation von Rissen in Stahlbeton

Di SHENGLIN
Lecturer
Nanjing Inst. of Techn.
Nanjing, China

Song QIGEN
Professor
Nanjing Inst. of Techn.
Nanjing, China

Shan BINGZI
Professor
Nanjing Inst. of Techn.
Nanjing, China

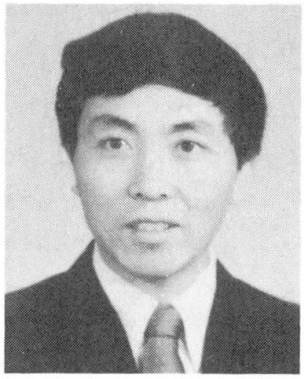

Di Shenglin, born 1951, got his master's degree of engineering at Nanjing Institute of Technology, Nanjing, Jiangsu. Now directed by professors Song Qigen and Shan Bingzi in the Research Division of Structural Mechanics, NIT, he was involved in computational mechanics of RC structures and finite element models for eight years.

SUMMARY

An analytical model has been developed to simulate the crack initiation and propagation. By separating and moving the nodes, the mesh of structure can be changed successively to follow the crack growth. In a computer program the nonlinear behavior of material and bond-slip relationship is taken into account. All the treatments are automatically executed by computer; the rationality of this model has been studied.

RÉSUMÉ

Un modèle analytique simule l'origine d'une fissure et sa propagation. En séparant et déplaçant les noeuds, le réseau de la structure peut être adapté pour suivre l'évolution de la fissure. Un programme d'ordinateur prend en considération le comportement non-linéaire du matériau et la relation adhérence-glissement. Tous les calculs sont exécutés à l'aide de l'ordinateur; le modèle semble rationnel.

ZUSAMMENFASSUNG

Ein numerisches Modell zur Beschreibung der Rissentstehung und deren Fortpflanzung wurde entwickelt. Durch Trennen und Verschieben von Knoten wird das Elementennetz dem Rissfortschritt angepasst. Im Computerprogramm wird nichtlineares Materialverhalten und Verbundverschiebung berücksichtigt. Die Rationalität dieses Modells ist untersucht worden.

1. INTRODUCTION

The crack initiation and propagation is one of the most important characteristics of concrete. In reinforced concrete structure, the cracks cause sudden changes in local stress levels and the local stress will be redistributed. The difference of crack distribution between different structures which are controlled by different strength criteria is obvious, so we must describe the crack initiation and propagation correctly.

There are three different approaches employed for crack modelling: (1) discrete cracking model; (2) smeared cracking model; (3) single crack within an element dealt with by fracture mechanics.

In the first approach, the difficulties are that the location and direction of the cracks are unknown in advance, so Ngo and Scordelis [1] have predicted the diagonal crack in simply supported beam. Based on the discrete cracking model, an approach for computer simulation of crack formation and growth has been developed in this paper. By separating and moving the nodes, the finite element mesh of structure can be changed successively to follow the crack propagation. The crack occurs and grows in accordence with the stress state, it is not necessary to predict the crack location and direction in advance.

2. FINITE ELEMENT SIMULATION MODEL

Consider the boundaries between neighboring element as checking line, if the average stress of two neighboring elements achieve the tensile strength of concrete, f_t', a crack will form along this checking line. According to the crack situation of neighboring boundaries, we can make different treatment, that include, (1) add an extra node, renumber the nodes and equations, separate the corresponding node as shown in Fig.1(a-e); (2) change the direction of cracked boundary to perpendicular to direction of σ_1; (3) calculate the displacement of moved nodes by Lagrangian interpolation formula.

The range in which the nodes can be moved is limited to avoid distorting the element shape exeessively, see Fig.1(f). For simplification, the node can only be moved along one direction, e.g. if the checking line along X coordinate is cracked, the node of this

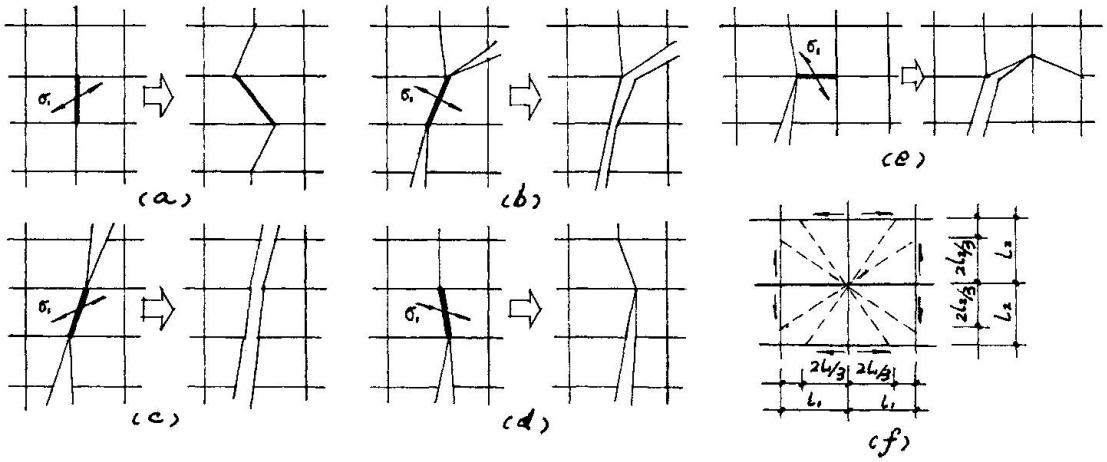

Fig. 1

border can only be moved in the direction of Y coordinate, vice cersa.

If some nodes are disjointed, the program will compute the equivelant node forces of relative elements and release them in next iteration to reflect the stress redistribution occured in actural structures. e.g. assuming node r will be disjointed, we add a new node r_n and call the original node r_o (Fig.2), the equivelant node force of element e_i respect to node r_o

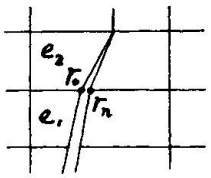

Fig. 2 (m=2)

$$\{P\}^{e_i}_{r_o} = \int_{A_{e_i}} [B]^T_{r_o} \{\sigma\}_{e_i} \cdot t dA \qquad (1)$$

where, t,A= the thickness and area of element e_i; $[B]_{r_o}$=node submatrix of strain. Summing up the contribution of all elements

$$\{P\}^{eq}_{r_o} = \sum_{i=1}^{m} \{P\}^{ei}_{r_o}, \quad \{P\}^{eq}_{r_n} = -\{P\}^{eq}_{r_o} \qquad (2)$$

is obtained, in which m=number of elements which are linked to node r_o.

According to the experimental results[2], though the bond action at each side of crack is weakened, the range is limited, so if we take the stiffness of linkage element as zero in such a case, a considerable error will be caused. In this program, when the crack crosses the reinforcement and the node is separated, we add an extra linkage element to link the new node of concrete to the same

node of reinforcement and then adjust the longitudinal stiffness of these linkage element.

When all the checking lines have been examined, the computer execute a new iteration using the released equivelant node force vector. If in an iteration, there is no new crack occured or propagated and also no element feil, the loading increment of next step will be added.

3. NONLINEAR ANALYSIS

A computer program has been set up for reinforced concrete plane problem. Using the quadratic element for both concrete and reinforcement, one dimension element for stirrup, the program has accepted the tangential stiffness increment method.

The stress-strain relation of concrete under biaxial compression can be expressed as

$$\sigma = \frac{a+b\epsilon}{1+c\epsilon+d\epsilon^2} \tag{3}$$

the constant a,b,c,d can be given by

$$\epsilon = 0, \quad \sigma = 0, \quad \frac{d\sigma}{d\epsilon} = E_0 \quad ;$$

$$\epsilon = \epsilon_c, \quad \sigma = \frac{\sigma_c}{1-\alpha_i\mu}, \quad \frac{d\sigma}{d\epsilon} = 0 \quad . \tag{4}$$

Where σ_c, ϵ_c=stress and strain at uniaxial compressive failure;

$$\alpha_1 = \sigma_1/\sigma_2 \ , \ \alpha_2 = \alpha_1^{-1} \ ;$$

E_0= initial elastic modulus.

then we have

$$E_i = \frac{d\sigma_i}{d\epsilon_i} = \frac{E_0\left[1-(\frac{\epsilon_i}{\epsilon_{ic}})^2\right]}{\left[1+(\frac{1}{1-\alpha_i\mu}\cdot\frac{E_0}{E_s}-2).\frac{\epsilon_i}{\epsilon_{ic}}+(\frac{\epsilon_i}{\epsilon_{ic}})^2\right]} \tag{5}$$

(i=1,2)

The concrete is considered as an orthotropic body, the modulus of elasticity in compression is calculated from eq.(5), in tension is E_0. The reinforcement is considered as idealized elasto-plastic material. The failure criteria is based upon Kupfer's work[4].

4. NUMERICAL RESULTS

A simply supported beam (Fig.3a) is analysed to study the rationality of this approach. After two loading increments, the cracks developed as shown in Fig.3b, In the second calculation, we load the same two loading increments on such a cracked beam at the same time. Because of the same equilibrium state, the correct results of the second computing must be the same as the first one. In fact, the error are very small(less than 4% in general).

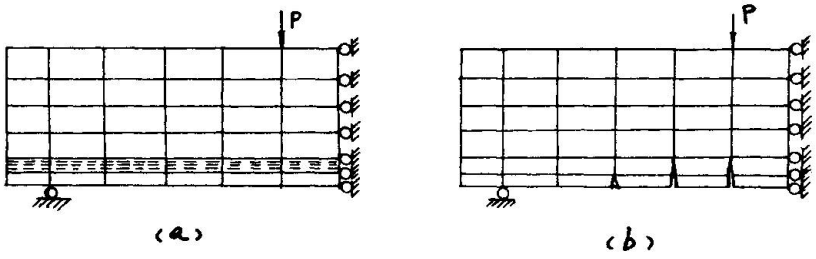

Fig. 3

To examin the whole analytical model and program, a specimen, shown in Fig.4, has been computed. Using 171 concrete elements, we obtained the crack distribution by computer (Fig.5), the crack distribution and direction agree well with the experimental results. The comparison of crack width is not satisfactory, it is obvious that the interlock action in the crack should be included, see Table 1.

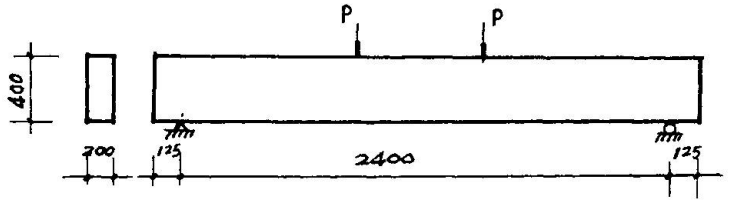

Fig.4 Specimen (mm)

width of crack	load	analysis	experiment
average	4t	0.090	0.057
	8t	0.170	0.080
maximum	4t	0.130	0.060
	8t	0.300	0.150

Table 1 Comparison of crack width

We have also got a lot of message 3 , such as deflection, stress and the properties of total structure. Combining with the experimental results, the analytical results can help us in study of RC structures.

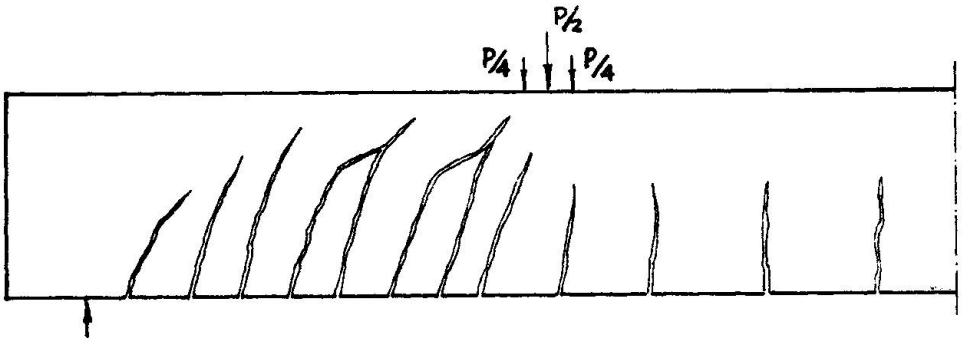

Fig.5 a analytical crack distribution of specimen

REFERENCES

1. Ngo D. and Scordelis A.C., Finite Element Analysis of RC Beam. ACI Journal, March 1967.

2. Song Qigen, Shan Bingzi, Di Shenglin, Study of Reinforced Concrete Bond Properties. International Symposium on Fundamental Theory of RC and PC,Nanjing, PRC, 1986.

3. Di Shenglin, Nonlinear Finite Element Analysis of RC Beams. Journal of Nanjing Institute of Technology, No.2, 1984.

4. Kupfer H.B., Behavior of Concrete Under Biaxial Stress. ACI Journal, August 1969.

Direct Iteration in Nonlinear Analysis of 3-Dimensional Concrete Structures

Méthode d'itération et analyse non-linéaire de structures tridimensionnelles en béton

Direkter Iteration bei der nichtlinearen Berechnung von räumlichen Betonkonstruktionen

Jiang JIAN-JING
Tsinghua University
Beijing, China

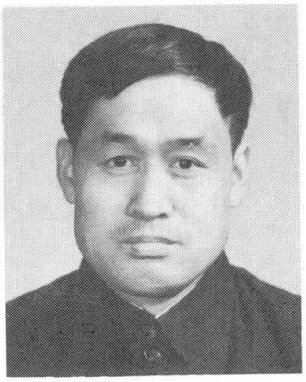

Jiang Jian-Jing, born in 1938, graduated from Tsinghua University in 1963 and received a Dr. Degree from Chalmers University in 1983. Now he is the director of R.C. structure division at Tsinghua University. He has been investigating mainly in finite element analysis and computer simulation of concrete structures.

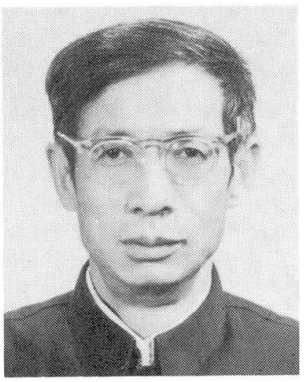

Zhu Jin-Quan, born in 1934, graduated from Tsinghua University in 1957. Now he is the Associate Dean of Civil Engineering Department at Tsinghua University. He has been investigating mainly in reinforced concrete structures.

Zhu JIN-QUAN
Tsinghua University
Beijing, China

SUMMARY

In this paper the direct iteration method for nonlinear analysis of three-dimensional reinforced concrete structures is studied. The paper presents a nonlinearity index, which is in term of second invariant stresses deviator tensor. Much computer time can be saved by using this nonlinearity index. One example is included and numerical results are compared with the experimental results. The comparison shows that this method may be recommended for practical use.

RÉSUMÉ

La contribution traite de la méthode d'itération directe pour l'analyse non-linéaire de structures tridimensionnelles en béton armé. Elle présente un index de non-linéarité, qui est un vecteur de tension de second ordre. Un temps d'ordinateur considérable peut être économisé en utilisant cet index de non-linéarité. Quelques exemples sont présentés et les résultats numériques comparés avec les résultats expérimentaux. La comparaison montre que cette méthode peut être recommandée dans la pratique.

ZUSAMMENFASSUNG

In diesem Beitrag wird die direkte Iterationsmethode für nichtlineare Berechnungen von räumlichen Stahlbetonkonstruktionen studiert. Der Beitrag stellt einen Nichtlinearitätsindex vor, der die zweite Invariante des Tensors der Deviatorspannungen verwendet. Mit diesem Index kann viel Rechenzeit gespart werden. Beispiele numerischer Berechnungen werden mit Versuchsresultaten verglichen. Der Vergleich zeigt, dass diese Methode der Praxis empfohlen werden kann.

1. INTRODUCTION

Three dimensional concrete structures are widely used in massive footing of huge machine, offshore platform, concrete reactor vessel, etc. But its detailed behaviour under various stress combination has not been full understood. In this paper the nonlinear finite element techniques are used for analysis of 3-D reinforced concrete structure from beginning of loading to failure of structure. In this paper the reinforcement is regarded as a steel membrance in the concrete, but different constitutive relationships are adopted for two different materials. The nonlinearity and crack growth of concrete, the yield of reinforced bars are considered in the analysis. The direct iteration method is used for solving the nonlinear finite element equation systems, which is quite efficient for the full range of nonlinear analysis. This method is first proposed by Ottosen [1]. Here this method will be extended to analyse three dimensional reinforced concrete structure. In Ottosen's model, the nonlinearity index is defined in term of σ_{3f}/σ_3, in which the interactive calculation is needed to get β. In this paper another nonlinearity index $\sqrt{J_{2f}}/\sqrt{J_2}$ is proposed, which can be directly calculated from the stress state and have evident geometrical means in stress space.

2. FINITE ELEMENT FORMULATION

Taking into consideration the effect of reinforcement. The eight-node isotropic element with reinforcement membrance is used. In this case the strain in the reinforcement is assumed to be the same as the surrounding concrete. Thus two materials are integrated into a single element but have separate stress-strain relations. A detail explanation can be found in Reference [2]. Here only the formula which are used in this paper are written as follows.

The stress-strain relation is

$$[\sigma]=[D][\varepsilon]$$

where [D] is the material matrix, which is change with the stress level. The stiffness matrix can be calculated by using standard procedure, i.e.

$$[Kc]=\iiint_V [B]^T [Dc][B]dv$$

where [B] - geometric matrix of solid elements
[Dc] - material matrix of concrete

The contribution of reinforcement membrane to stiffness matrix of element may be calculated as follows

$$[Ks]=t\iint_A [B]^T [L]^T [Ds][L][B]dA$$

where [B] - geometric matrix of solid elements
[L] - matrix of coordinate translation
[Ds] - material matrix of reinforced bar
t - equivalent thickness in reinforced direction.

Then the total stiffness matrix of element [K] can be calculated as

$$[K] = [Kc] + [Ks]$$

3. CONSTITUTIVE RELATION FOR CONCRETE

From the test of concrete under compressive stresses shows that the nonlinear strain is existed at beginning of loading and hasn't evident initial yield surface. On the other hand the stress-strain relation of concrete under triaxial stress condition has not yet been full understood. In this case the Ottosen's nonlinear elastic model is available for monotonously increasing load.

In order to evaluate the modulus of elasticity of concrete at different stress level, three things have been decided upon first, i.e.

(1) The failure criterion of concrete;
(2) The equivalent uniaxial stress-strain formulation of concrete;
(3) The nonlinearity index of concrete.

The failure criterion under triaxial stress state proposed by Ottosen is assumed in this paper. However, some other failure surfaces, such as Mohr-coulomb, Drucker-Prager, W.F.Chen, Willianm-Watnke have been implemented in the program. From the expression of the stress-strain relation under uniaxial loading, the secant modulus of concrete, Ec, can be determined from the uniaxial expression by using the nonlinearity index. Here the following expression proposed by Sargin [4] is adopted:

$$-\frac{\sigma}{f_c'}=\frac{-(Eo/Ep)(\varepsilon/\varepsilon_p)+(D-1)(\varepsilon/\varepsilon_p)^2}{1-((Eo/Ep)-2)(\varepsilon/\varepsilon_p)+D(\varepsilon/\varepsilon_p)^2}$$

in which tensile stress and strain are taken as positive. ε_p is the strain at peak stress f_c', Eo is the initial modulus, and Ep is the secant modulus corresponding to $\varepsilon=\varepsilon_p$. D is a parameter which mainly affects the descending segment of the stress-strain curve (Fig. 1). The nonlinearity index β is defined as the ratio of σ/f_c' . Thus the secant modulus of concrete Ec can be evaluated as

$$Ec=0.5Eo-\beta(0.5Eo-Ep)\pm\sqrt{[0.5Eo-\beta(0.5Eo-Ep)]^2+\beta Ep^2\ [D(1-\beta)-1]}$$

where the positive sign is used for the ascending part and the negative sign is used for descending part of the curves.

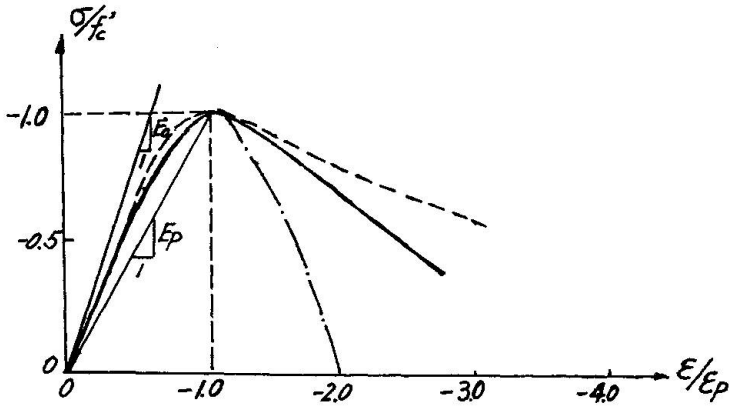

Fig. 1

Under uniaxial loading nonlinearity index β is determined by the scalar stress σ only. How can β be determined under general stress condition? Ottosen suggests

(Fig.2):

$$\beta = \sigma_{3f}/\sigma_3$$

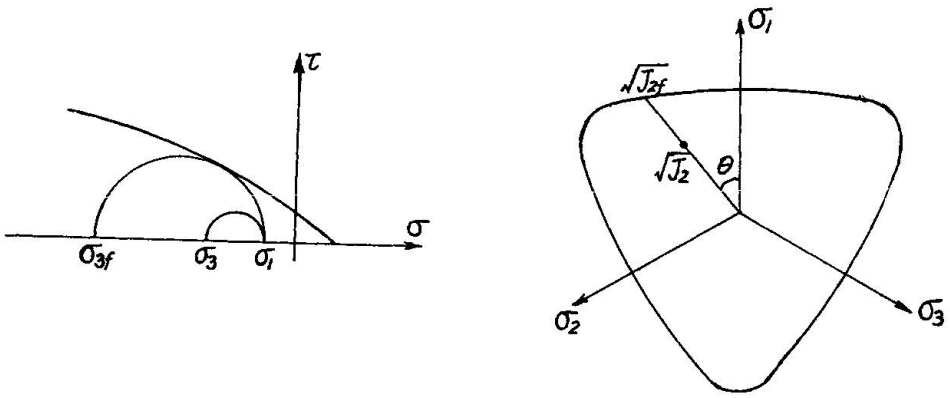

(a) (b)

Fig. 2

where σ_3 is the third principal stress
σ_{3f} is the failure value of σ_3 provided σ_1 and σ_2 are unchanged.

In order to determine the σ_{3f}, the try and error method should be used. In this paper the β value is suggested to be calculated as follows:

$$\beta = \sqrt{J_{2f}}\,/\sqrt{J_2}$$

where J_2 is the second invariant of stress deviator tensor
J_{2f} is the failure value provided I_1 and θ keep unchanged.

4. DIRECT ITERATION METHOD

The finite element equation

$$[K][U] = [P]$$

is a set of nonlinear equations, in which, [U] the total stiffness matrix changes with the stress level. Here, the "direct iteration method" is developed to solve the nonlinear equations. The iterative steps are as follows:

(1) Evaluate the first approximate displacement $[U_1]$ with the initial stiffness matrix $[K_1]$.

(2) Calculate the strain of each element from the displacement $[U_1]$.

(3) Calculate the stress for each element.

(4) Calculate nonlinearity index β.

(5) Evaluate the secant modulus of concrete, and form the updated material matrix

[Dc].

(6) Check the tension cut-off condition: if $\sigma_1 > f'$, modify [Dc].

(7) Calculate the stress of the reinforcement and check the yielding condition: if $\sigma_3 > f_y'$, modify the material matrix [Ds].

(8) Calculate the element stiffness matrix [Kc] and assemble the structural stiffness $[K_2]$.

(9) Evaluate the next approximate displacement $[U_2]$ with $[K_2]$ by

$$[U_2] = [K_2]^{-1} [P]$$

(10) Check the convergence condition: if $\|\delta u\| \leq \varepsilon$, stop the iteration and output the results, where ε is the convergence tolerance; otherwise, replace $[U_1]$ with $[U_2]$, go to step (2), and repeat the procedure.

5. EXAMPLE

The footing structure, Fig. 3, was tested by Nylander. The footing is loaded by a jack, and fixed to the ground by 12 steel bars. Swedish deformed bars (kamstal) of type Ks 60 were used as reinforcement. The actual average yield stress is f_y'=621 MPa. The amount of reinforcement is 17ϕ8 and 16ϕ8, see Fig. 3. The load-deflection curve obtained from experiment is shown in Fig. 4. The deflection of the centre obtained from calculation is also shown in Fig. 4 by a dashed line. The strain at the centre of the reinforcement is shown in Fig. 5 in which the solid line shows the experimental result and the dashed line shows the analytical results by this program.

It can be concluded that the calculated load-displacement curve is in reasonable agreement with the experimental data that the analytical stress in the centre reinforcement can reflect the main characteristics of the experimental results. The calculated failure load is about 11% higher than that experimentally obtained. It is reasonable for the concrete structure.

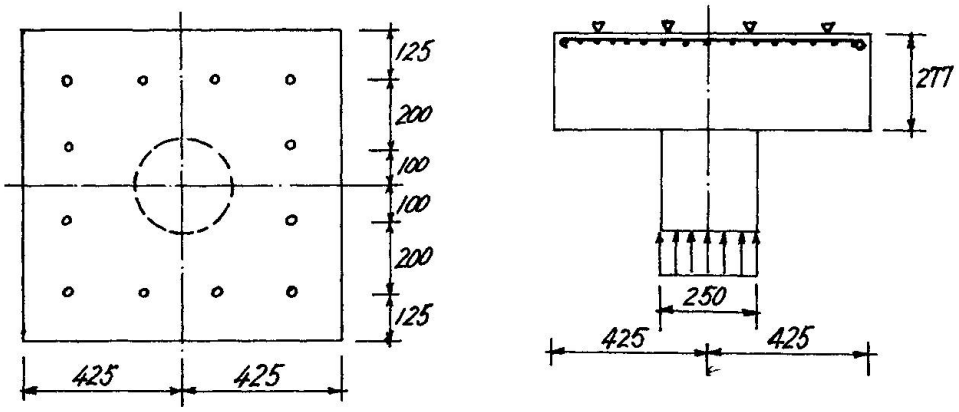

Fig. 3

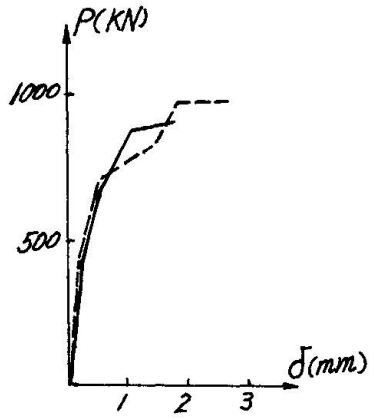

Fig. 4

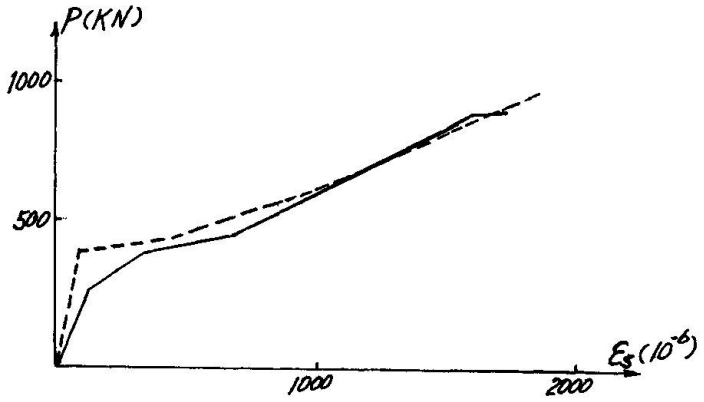

Fig. 5

REFERENCES

[1]. Ottosen, N.S.,: Constitutive model for short-time loading of concrete, J. Engng. Mech. Div. ASCE, vol. 105, No. EM1, February, 1979, PP127-141

[2]. Zienkiewicz, O. C., Owen, D.R.H., Phillips, D.V. and Nayak, G.C.,: Finite element method in analysis of reactor vessels, Nuclear engineering and design, 20(1972) PP507-541

[3]. Jiang, J.J.,: Finite element techniques for static analysis of structures in reinforced concrete,Department of structural mechanics,Chalmers University of technology, Sweden,1983

[4]. Sargin, M.,: stress-strain relationship for concrete and analysis of structural concrete sections, study No. 4, solid Mechanics Division, University of Waterloo, Ontario, Canada, 1971

Framework Model for the Simulation of Fracture Behaviour of Concrete

Modèle de treillis pour la simulation du comportement à la rupture du béton

Ein Fachwerkmodell zur Simulation des Bruchverhaltens von Beton

Ulrich RODE
Civil Engineer
Ruhr-Universität
Bochum, FRG

Ulrich Rode, born in 1957, works as assistant in civil engineering, specially for material technology. He studied at the University of Bochum and received his Dipl.-Ing. degree in 1985.

SUMMARY
A framework model is used for the computer simulation of fracture behaviour of concrete. During the loading process the model degenerates to total collapse due to the failure of struts. Without delineating the geometrical correct shape of particles in material structure the model can be used for microscopical or macroscopical studies. The results of the simulation of a uniaxial tension test are presented.

RÉSUMÉ
Un modèle de treillis est utilisé pour la simulation du comportement à la rupture du béton. Au cours du processus de charge, le modèle dégénère jusqu'à ruine totale par suite de rupture des diagonales. Bien qu'il ne décrive pas la forme géométrique correcte des particules du matériau, le modèle peut être utilisé pour des études microscopiques et macroscopiques. Les résultats sont présentés pour la simulation d'un essai de traction uniaxiale.

ZUSAMMENFASSUNG
Für die Computersimulation des Bruchverhaltens von Beton wird ein Fachwerkmodell benutzt, das durch das Versagen von Stäben während der Belastungsgeschichte bis zum Totalkollaps degeneriert. Ohne die geometrische Gestalt der Partikel im Materialgefüge abzubilden, kann das Modell für mikroskopische und makroskopische Studien verwendet werden. Die Ergebnisse der Simulation eines Zugversuches mit ideal einachsiger Lasteinleitung werden vorgestellt.

1. INTRODUCTION

In material research a numerical method is useful not only in supplying tests of specimens in laboratory, but also giving realistic informations about the crack opening and crack growth inside the specimen. In recent years several models for describing the fracture behaviour of brittle materials have been put forward. Some authors, e.g. /1/, use a mesh for FEM which delineates the structure of concrete exactly. At Bochum another way has been chosen. The model conception is based on Hrennikoff's /2/ idea of the solution of linear elastic continuum problems by framework models. This model allows simulations on micro- and macro levels without altering the number of elements. Only the strut parameters are changed due to the alteration of specimen size.

2. MODEL CONCEPTION

The strut arrangement results from the idea of modelling stress trajectories between equidistant lattice points /3/. The basis cell is a cube, see fig. 1, with edge struts, surface diagonal struts and space diagonal struts. The struts itself behave linear elastic up to given strain rates. On exceeding the maximum tensile or compressive strain the affected struts are removed from the system, representing cracks. Due to the parameter quantification, large displace-

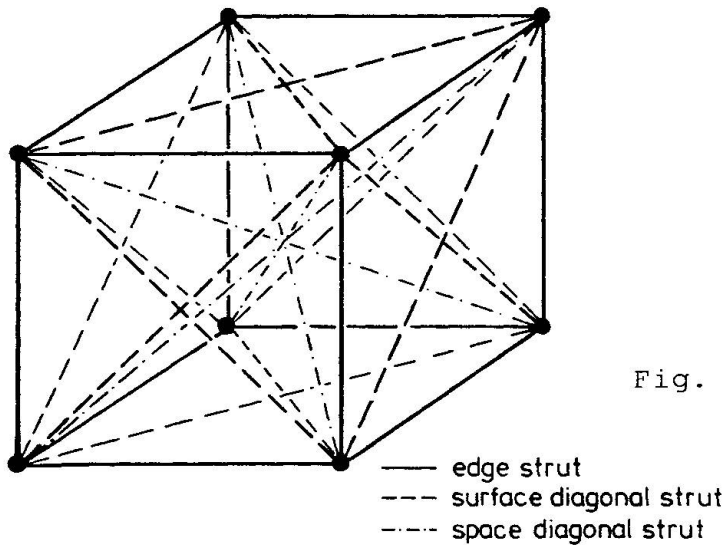

Fig. 1: Basis framework cube

ments may hardly occur. But in heavily degenerated states strut series may buckle or snap through. Thus, a fully geometrically and physically nonlinear analysis of the system has to be performed.

The basic program system has been developed in 1984 /4/. Special numerical techniques have been adapted to perform the simulation analysis on a vector computer effectivelly and fully automatized. The following variations are possible:

- 2D/3D simulations
- uniaxial / multiaxial loading
- compression / tension tests
- load / displacement control
- rigid load induction / "weak" load induction
- influence of viscosity

Additionally, the program system allows an implementation of any material law, e.g. the input of a stress-crack width diagram, which results from the fictitious crack model of Hillerborg /5/.

3. MODELLING CONCRETE

As mentioned before, the model conception allows to choose any level of delineating concrete structure /6/. According to the specimen size the strut parameters have to be altered. Fig. 2 shows an example for microscopical studies. A single strut represents the stress flow mainly through an aggregate particle, another one mainly through the mortar matrix, and a third one is affected by the bond between matrix and aggregate. Fig. 3 shows an example for macroscopical studies. With a given aggregate size distribution and concentration, the three-dimensional composite structure of concrete is simulated to specify the strut parameters. Since exact modelling of the real structure is not required, the strut parameters are stochastically endowed with values by a computerized random number process.

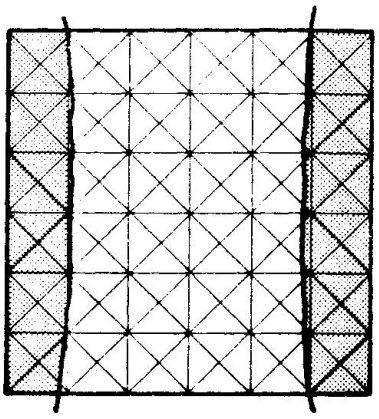

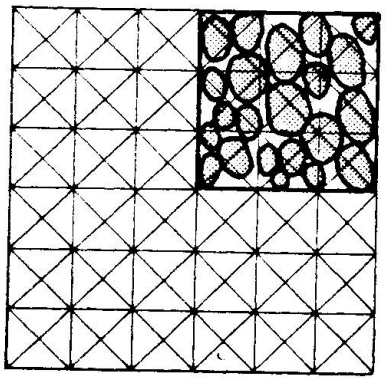

Fig. 2: Example for simulations on a microlevel

Fig. 3: Example for simulations on a macrolevel

4. EXAMPLE

In this chapter the simulation of an ideal uniaxial tension test at a square plane framework will be presented. The concrete is delineated on a macro level. The struts behave linear elastic without any influence of viscosity. The strut parameters are only defined by the stiffness, the tensile strength and the compressive strength. The typical nonlinear behaviour of the total system is determined only by degeneration or cracking, respectively. All quantities of the strut parameters are normally distributed with a variance of 50 %, modelling a very inhomogenous concrete.

The simulation framework consists of 31 x 31 nodes and 3660 struts. The loading acts on the upper edge of the system in a way, that all nodes on this edge displace equally in vertical and freely in horizontal direction. The opposite edge is supported correspondingly. To calculate the load-displacement path up to the total collapse a displacement control is used here.

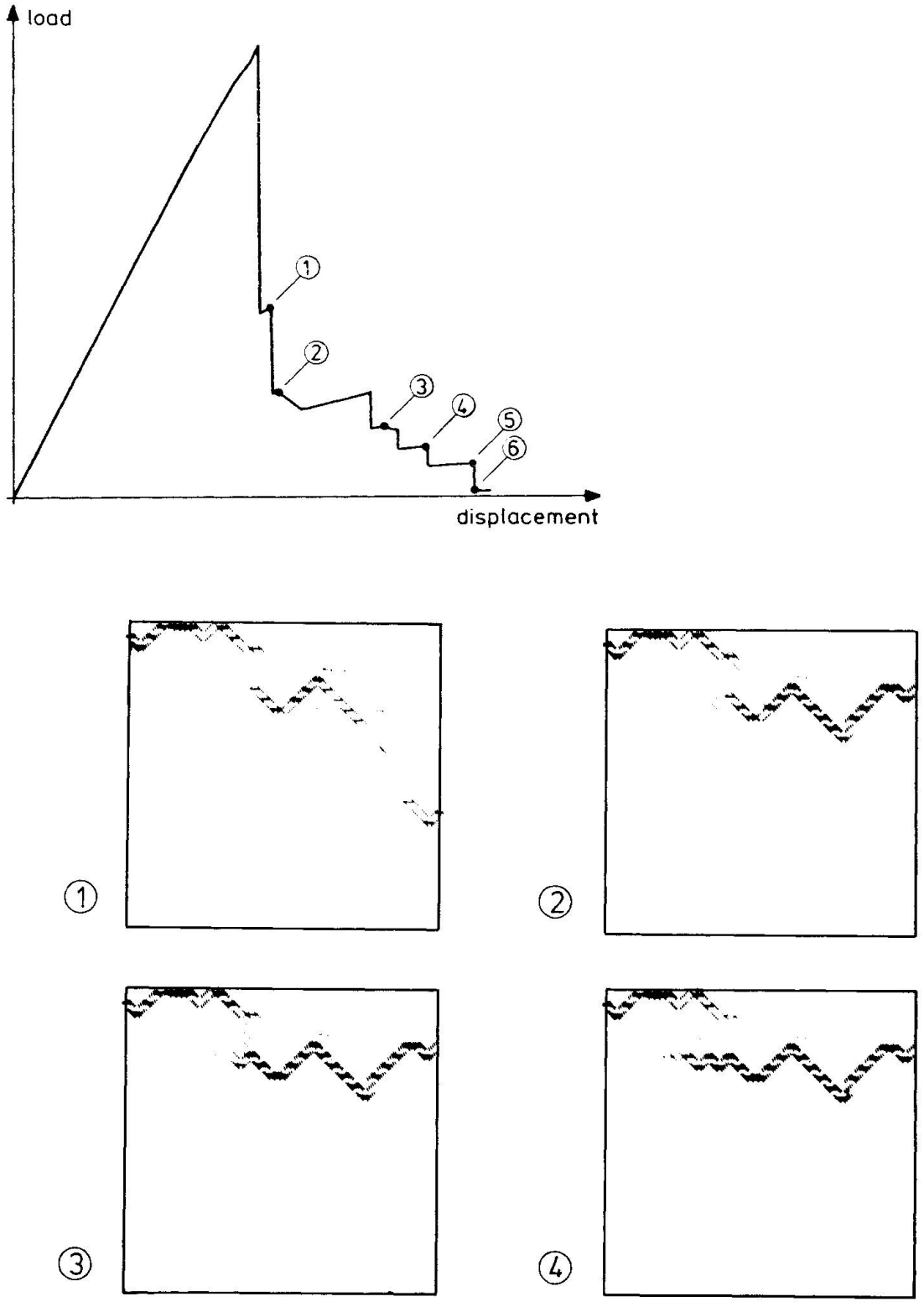

Fig. 4: Results of the simulation of an uniaxial tension test at a plane framework

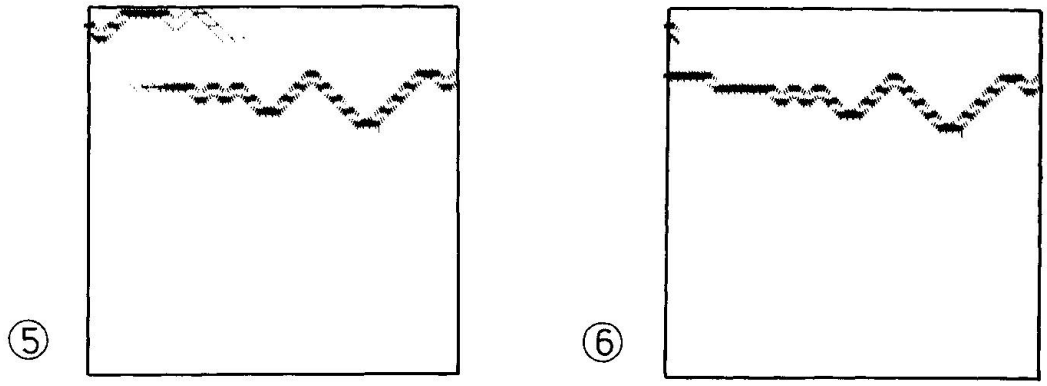

Fig. 4: continued

Fig. 4 shows the graphical interpretation of the tension test simulation. Load-displacement curve and crack plots for six selected load levels are given. According to the strut parameters the first cracks appear randomly. At the unloading branch several horizontal cracks are visible but only one crack runs in horizontal direction and marks the failure mechanism, while the other cracks close just before the total collapse.

The result of this simulation study shows the general applicability of the presented framework model for simulations of fracture behaviour of concrete.

5. REFERENCES

/1/ Wittmann, F.H., Roelfstra, P.E. and Sadouki, H.:
Simulation and Analysis of Composite Structures,
Material science and Engineering, 68 (1984-1985).

/2/ Hrennikoff, A.:
Solution of Problems of Elasticity by the Framework method. Journal of Appl. Mech. 8 (1941).

/3/ Schorn, H.:
Zur Einführung numerischer Berechnungsverfahren in der Ermittlung strukturorientierter Stoffgesetze, Strukturmechanik und Numerische Verfahren, Hrsg.: R. Diekkämper, H.-J. Niemann, Verlag R. Müller, Köln 1982.

/4/ Diekkämper, R.:
Ein Verfahren zur numerischen Simulation des Bruch- und Verformungsverhaltens spröder Werkstoffe, Diss., Technisch-wissenschaftliche Mitteilungen Nr. 84-7, Institut für Konstruktiven Ingenieurbau, Ruhr-Universität Bochum, Dezember 1984

/5/ Hillerborg, A.:
Analysis of One Single Crack, Fracture Mechanics of Concrete, pp. 223-249, edited by F.H. Wittmann, Elsevier Science Publishers B.V., Amsterdam 1983.

/6/ Schorn, H., Rode, U.:
Numerische Simulation von Zugrißöffnungen im Beton, Deutscher Verband für Materialprüfung e.V., Vorträge der 18. Sitzung des Arbeitskreises Bruchvorgänge, Aachen 1986.

Leere Seite
Blank page
Page vide

Numerical Models for the Non-Linear Analysis of Prestressed Concrete Frames

Modèles numériques pour l'analyse non-linéaire de cadres en béton précontraint

Numerische Modelle für die nichtlineare Berechnung von Spannbetonrahmen

Gian Michele CALVI
Researcher
ISMES
Bergamo, Italy

G.M. Calvi, born 1957, received his M.S. in structural engineering from the University of California, Berkeley, in 1985 and recently completed the requirements for his Doctorate degree at the Politecnico di Milano. He has been involved in research related to seismic behaviour of reinforced masonry and prestressed concrete structures.

A. Gobetti, born 1947, graduated at the University of Pavia in 1971, where he is presently Associate Professor of Dynamics of Structures. His research fields concern the numerical techniques for the solution of structural problems.

Armando GOBETTI
Assoc. Prof.
University of Pavia
Pavia, Italy

SUMMARY

After a brief overview of the models currently used for prestressed concrete structures, a model originally developed by the authors is discussed in detail. Its main goal seems to be the simplicity in which shear deformations and slippage of the cables are considered.

RÉSUMÉ

Après avoir passé en revue les modèles actuellement employés pour les structures en béton précontraint, les auteurs présentent leur propre modèle. Le résultat le plus important que l'on peut attendre de ce modèle est la simplicité dans l'expression de la déformation due à l'effort tranchant et de l'écoulement des câbles.

ZUSAMMENFASSUNG

Nach einer kurzen Übersicht über die Modelle, die heute für Spannbeton gebräuchlich sind, wird ein von den Autoren entwickeltes Modell im einzelnen besprochen. Das wichtigste Ergebnis ist, dass Schubverformung und Kabelschlupf sehr einfach behandelt werden können.

1. FOREWORD

The design of prestressed concrete structures must satisfy the requirements of safety and serviceability, as all other kinds of structures.
While this can be accomplished in most cases by following approximate or empirical procedures, it is also desirable to have refined models which can trace the structural response throughout their elastic, cracking, inelastic and ultimate ranges.
The use of these models can be either providing a firmer basis for the codes and analyzing unusual and complex structures.
The purpose of this paper is twofold: first a brief overview of the currently used models is given, then some more details are given about a model developed by the authors.

2. PROBLEMS IN MODELLING PRESTRESSED CONCRETE FRAMES

When dealing with prestressed members any model should be evaluated with respect to some important and peculiar problems.

Time dependent effects, due either to load history, temperature history, creep, shrinkage and aging of concrete and relaxation of the prestressing cables, have the outmost importance because of the character of imposed deformation of the prestressing action.

Bond between tendons, mortar and concrete is a qualifying point: refined model should give the possibility of simulating bonded and unbonded tendons, and in the former case should incorporate a law for the progressive deterioration and failure of bond connections.

Shear deformations and effects of the prestressing action on shear cannot always be neglected, particurarly when dealing with deep beams.

Planarity of the section is not guaranteed due to shear and torsions, and is not respected at all after some slippage between cables and concrete has occurred.

Connections between elements, mainly beam-column connections, may create problems to some models, effective for one-dimensional structures.

The constitutive relations are sometime based on well established laws for concrete and steel, sometimes on the contrary are obtained through euristic corrections of the usual relations for concrete beams.

Finally computer time and memory may be very penalizing for too refined or bad conditioned elements.

3. CURRENT MODELS

Models based on quite different ideas are presently implemented to simulate the behavior of PC beams. The most commonly used ones will be briefly presented in what follows.

3.1 Traditional beam elements whith corrections

This is conceptually the simplest and most euristic approach /2/. The usual moment-rotation relations are used, correcting at each time step the stiffness of the elements in order to take into account the actual non-linearity.
The prestressing action is introduced as an external force, but the reduction in stiffness keeps it equivalent to an imposed deformation. The sections are considered to remain plane, bond and shear are not explicity taken into account.
Most of the job consist in getting the right correction factors for cracking, time dependent effects, tension stiffening.

3.2. Integration of sectional M-ϕ relations

A second approach is based on the use of sectional results, obtained normally through programs which divide any section into layers with different stress-stain relations. Equilibrium and planarity of the section are then imposed to get moment-curvature relations /7/.
The prestressing action is taken into account prestressing some steel layers, bond is supposed to be perfect, time dependent effects are usually neglected.
A number of choices is then possible to get the overall stiffness of a beam element:

1. Each beam can be identified by one or more sections, using constant, linear or higher order variation of the stiffness properties along the member;
2. The moment-curvature relations can be piecewise linearized, or the actual M - ϕ can be used and the stiffness of each section computed at each step within the F.E. analysis /1/. In this case the procedure way be very time consuming.

3.3. Layer and filament models

A beam element is decomposed in a number of straight layers or filament each of them with a monodimensional stress-strain law which can take into-account also time dependent effects.
Pretensioned, bonded and unbonded postensioned cables can be simulated, shear deformations are neglected.
The elements cross sections should have a simmetry in the case of layers models, can be of any shape in the case of filament models.
The tendons are straight, but not necessarily horizontal within the element /11/.

4. BIDIMENSIONAL LAYERS MODEL

This model, recently implemented by the authors, differs from the layer model mainly because of the layers are here modeled as plane stress elements instead of one-dimensional.
The advantages of such a model may be summarized as follows:

1. the shear deformations are considered, which is particulary important for deep beams.
2. It is possible to take into account the interactions between axial action, shear and bending moment.
3. The sections can assume up to a second order polynomial shape.
4. The number of layers is much smaller than in the case of a mono-dimensional layer model.

4.1. Analytical Formulation

The adopted approach is the Displacement Finite Element Formulation.
The displacement fields are defined over a bidimensional domain, subdivided into strips through the height of the beam.
The strain-displacement relations for the Timoshenko beam theory may be written as:

$$\varepsilon_{RR} = - S \frac{\partial \theta}{\partial R} + \frac{\partial u}{\partial R}$$
$$\varepsilon_{RS} = - \theta + \frac{\partial v}{\partial R} \qquad (1)$$

Where R and S are coordinates related to a sectional reference system, which may vary along the beam because of the variability in the shape of the cross section; u , v and are the generalized dislacement components, according to a classical Lagrangian formulation, referred to an absolute reference system.

The commonly used Bernoulli-Navier formulation, which requires the planarity of the sections, assumes:

$$\theta = \frac{dv}{dR} \tag{2}$$

and consequently equations (1) assumes the form:

$$\varepsilon_{RR} = - S \frac{d^2v}{dR^2} + \frac{du}{dR}$$
$$\varepsilon_{RS} = 0 \tag{3}$$

This formulation requires the continuity in C^1 for the discrete variables in the shape functions: they have to be at least of the third order in R for v and of the first order for u (see table 1).
The use of the Timoshenko theory gives many advantages and one problem:
- the shape functions have to be continuous in C°, they can be the same for u, v and θ (see table 1).
- Three nodes elements can be used, so that curved beams can be represented, the layers can have curvilinear borders, sensible modifications in the cross section shape do not give problems.
- The shear deformations are directly taken into account.
- The problem is that the strain tensor components are not of the same order, so that the shear effects are overestimated when the height of the beam becomes smaller and smaller.

This difficulty has been successfully overjumped by fictitiously reducing the degree of ε_{RS} and setting the ε_{RS} and the ε_{RS} reduced at the same values at the Gauss integration points.
For the prestressing steel layers the strain displacement relations are modified as follows:

$$\varepsilon_{RR} = - \frac{\partial\theta}{\partial R} + \frac{\partial u}{\partial R} + \varepsilon_o + \frac{\partial \Delta u}{\partial R}$$
$$\varepsilon_{RS} = - \theta + \frac{\partial v}{\partial R} \tag{4}$$

Where ε_o is the initial strain due to prestressing and Δu is the slippage between cable and concrete after the bond has been destroyed.

4.2. Constitutive Equations

The constitutive equations have to be biaxial for concrete and steel and have to treat the bond between steel and concrete.
Concrete. The relations presented by Kupfer and Gerstle /8/ have been used. They separate the hydrostatic and deviatoric behavior:

$$\sigma_o = 3K \varepsilon_o$$
$$\sigma_o = 2G \gamma_o \tag{5}$$

finding a very good correlation between the experimental results and the following equations:

$$G_S/G_O = 1 - a (\tau_o/fcu)^m$$
$$G_T/G_O = \frac{(G_S/G_o)^2}{m - G_S/G_O (m - 1)}$$
$$K_S/K_O = G_S/G_O \, e^{(c\gamma_o)^P} \tag{6}$$
$$K_T/K_O = \frac{G_T/G_o}{e^{-(c\gamma_o)^P} (1 - p(c\gamma_o)^P)}$$

where G_S and K_S are the secant moduli,
G_T and K_T are the tangent moduli,
G_o, K_o, a, m, c, and p are constants given as a function of ultimate monoaxial strength f_{cu}

The biaxial strength is then given by the expressions:

compression-compression $(\sigma_1/fcu + \sigma_2/fcu)^2 + \sigma_1/fcu + 3.65\ \sigma_2/fcu = 0$

compression-tension $\sigma_2/ftu = 1 + 0.8 \sqrt[3]{\sigma_1/fcu}$ (7)

tension-tension $\sigma_2 = f_{tu} = 0.64 \sqrt[3]{f_{cu}^2}$

The material stiffness matrix is:

$$4G\,\frac{3K+G}{3K+4G}\begin{bmatrix} 1 & \frac{3K-2G}{2(3K+G)} & 0 \\ \frac{3K-2G}{2(3K+G)} & 1 & 0 \\ 0 & 0 & \frac{3K+4G}{4(3K+G)} \end{bmatrix} \qquad (8)$$

setting $\sigma_y = 0$ the final relations for concrete are obtained:

$$\begin{bmatrix} \sigma_{RR} \\ \sigma_{RS} \end{bmatrix} = \begin{bmatrix} \frac{9KG}{3K+D} & 0 \\ 0 & G \end{bmatrix} \times \begin{bmatrix} \varepsilon_{RR} \\ \varepsilon_{RS} \end{bmatrix} \qquad (9)$$

Steel. The Von Mises plastic potential has been used, with an isotropic hardening taken from the CEB quintic for prestressing steel:

$$\varepsilon_S = 0.823\,\left(\frac{\sigma_S}{f_{y0.2}} - 0.77\right)^5 \qquad \sigma_S > 0.7\,\frac{f_{y0.2}}{E_S}$$

$$\varepsilon_S = \frac{\sigma_S}{E_S} \qquad \sigma_S < 0.7\,\frac{f_{y0.2}}{E_S} \qquad (10)$$

By conformity and normality the following expression for the plastic velocity of deformation is obtained:

$$\dot{\varepsilon}_{ij}^{(p)} = \bar{H}\,\frac{\partial f}{\partial \sigma_{kl}}\,\dot{\sigma}_{kl}\,\frac{\partial f}{\partial \sigma_{ij}} \qquad (11)$$

where

$$\bar{H} = \frac{1}{\frac{\partial f}{\partial \varepsilon_{mn}^{(P)}} + \frac{\partial f}{\partial \chi}\,\frac{\partial \chi}{\partial \varepsilon_{mn}^{(P)}}\,\frac{\partial f}{\partial \sigma_{mn}}}$$

and

$$f(\sigma_{ij},\ \dot{\varepsilon}_{ij}^{(P)},\ \chi(\dot{\varepsilon}_{ij}^{(P)})) = 0 \qquad (12)$$

by consistency.

With some manipulation the material stiffness matrix is obtained:

$$\begin{bmatrix} \Delta\sigma_{RR} \\ \Delta\sigma_{RS} \end{bmatrix} = \frac{1}{\frac{4\bar{H}}{9G}\sigma_{RR}^2 + \frac{4\bar{H}}{E}\sigma_{RR}^2 + \frac{1}{EG}} \begin{bmatrix} 4\bar{H}\sigma_{RS}^2 + \frac{1}{G} & -\frac{3}{4}\bar{H}\sigma_{RR}\sigma_{RS} \\ -\frac{4}{3}\bar{H}\sigma_{RR}\sigma_{RS} & \frac{4}{9}H\sigma_{RR}^2 + \frac{1}{E} \end{bmatrix} \begin{bmatrix} \Delta\varepsilon_{RR} \\ \Delta\varepsilon_{RS} \end{bmatrix} \tag{13}$$

with

$$\bar{H} = 9.2587534 \frac{\sqrt[5]{(\varepsilon_p/0.823)^4}}{f_{y0.2}^2 \sigma_{RR} (0.7 + \sqrt[5]{\varepsilon_p/0.823})}$$

For the ordinary steel hardening has been neglected because it is not usually reached: the ultimate strain of the prestressing steel is normally lower than the hardening strain of the ordinary steel.
Its constitutive equation is consequently simply elastic-perfectly plastic.

Bond. The bond between steel and concrete is presently considered as rigid-plastic, but it could be easily transformed in a multi-linear relation.
At every step the stresses at the border of the concrete layers are checked at the joint position: if a failure occurs the bond ties are supposed to be broken.
As a consequence the height variable S for the steel layer is not any more taken with reference to the N.A.of the section, but with reference to the N.A. of the layer. In such a way the moment of inertia of the steel layer is not any more contributing to the whole section moment of inertia.
Moreover a new unknown variable Δu (eq.2) is considered, which is the displacement of the steel layer at the joint where the failure has occumed.
Of course this means that a new row and a new column are inserted in the stiffness matrix.
Two different strategies are possible, depending on the meaning of Δu: it may be taken as the total displacement of the cable joint or as the displacement of the cable joint with respect to the deformed position of the section. To clarify the ideas let's consider a two elements, three joints, two layers example in the simpler formulation.
The stiffness matrix can be written as follows:

$$\begin{bmatrix} F_{u1} \\ F_{v1} \\ F_{\theta 1} \\ F_{u2} \\ F_{v2} \\ F_{\theta 2} \\ F_{u3} \\ F_{v3} \\ F_{\theta 3} \\ F_{\Delta u} \end{bmatrix} = \begin{bmatrix} K_{1,1} & 0 & 0 & K_{1,4} & 0 & 0 & 0 & 0 & 0 & K_{1,10} \\ & K_{2,2} & K_{2,3} & 0 & K_{2,5} & K_{2,6} & 0 & 0 & 0 & 0 \\ & & K_{3,3} & 0 & K_{3,5} & K_{3,6} & 0 & 0 & 0 & 0 \\ & & & K_{4,4} & 0 & 0 & K_{4,7} & 0 & 0 & 0 \\ & & & & K_{5,5} & K_{5,6} & 0 & K_{5,8} & K_{5,9} & 0 \\ & & & & & K_{6,6} & 0 & K_{6,8} & K_{6,9} & 0 \\ & & & \text{sym.} & & & K_{7,7} & 0 & 0 & 0 \\ & & & & & & & K_{8,8} & K_{8,9} & 0 \\ & & & & & & & & K_{9,9} & 0 \\ & & & & & & & & & K_{10,10} \end{bmatrix} \begin{bmatrix} u_1 \\ v_1 \\ \theta_1 \\ u_2 \\ v_2 \\ \theta_2 \\ u_3 \\ v_3 \\ \theta_3 \\ \Delta u \end{bmatrix} \tag{14}$$

Some significant terms of the stiffness matrix are explicitly given in table 2, before and after the bond failure at joint 2.

5. CONCLUSIONS

The main points to be considered when dealing with modeling P.C. frames are discussed, showing that a choice should be operated case by case to take into account the most important effects and to disregard the others.
An original model is presented: it seems to be a good compromise between

simplicity of calculation and refinement in the material modeling.
The model deals satisfactorily with the problems of bond, shear, connections and constitutive relationships, but presently disregards the time dependent effects.
Many simulations of different structure are needed in order to check the effectiveness of the model; then further refinements might be implemented.
The most important of them seem to be to consider a multilinear law for bond and to take into account time dependent effects.
A particular problem deals with the constitutive equations for concrete, estensively discussed in /3/; in the present model it seems to be necessary to take into account the effect of confinement due to steel.

6. REFERENCES

/1/ CALVI G.M., Cyclic Behavior of Partially Prestressed Continuous Beams - M.S. thesis, Div. of Struct. Eng. and Struct. Mech., Dept. of Civ. Eng., University of California, Berkeley, May, 1985

/2/ CAUVIN A., Non linear Analysis of Prestressed Concrete Continuous Beams and Frames - Proceedings, Int. Symp. on Non-linearity and Continuity in Prestressed Concrete, Un. of Waterloo, Ontario, Canada, July, 1983

/3/ C.E.B. TASK GROUP 6, Concrete under Multiaxial States of Stress. Constitutive Equations for Practical Design - Bull. N.156, June, 1983

/4/ CRISFIELD M.A., A Quadratic Mindlin Element using Shear Contraints - Computer and Structures, 1984, 833-852

/5/ GOBETTI A., A Finite Element Model for Geometrically Nonlinear Elastoplastic Plane Frame Structures, Rep. N. 25, Dept. of Struct. Mech., Un. of Pavia, Italy, 1986

/6/ HUGHES T.J.R., The Heterosis Finite Element Methods for Plate Bending - Computers and Structures, 1978, 445-450

/7/ KABA, S.A., MAHIN, S.A, Interactive Computer Analysis Methods for Predicting the Inelastic Behavior of Sections, Rep. No. UCB/EERC-83/18, EERC, Univ. of California, Berkeley, July 1983

/8/ KUPFER, H.B. and GERSTLE, K.H., Behavior of concrete under biaxial stresses, Journ. of the Eng. Mech. Div., ASCE, VOL.99, N. EM4, Aug., 1973

/9/ MINDLIN R.D., Influence of Rotatory Inertia and Shear on Flexural Motions of Isotropic Elastic Plates , Journ. of App. Mech., 1951, 31-38

/10/ PRATHAP G., An Optimaly Constrained 4-Node Quadrilateral Thin Plate Bending Element - Computers and Structures, 1984, 789-794

/11/ SCORDELIS A., Analitycal Models for Non linear Material, Geometric and Time-Dependent Effects - Proc., Int. Symp. on Nonlinearity and Continuity in Prestressed Concrete, Un. of Waterloo, Ontario, Canada, July 1983.

$N_{v,1} = \frac{1}{2} - \frac{3}{2}\frac{R}{l} + 2\frac{R^3}{l^3}$	$N_{u,v,\theta,1} = \frac{2R^2}{l^2} - \frac{R}{l}$
$N_{v,2} = \frac{1}{2} + \frac{3}{2}\frac{R}{l} - 2\frac{R^3}{l^3}$	$N_{u,v,\theta,2} = \frac{2R^2}{l^2} + \frac{R}{l}$
$N_{\theta,1} = \frac{l}{8} - \frac{R}{4} - \frac{R^2}{2l} + \frac{R^3}{l^3}$	$N_{u,v,\theta,3} = 1 - \frac{4R^2}{l^2}$
$N_{\theta,2} = -\frac{l}{8} - \frac{R}{4} + \frac{R^2}{2l} + \frac{R^3}{l^3}$	
$N_{u,1} = \frac{1}{2} - \frac{R}{l}$	
$N_{u,2} = \frac{1}{2} + \frac{R}{l}$	
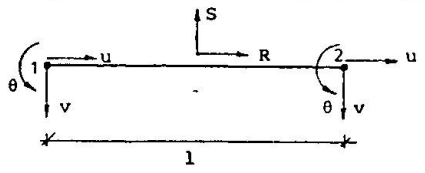	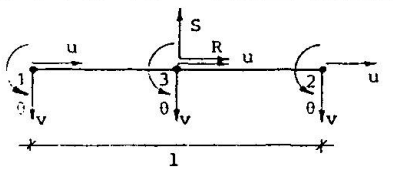

Table 1 – shape functions according to the Bernoulli-Navier and the Timoshenko formulations

	Before bond failure at joint 2	After bond failure at joint 2
$K_{1,1}$	$\int_I E_I N_1'^2 dv + \int_{II} E_{II} N_1'^2 dv$ (1)	same
$K_{1,4}$	$\int_I E_I N_1' N_2' dv + \int_{II} E_{II} N_1' N_2' dv$ (1)	$\int_I E_I N_1' N_2' dv$ (1)
$K_{1,10}$	0	$\int_{II} E_{II} N_1' N_2' dv$ (1)
$K_{2,2}$	$\int_I G_I N_1'^2 dv + \int_{II} G_{II} N_1'^2 dv$ (1)	same
$K_{2,3}$	$\int_I G_I N_1' N_1 dv + \int_{II} G_{II} N_1' N_1 dv$ (1)	same
$K_{2,5}$	$\int_I G_I N_1' N_2' dv + \int_{II} G_{II} N_1' N_2' dv$ (1)	same
$K_{2,6}$	$\int_I G_I N_1' N_2 dv + \int_{II} G_{II} N_1' N_2 dv$ (1)	same
$K_{3,3}$	$\int_I (E_I S_I^2 N_1'^2 + G_I N_1^2) dv + \int_{II} (E_{II} S_{II}^2 N_1'^2 + G_{II} N_1^2) dv$ (1)	same
$K_{3,5}$	$\int_I G_I N_1 N_2' dv + \int_{II} G_{II} N_1 N_2' dv$ (1)	same
$K_{3,6}$	$\int_I (G_I N_1 N_2 + E_I S_I^2 N_1 N_2) dv + \int_{II} (G_{II} N_1 N_2 + E_{II} S_{II}^2 N_1 N_2) dv$ (1)	$\int_I (G_I N_1 N_2 + E_I S_I^2 N_1 N_2) dv$ (1)
$K_{4,4}$	$\int_I E_I N_2'^2 dv + \int_{II} E_{II} N_2'^2 dv$ (1) + $\int_I E_I N_1'^2 dv + \int_{II} E_{II} N_1'^2 dv$ (2)	$\int_I E_I N_2'^2 dv$ (1) + $\int_I E_I N_1'^2 dv$ (2)
$K_{5,5}$	$\int_I G_I N_2'^2 dv + \int_{II} G_{II} N_2'^2 dv$ (1) + $\int_I G_I N_1'^2 dv + \int_{II} G_{II} N_1'^2 dv$ (2)	same
$K_{5,6}$	$\int_I G_I N_2' N_2 dv + \int_{II} G_{II} N_2' N_2 dv$ (1) + $\int_I G_I N_1' N_1 dv + \int_{II} G_{II} N_1' N_1 dv$ (2)	same
$K_{6,6}$	$\int_I (E_I S_I^2 N_2'^2 + G_I N_2^2) dv + \int_{II} (E_{II} S_{II}^2 N_2'^2 + G_{II} N_2^2) dv$ (1) + $\int_I (E_I S_I^2 N_1'^2 + G_I N_1^2) dv + \int_{II} (E_{II} S_{II}^2 N_1'^2 + G_{II} N_1^2) dv$ (2)	$\int_I (E_I S_I^2 N_2'^2 + G_I N_2^2) dv + \int_{II} G_{II} N_2^2 dv$ (1) + $\int_I (E_I S_I^2 N_1'^2 + G_I N_1^2) dv + \int_{II} G_{II} N_1^2 dv$ (2)
$K_{10,10}$	0	$\int_{II} E_{II} N_2' dv$ (1) + $\int_{II} E_{II} N_1^2 dv$ (2)

Table 2 - Timoshenko formulation: some terms of the stiffness matrix (I layer, 1 joint, (1) element)